TOPICS IN ORGANOMETALLIC CHEMISTRY

25

Volume Editor Thomas R. Ward

Bio-inspired Catalysts

Springer

25

Topics in Organometallic Chemistry

Topics in Organometallic Chemistry

Recently Published and Forthcoming Volumes

Metal Catalysts in Olefin Polymerisation
Volume Editor: Z. Guan
Vol. 26, 2009

Bio-inspired Catalyst
Volume Editor: T. R. Ward
Vol. 25, 2009

Directed Metallation
Volume Editor: N. Chatani
Vol. 24, 2007

Regulated Systems for Multiphase Catalysis
Volume Editors:W. Leitner, M. Hölscher
Vol. 23, 2008

Organometallic Oxidation Catalysis
Volume Editors: F. Meyer, C. Limberg
Vol. 22, 2007

N-Heterocyclic Carbenes in Transition Metal Catalysis
Volume Editor: F. Glorius
Vol. 21, 2006

Dendrimer Catalysis
Volume Editor: L.H. Gade
Vol. 20, 2006

Metal Catalyzed Cascade Reactions
Volume Editor: T. J. J.Müller
Vol. 19, 2006

Catalytic Carbonylation Reactions
Volume Editor: M. Beller
Vol. 18, 2006

Bioorganometallic Chemistry
Volume Editor: G. Simonneaux
Vol. 17, 2006

Surface and Interfacial Organometallic Chemistry and Catalysis
Volume Editors: C. Copéret, B. Chaudret
Vol. 16, 2005

Chiral Diazaligands for Asymmetric Synthesis
Volume Editors: M. Lemaire, P. Mangeney
Vol. 15, 2005

Palladium in Organic Synthesis
Volume Editor: J. Tsuji
Vol. 14, 2005

Metal Carbenes in Organic Synthesis
Volume Editor: K.H. Dötz
Vol. 13, 2004

Theoretical Aspects of TransitionMetal Catalysis
Volume Editor: G. Frenking
Vol. 12, 2005

Ruthenium Catalysts and Fine Chemistry
Volume Editors: C. Bruneau, P. H. Dixneuf
Vol. 11, 2004

New Aspects of Zirconium Containing Organic Compounds
Volume Editor: I. Marek
Vol. 10, 2004

Precursor Chemistry of Advanced Materials
CVD, ALD and Nanoparticles
Volume Editor: R. Fischer
Vol. 9, 2005

Metallocenes in Stereoselective Synthesis
Volume Editor: T. Takahashi
Vol. 8, 2004

Transition Metal Arene π-Complexes in Organic Synthesis and Catalysis
Volume Editor: E. P. Kündig
Vol. 7, 2004

Bio-inspired Catalysts

Volume Editor: Thomas R. Ward

With Contributions by
E.W. Dijk · B.L. Feringa · G. Roelfes
Q. Jing · K. Okrasa · R.J. Kazlauskas
M.T. Reetz · S. Abe · T. Ueno · Y. Watanabe
J. Steinreiber · T.R. Ward

The series *Topics in Organometallic Chemistry* presents critical overviews of research results in organometallic chemistry. As our understanding of organometallic structure, properties and mechanisms increases, new ways are opened for the design of organometallic compounds and reactions tailored to the needs of such diverse areas as organic synthesis, medical research, biology and materials science. Thus the scope of coverage includes a broad range of topics of pure and applied organometallic chemistry, where new breakthroughs are being achieved that are of significance to a larger scientific audience.
The individual volumes of *Topics in Organometallic Chemistry* are thematic. Review articles are generally invited by the volume editors.
In references *Topics in Organometallic Chemistry* is abbreviated *Top Organomet Chem* and is cited as a journal.

Springer WWW home page: springer.com
Visit the TOMC content at springerlink.com

ISBN 978-3-540-87756-1 e-ISBN 978-3-540-87757-8
DOI 10.1007/978-3-540-87757-8

Topics in Organometallic Chemistry ISSN 1436-6002

Library of Congress Control Number: 2008941074

Cover design: WMX Design GmbH, Heidelberg, Germany

Printed on acid-free paper

springer.com

Volume Editor

Prof. Thomas R. Ward

Department of Chemistry
University of Basel
Spitalstrasse 51
4056 Basel
Switzerland
thomas.ward@unibas.ch

Editorial Board

Topics in Organometallic Chemistry
Also Availabe Electronically

For all customers who have a standing order to Topics in Organometallic Chemistry, we offer the electronic version via SpringerLink free of charge. Please contact your librarian who can receive a password or free access to the full articles by registering at:

springerlink.com

If you do not have a subscription, you can still view the tables of contents of the volumes and the abstract of each article by going to the SpringerLink Homepage, clicking on “Browse by Online Libraries”, then “Chemical Sciences”, and finally choose Topics in Organometallic Chemistry.

You will find information about the

– Editorial Board
– Aims and Scope
– Instructions for Authors
– Sample Contribution

at springer.com using the search function.

Color figures are published in full color within the electronic version on SpringerLink.

Preface

In order to meet the ever-increasing demands for enantiopure compounds, heterogeneous, homogeneous and enzymatic catalysis evolved independently in the past. Although all three approaches have yielded industrially viable processes, the latter two are the most widely used and can be regarded as complementary in many respects. Despite the progress in structural, computational and mechanistic studies, however, to date there is no universal recipe for the optimization of catalytic processes. Thus, a trial-and-error approach remains predominant in catalyst discovery and optimization.

With the aim of complementing the well-established fields of homogeneous and enzymatic catalysis, organocatalysis and artificial metalloenzymes have enjoyed a recent revival. Artificial metalloenzymes, which are the focus of this book, result from combining an active but unselective organometallic moiety with a macromolecular host.

Kaiser and Whitesides suggested the possibility of creating artificial metalloenzymes as long ago as the late 1970s. However, there was a widespread belief that proteins and organometallic catalysts were incompatible with each other. This severely hampered research in this area at the interface between homogeneous and enzymatic catalysis. Since 2000, however, there has been a growing interest in the field of artificial metalloenzymes for enantioselective catalysis.

The current state of the art and the potential for future development are presented in five well-balanced chapters. G. Roelfes, B. Feringa et al. summarize research relying on DNA as a macromolecular host for enantioselective catalysis. T. Ueno, Y. Watanabe et al. delineate the potential of exploiting the void space present in apoenzymes. R. Kazlauskas et al. outline the potential of replacing zinc in carbonic anhydrase with manganese to yield an artificial peroxidase. In the spirit of the directed evolution of enzymes, M. Reetz describes his efforts towards the application of Darwinian protocols to artificial metalloenzymes. Finally, J. Steinreiber and T. Ward summarize the progress in the field of artificial metalloenzymes based on biotin-avidin technology.

The results presented in this book highlight the enormous synergistic potential of combining organometallic moieties with protein scaffolds to yield artificial metalloenzymes for enantioselective catalysis.

Basel, October 2008 Thomas R. Ward

Contents

Top Organomet Chem (2009) 25: 1–24
DOI:10.1007/3418_2008_2

DNA in Metal Catalysis

Ewold W. Dijk, Ben L. Feringa, and Gerard Roelfes

Abstract The DNA molecule, which contains the blueprint of life, has played a pivotal role in the biological revolution. In recent years, many non-biological applications of this remarkable molecule have been explored. In this chapter we will review the use of DNA in metal catalysis. Three general approaches will be discussed: metal-dependent DNAzymes, DNA-templated catalysis, and the recently introduced concept of DNA-based asymmetric catalysis

Key words: DNA, DNA-based asymmetric catalysis, DNA-templated catalysis, Hybrid catalysis, Metal-dependent DNAzymes

Contents

E.W. Dijk, B.L. Feringa(✉) and G. Roelfes(✉)
Department of Organic and Molecular Inorganic Chemistry, Stratingh Institute for Chemistry, University of Groningen, Nijenborgh 4, 9747 AG Groningen, The Netherlands
e-mail: b.l.feringa@rug.nl
e-mail: j.g.roelfes@rug.nl

Abbreviations

A	Adenosine
bpy	2,2′-Bipyridine
C	Cytidine
D–A	Diels–Alder
dA	Deoxyadenosine
dC	Deoxycytidine
DCM	Dichloromethane
dG	Deoxyguanosine
ds-DNA	Double-stranded DNA
dT	Deoxythymidine
DTT	Dithiothreitol
G	Guanosine
HRP	Horseradish peroxidase
MMPP	Magnesium bis(monoperoxyphthalate)
MPIX	Mesoporphyrin IX
NMM	N-Methylmesoporphyrin
Nu	Nucleophile
PNA	Peptide nucleic acid
ss-DNA	Single-stranded DNA
st-DNA	Salmon testes DNA
tpy	2,2′:6′,2″-Terpyridine
TSA	Transition state analog
U	Uridine

1 Introduction

The very special properties of DNA, one of the icons of modern science, make it one of the most versatile molecules in chemistry. In nature, it serves as the carrier of genetic information and as such is one of the cornerstones of life [1]. In vitro, a very diverse set of applications have been explored, ranging from programmable building blocks in bionanotechnology [2] to scaffolds for catalysis. In this review, we will focus on this last aspect, with a particular emphasis on metal catalysis. Three approaches will be discussed: DNAzymes, DNA-templated catalysis, and DNA-based asymmetric catalysis (Fig. 1). Artificial DNA–metal base pairing [3] will not be covered, as no catalysis using these systems has been reported to date.

2 DNAzymes

The discovery [4, 5] of naturally occurring ribozymes – RNA molecules with catalytic activity – made it clear that proteins are not the only biopolymers capable of catalysis in nature. At present, a large number of natural RNAzymes are known,

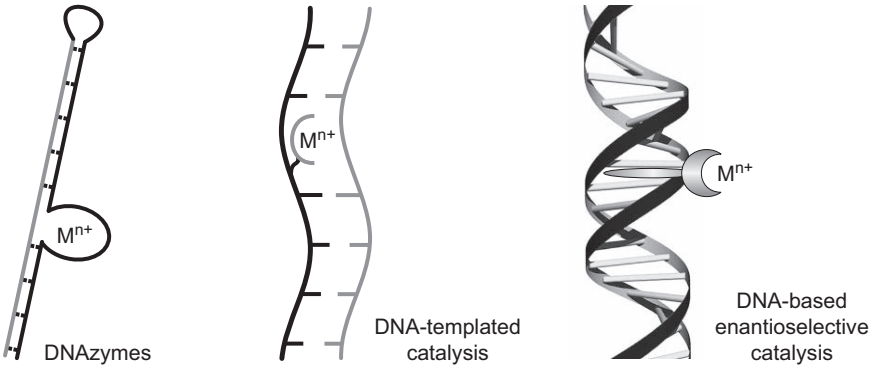

Fig. 1 The three approaches to DNA-based catalysis described in this chapter

including tetrahymena, hairpin and hammerhead ribozymes [6]. In addition, the ribosome has been established to be a ribozyme [7]. Inspired by these natural systems, synthetic ribozymes were created using in vitro selection and amplification schemes [8]. The catalytic repertoire of synthetic ribozymes obtained in this way ranges from nucleotide-modifying reactions to more synthetically useful C–C bond forming reactions such as the aldol, Michael, and Diels–Alder reactions [9, 10].

Although no catalytically active DNAs are known in nature, the chemical similarity between DNA and RNA led to the fundamental scientific question whether DNA could catalyze reactions. Furthermore, from a practical point of view, DNA has several advantages over RNA. These include a higher chemical stability and its availability at low cost by means of automated DNA synthesis.

Herein, a brief discussion on DNAzymes will be given, with a focus on the role of metal ions for their activity. The term DNAzyme (or deoxyribozyme, DNA enzyme) will only be used for single-stranded DNAs that possess catalytic activity due to folding into complex tertiary structures [11]. Analogously to RNAzymes, DNAzymes are usually obtained by means of in vitro selection schemes. Typically, this selection procedure results in DNAzymes that are *cis*-acting (Fig. 2a); the substrate and catalyst strands are covalently linked together in the same polynucleotide backbone. This implies that the catalyst is modified during the reaction and, hence, only single turnover can be obtained. Sometimes it is attempted to convert an active *cis*-acting catalyst into a *trans*-acting one (Fig. 2b) by rational design. This entails that the covalent link between the catalytic part and the substrate is removed, and multiple turnovers may occur.

2.1 The Role of Metal Ions

Because of the limited functional diversity of the available building blocks for polynucleotides the intrinsic reactivity of DNA is in principle restricted, especially in comparison to enzymes. It has been suggested that metal ion cofactors could be

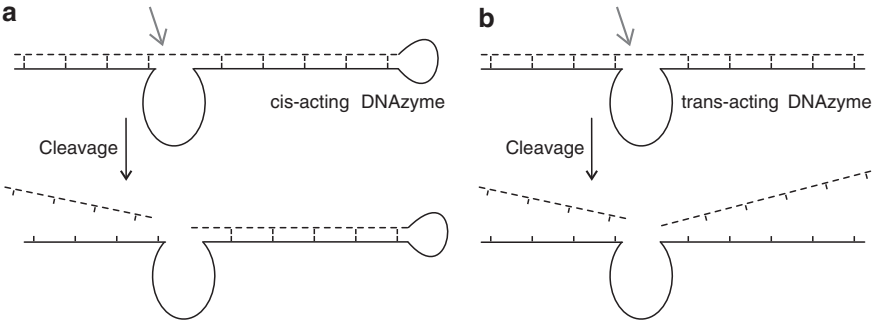

Fig. 2 Schematic representation of *cis*-acting (**a**) and *trans*-acting DNAzymes (**b**). The *cis*-acting DNAzymes contain a covalent link between the catalyst (*solid line*) and substrate (*dashed line*) domains, whereas *trans*-acting DNAzymes do not. The *arrows* indicate the site where a cleavage reaction generally takes place

important in overcoming this limitation and in increasing the scope of DNA-mediated catalytic transformations, their catalytic efficiency and their selectivity [12]. Although our understanding of the role of metal ions in DNAzyme catalysis is still rather limited, two modes of action are generally recognized. The first is direct assistance in the chemical reaction, either as a Lewis acid, or as a result of the redox activity of the metal center. Alternatively, metal ions can play a structural role and may induce a catalytically active tertiary structure in the DNAzyme, e.g., by minimizing electrostatic repulsions between backbones or by (weak) chelation between two distal metal binding sites. These roles can be exerted via several binding modes, such as (i) nonspecific binding to the backbone phosphates, neutralizing their negative charge; (ii) binding in localized pockets of concentrated negative electrostatic potential; (iii) inner-sphere coordination (direct interactions between the metal ion and functional groups at the polynucleotide); and (iv) outer-sphere binding (interactions between the metal-coordinated water molecules and the polynucleotide) [13]. Often it is difficult to distinguish between these different roles.

Exact identification of the metal binding sites, which might facilitate the specification of the role of a particular metal ion, has not been reported in DNAzyme systems to date. In some examples, the metal ion was shown to induce global folding in the system, but only for specific metals [14]. Other studies revealed an overall correlation between reaction rate and the pK_a of the hydrated metal ions, suggesting an assisting function in a rate-determining proton transfer step [15–20]. However, the existence of DNAzymes that function independently of any divalent metal ions at all [21–23] indicates that although metal ions generally greatly facilitate catalysis, some oligonucleotide structures are active enough by themselves and, therefore, divalent metal ions are not an absolute requirement for reactivity.

Two classes of DNAzymes will be discussed in more detail here, namely the DNAzymes catalyzing the cleavage of RNA and the metallation of porphyrins. Other transformations catalyzed by DNAzymes include oxidative DNA cleavage

and the ligation of RNA and DNA. For more general information about DNAzymes the reader is referred to a number of excellent reviews [24–29].

2.2 RNA-Cleaving DNAzymes

The first DNAzymes reported were capable of cleaving RNA substrates (Fig. 3) [8, 30]. This is still the most prevalent activity for DNAzymes found to date. From a starting pool of ~10^{14} ss-DNA molecules, using an in vitro selection strategy, Pb^{2+}-dependent DNAzymes capable of hydrolyzing a single RNA phosphodiester bond embedded in a DNA strand were identified by Breaker and Joyce [31]. After five rounds of selection with progressively decreasing reaction times, the pool of DNAzymes exhibited a reaction rate of ~0.2 min^{-1}, which is around 10^4-fold faster than the background cleavage rate under the same conditions.

An intermolecular (*trans*) version of the reaction was achieved by identification and subsequent redesign of the most active DNAzyme. This resulted in site-specific cleavage of a 19-nucleotide chimeric substrate by a 38-nucleotide Pb^{2+}-dependent DNAzyme with a turnover rate of 1 min^{-1} at 23 °C. However, all-RNA substrates were left untouched by this system.

In a subsequent study, a similar in vitro selection strategy was applied towards Mg^{2+}-, Mn^{2+}-, and Zn^{2+}-dependent DNAzymes with RNAse activity [32]. Although the reaction with the resultant DNA enzymes proceeded around 17 times slower than with the Pb^{2+}-based system, focus remained on the Mg^{2+}-dependent systems, as they might eventually be active under intracellular conditions. Next, a *trans*-acting catalyst capable of 17 turnovers of a chimeric substrate within 5 h was developed. The most active clone was suggested to contain a three-stem junction, based on the sequence. This makes the structure more complex than that of its Pb^{2+}-dependent analog.

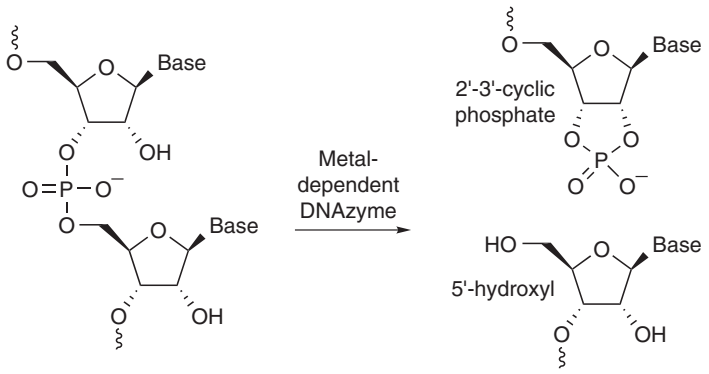

Fig. 3 Cleavage of RNA by a metal-dependent DNAzyme

Santoro and Joyce devised an in vitro selection procedure for the development of DNA enzymes capable of cleaving longer RNA strands at a specific position between a purine and a pyrimidine in the substrate [33]. In earlier studies, only a single cleavable ribonucleotide linkage, flanked by deoxyribonucleotides, had been present in the substrate domain during selection. After eight to ten selection rounds, two classes of active DNAzymes were found that cleaved the target RNA at two distinct positions. They were named 8-17 and 10-23, after the selection round and clone number (Fig. 4). After reselection and under optimal conditions (50 mM $MgCl_2$, pH 8.0, 37 °C), values for catalytic efficiency (k_{cat}/K_m) reached 4.5×10^9 M^{-1} min^{-1}, which is at least as good as that of ribonuclease enzymes [34]. The high substrate affinity due to specific Watson–Crick base pairing interactions contributes significantly to catalytic efficiency. Both DNAzymes were transformed into a *trans*-active form by removing the loop region between catalyst and substrate strand, resulting in multiple turnovers under simulated physiological conditions. Reselection from a pool of 8-17–related DNA sequences broadened the substrate scope, resulting in DNAzymes capable of cleavage at junctions between any two nucleotides [35].

Mechanistic studies on the 10-23 DNAzyme [18] revealed a metal-assisted deprotonation of the 2′-hydroxyl of the ribose moiety in the RNA strand adjacent to the cleavage site of the substrate. This was based primarily on the observed dependence of the rate on the concentration and the nature of the divalent metal ion, and on pH-dependence studies. Between pH 6.5 and 8.5, the log of k_{cat} increased linearly with pH, with a slope of 0.94, which suggests a single deprotonation event in the rate-determining step. Substrates containing a single base mismatch gave rise to a three- to >12,000-fold reduction in catalytic efficiency. The X-ray structure of the 10-23 DNAzyme/RNA substrate complex shows five double-helical domains separated by two four-way junctions, stabilized by metal ions coordinated to the nucleotides at these junctions [36]. However, it was concluded that this structure did not reflect the active conformation in solution. The sequence requirements of the catalytic core, consisting of 15 nucleotides, were studied by systematic mutagenesis [37, 38]. The extremities of the core were very sensitive to mutations, which led to dramatic loss of activity. The importance of specific hydrogen-bond acceptors and donors in the structure was also assayed by introduction of unnatural nucleotides like inosine, deoxypurine, and 2-aminopurine in the core. Thus, the keto and exocyclic amino groups essential for catalysis were identified.

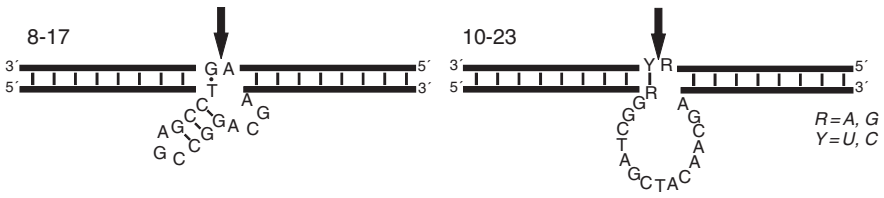

Fig. 4 Schematic representation of the metal-dependent 8-17 and 10-23 DNAzymes. The cleavage site in the RNA substrate strand (*gray*) is indicated by an *arrow*

The importance of backbone-phosphates in the catalytic core of 10-23 was assayed by systematic modification of each core phosphate with a phophorothioate analog, showing the importance of specific oxygen atoms in the core for metal binding [39]. Several phosphate oxygen atoms and a carbonyl oxygen at a central guanosine showed an interaction with the metal ion, indicated by a decrease in catalytic activity upon substitution at these positions with a sulfur atom. In conclusion, although the metal ion plays an important role for catalysis by the 10-23 DNAzyme, it is not yet clear whether this role is structural or catalytic.

Detailed studies of the 8-17 DNAzyme showed that its catalytic activity in the presence of Ca^{2+} was up to 20-fold higher than in the presence of Mg^{2+} [40]. The nucleotides positioned at both ends of the single-stranded ACGA loop in its core were shown to be responsible for this greater rate for the Ca^{2+}-catalyzed reaction relative to Mg^{2+}, indicating a possible metal ion binding site at that position. Studies on the rate dependence of 8-17 on pH and metal ions, similar to those performed for 10-23, again indicated the presence of a single binding site for activating ions and the metal-assisted deprotonation of the reactive 2′-hydroxyl group [15]. Mutational analysis of the catalytic core revealed two residues in the loop of the DNAzyme that form a network of hydrogen bonds with some other part of the structure [41]. Other, less crucial residues might be exposed to solvent molecules. The need for a stable stem in the core was confirmed; the presence of three G–C residues in the stem resulted in highest activity.

FRET studies with an 8-17 variant containing fluorophores at all three branches [42] revealed a two-step folding process with both steps induced by a zinc ion. Later studies [14] showed a different folding behavior of 8-17 with different metal ions; Zn^{2+} and Mg^{2+} ions induced folding of the DNAzyme into a more active, compact conformation at low metal ion concentration, and cleavage only occurred at higher concentrations of the metal ions. In contrast, Pb^{2+} did not induce a change in conformation, although catalysis in the presence of Pb^{2+} was more efficient than with either Zn^{2+} or Mg^{2+}. Apparently, the binding mode of Pb^{2+} to the DNAzyme is different and no global conformational change, which is proposed to take place prior to binding of Zn^{2+} or Mg^{2+}, is needed for catalysis to occur. Alternatively, the DNAzyme might be pre-folded into a Pb^{2+}-binding structure, and no further structural changes are necessary to induce efficient cleavage of the RNA substrate. A single-molecule FRET investigation into the metal-dependent folding, cleavage, and product release of the fluorophore-labeled DNAzyme showed a different reaction pathway in the presence of Pb^{2+} than in the presence of Zn^{2+} or Mg^{2+} [43].

Some effort has been invested in identifying the mechanistic similarities between DNAzymes and ribozymes. Comparison of both systems in terms of dependence on metal ions, stem length, pH, solvent isotope effects, and cleavage activity against a full-length messenger RNA showed evidence for a closely related mechanism of action for both RNAzymes and DNAzymes [16, 17, 19, 44]. This was proposed to involve a rate-determining metal-assisted deprotonation at the 2 -hydroxyl in the substrate during the chemical cleavage step, with a large influence of the binding helix between the substrate and (deoxy)ribozyme on the overall cleavage activity.

Further derivatization of the 8-17 DNAzyme resulted in catalysts that could be activated [45, 46] or switched on and off by light [47, 48], or allosterically activated by ATP [9, 49–51] or oligonucleotides [52–55]. Many more variations of RNA-cleaving DNAzymes have been reported since the original discovery by Santoro and Joyce, as recently reviewed [56].

2.3 Applications of RNA-Cleaving DNAzymes

RNA-cleaving DNAzymes have found a variety of different applications. Selective targeting of mRNA in vivo, in order to suppress the expression of specific genes that cause disease, is an obvious field of application of deoxyribozymes. Efforts in this direction have been reviewed [57, 58].

Since some DNAzymes depend on specific metal ions for activity, they can be employed for the detection of those ions. In the first example, a previously reported [59] DNAzyme was labeled with a Dabcyl fluorescence quencher at the 3′-end and the corresponding RNA substrate with a TAMRA fluorophore at the 5′-end [60]. Upon addition of Pb^{2+} ions, the substrate was cleaved, resulting in dissociation from the DNA enzyme strand. This led to spatial separation of the fluorophore–quencher pair, resulting in fluorescence (Fig. 5). The sensor system was over 80 times more responsive to Pb^{2+} than to other metal ions, and had a quantifiable detection range of 10 nM to 4 μM. A similar strategy was developed for the detection of Cu^{2+} by a DNAzyme that oxidatively cleaves DNA [61]. The system showed a dynamic range of 35 nM to 20 μM and had a metal ion selectivity of a factor of 2000 for Cu^{2+} over other metal ions. A comparable system was reported for the detection of the uranyl cation (UO_2^{2+}), with millionfold selectivity over other metal ions and parts-per-trillion sensitivity.

A different approach to DNAzyme sensors relies on the visual properties of aggregated gold nanoparticles [62–64]. The substrate for the DNAzyme is designed so that

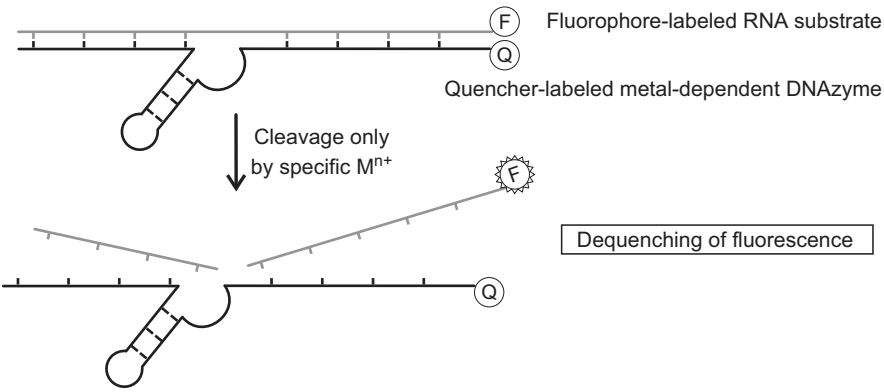

Fig. 5 Schematic representation of a fluorophore (*F*)- and quencher (*Q*)-labeled DNAzyme–substrate complex serving as a selective sensor for metal ions

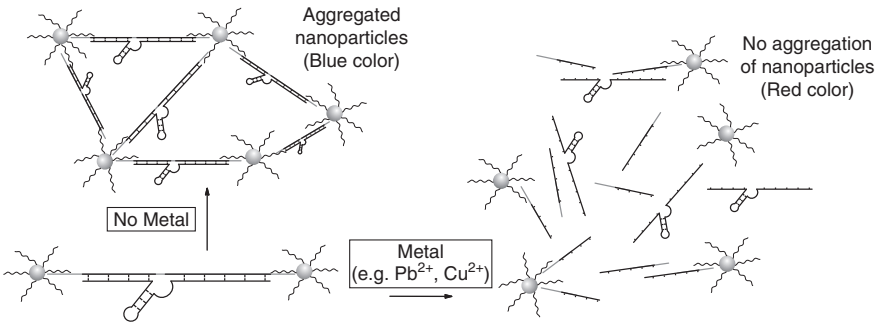

Fig. 6 Representation of metal ion sensors based on DNAzymes and gold nanoparticles

it can hybridize to DNA strands that are attached to nanoparticles. This causes aggregation of the gold nanoparticles, giving rise to a characteristic blue color. In the presence of Pb^{2+} ions, however, the DNAzyme catalyzes the cleavage of the substrate strand and aggregates of nanoparticles do not form. This results in a characteristic red color (Fig. 6). Quantitative analysis of Pb^{2+} could be achieved by UV–Vis spectroscopy. This concept has been improved further and expanded to other analytes [65–67].

In addition to chemical sensors, DNAzymes have found applications in molecular logic gates [68–70] and molecular motors [71, 72].

2.4 Other Oligonucleotide Modifications Catalyzed by DNAzymes

Not only RNA substrates can be cleaved by DNAzymes: oxidative DNA cleavage by metal-dependent deoxyribozymes has also been reported. A *cis*-acting Cu^{2+}-dependent DNAzyme was obtained, showing a millionfold rate enhancement relative to the uncatalyzed rate of DNA cleavage [73]. The DNAzymes were engineered into a *trans*-acting "restriction enzyme", capable of targeting any desired nucleotide sequence [74, 75]. Cleavage occurred at several closely grouped sites, suggesting the oxidative cleavage pathway involves diffusible radical species, e.g., hydroxyl radicals.

The first DNAzyme capable of the ligation of DNA, using an activated DNA substrate, was dependent on Zn^{2+} or Cu^{2+} and gave a 3400-fold rate increase relative to a simple, nonfolded complementary template [76]. With the exception of DNA-templated ligation of DNA [77], only a limited number of DNAzymes capable of DNA ligation have been reported to date. In one case, metal ions were not required to achieve activity [78], whereas another DNAzyme performed ligation in two separate steps, the first being pyrophosphate activation at the 5′ end of one DNA fragment, and the second step being the actual 3′–5′ ligation step [79, 80].

In contrast, RNA ligation by DNAzymes has been well documented [81]. The first Ca^{2+} or Mg^{2+}-dependent system gave nucleophilic opening of the 2′–3′ cyclic phosphate of one RNA strand by the 5′-hydroxyl group of the other, resulting in an

unnatural 2′–5′ linkage [82]. It had very stringent requirements for the nucleotides immediately surrounding the ligation site. For the corresponding *trans*-acting system, rate constants up to 0.18 min^{-1} were observed. However, only single turnovers could be achieved due to product inhibition. Evolution of ligating DNAzymes from the 8-17 and 10-23 motifs (which exclusively cleave 3′–5′ RNA linkages) only gave rise to 2′–5′ linkages of RNA substrates using divalent metal ions (Mg^{2+}, Ca^{2+}, Mn^{2+}) for activity [83]. Further optimization resulted in a DNAzyme that accepted almost any RNA substrate, albeit with a specifically required sequence around the ligation site [84]. Lariat RNA, a key intermediate in biological splicing, could also be obtained using this system [20, 85]. Modifications in the selection strategy [86, 87] or the DNAzyme [88] resulted in DNAzymes capable of performing native 3′–5′ ligation rather than unnatural 2′–5′ ligation.

Other modification reactions of (oligo)nucleotides catalyzed by DNAzymes include kinase (5′-phosphorylation) [89–92], DNA capping [93], self-depurination [94], and RNA tagging [95].

2.5 DNAzymes for the Metallation of Porphyrins

Very few examples of DNAzymes not using (oligo)nucleotides as their substrates have been reported. This is presumably because of the strong Watson–Crick interactions between the DNA catalysts and oligonucleotide substrates, which facilitates the design of selection schemes. Notable exceptions are DNAzymes that catalyze the metallation of porphyrins [96]. By the use of a transition state analog (TSA) for this reaction, an efficient DNAzyme was isolated that gave a 1400-fold rate enhancement in the metallation of mesoporphyrin IX (MPIX, Fig. 7a). Clones that strongly bound *N*-methylmesoporphyrin (NMM, a TSA in the metallation of MPIX) were tested for their ability to catalyze the insertion of Zn^{2+} and Cu^{2+} into MPIX. Several clones were indeed active in this reaction and kinetic measurements showed a rate enhancement of up to 1400 over the background reaction. The catalytic efficiency (k_{cat}/K_m) of the best system was 79 $M^{-1}\,min^{-1}$, about 40 times lower than that of a catalytic antibody capable of performing the same reaction [98]. No evidence was found for a metal-binding site close to the active site of the DNAzyme. The observed dependence of the catalytic activity on the metal ion composition of the medium (specifically K^+, and not Na^+) indicated the presence of guanine quartets in the enzyme's folded structure. A minimized and optimized system for porphyrin metallation, which showed a 3700-fold rate enhancement, was subjected to a detailed mechanistic analysis [99, 100]. It was established that the DNAzyme's activity was due to an increase of the basicity of the porphyrin substrate by 3–4 pH units. It was speculated that this is caused by a DNAzyme-induced distortion of the planar structure of MPIX, facilitating its metallation.

A simple 18-meric DNA sequence known to form a G-quartet structure in the presence of monovalent cations like K^+ or Na^+ showed efficient porphyrin metallation with Zn^{2+} ions, giving a k_{cat} of 1.0 min^{-1} [101]. Circular dichroism

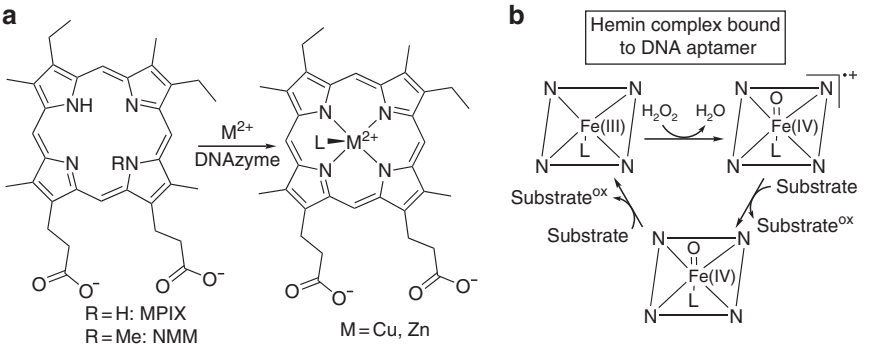

Fig. 7 (**a**) Porphyrin metallation catalyzed by DNAzymes. (**b**) Proposed mechanism for the peroxidation reaction catalyzed by the DNAzyme/hemin complex [97]

measurements indicated that a parallel G-quartet structure, with four or more strands, should be responsible for efficient catalysis.

Metallated porphyrins proved to be efficient cofactors in DNA-based catalysis. Fe^{3+}-protoporphyrin (hemin) gave significantly higher peroxidase activity when bound to a known porphyrin-binding DNA aptamer than when free in solution [97] (Fig. 7b). A combination of a hydrophobic binding pocket, which increases the solubility and prevents aggregation of hemin, tentative donation of an axial ligand to the Fe^{3+} center, and the presence of a relatively polar site close to the iron-oxo center presumably facilitates the peroxidation reaction. The DNAzyme's regio-, enantiomeric, and diastereomeric selectivity for the oxidation of various chiral phenolic substrates, compared to free hemin and the enzyme horseradish peroxidase (HRP) was determined [102]. Although oxidation rates with the DNAzyme as the catalyst were higher than with HRP in some cases, the kinetic discrimination between enantiomers, diastereomers, and regioisomers in a mixture was generally lower than that of HRP.

3 DNA-Directed and DNA-Templated Metal Catalysis

In DNA-directed catalysis, the primary role of DNA is that of substrate binding moiety responsible for bringing the (metal) catalyst into contact with the substrate, usually an oligonucleotide. In contrast to DNAzymes, a direct involvement of the oligonucleotide in catalysis is not a priori envisioned. The catalyst comprises a synthetic ligand for binding a catalytically active metal ion and a DNA strand that is complementary to a target oligonucleotide (Fig. 8a). The DNA strand brings the active metal ion in close proximity of the substrate. Furthermore, sequence-specific binding between the substrate and the template results in a highly selective reaction; mismatches in the sequence give rise to a strongly decreased reactivity.

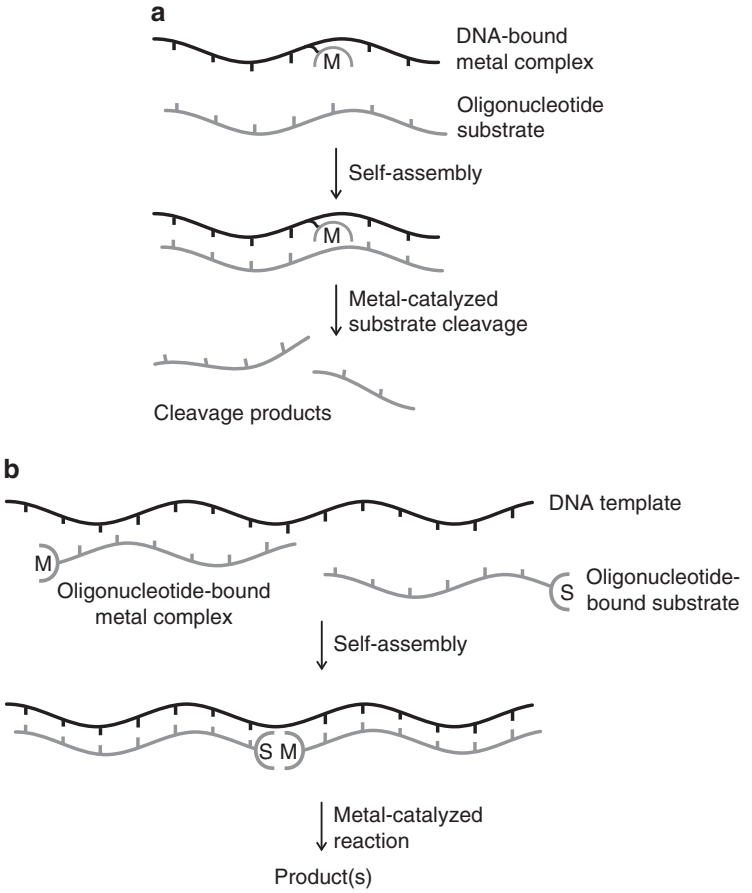

Fig. 8 Schematic representation of the concepts of DNA-directed catalysis (**a**) and DNA-templated catalysis (**b**)

In contrast, DNA-templated catalysis involves an oligonucleotide-bound metal catalyst that is brought into contact with an oligonucleotide-bound substrate by hybridization of both modified oligonucleotides on a DNA template strand, resulting in a high effective molarity and, as a result, increased reactivity (Fig. 8b). In this case, DNA, RNA, or PNA (peptide nucleic acids; synthetic DNA analogs with a peptide backbone) have a dual role as both template and as template binding moiety.

3.1 DNA-Directed Catalysis

DNA-directed catalysis was first reported by Vlassov and coworkers [103], who attached EDTA covalently to octathymidylate and showed that the modified oligonucleotide in the presence of Fe^{2+} and dithiothreitol (DTT) cleaved poly(A) and

poly(dA) substrates more efficiently than a noncomplementary poly(dT) substrate (Fig. 9a). This concept was extended further by attachment of EDTA to the 5′-terminal phosphate [104] or to an internal thymidine [105] of ss-DNA sequences. Upon addition of Fe^{2+} and DTT to the oligonucleotide-EDTA conjugate, complementary ss-DNA sequences were cleaved within 4–16 residues, both upstream and downstream of the EDTA-modified nucleotide.

Sequence-specific ds-DNA cuts were achieved by aligning an Fe^{2+}/EDTA-modified oligonucleotide along a DNA duplex via Hoogsteen pairing, resulting in the formation of a triple helix [106]. The addition of cations like spermine or $Co(NH_3)_6^{3+}$ was needed to overcome charge repulsion resulting from triplex formation. Single-base mismatches in the EDTA-modified oligonucleotide lowered the cleavage efficiency by at least an order of magnitude.

The concept of DNA-directed catalysis has been applied to many metal binding ligands other than EDTA, giving rise to catalysts capable of oxidative and/or hydrolytic cleavage of polynucleotide substrates.

Similar to the original system by Vlassov and coworkers, Fe^{2+}-porphyrin attached to heptathymidylate showed effective cleavage of poly(A) and poly(dA), but not poly(dT) [107]. In addition to cleavage reactions, nucleobase oxidation and crosslinking reactions could also be achieved using similar catalysts, depending on the reaction conditions chosen [108]. Other systems with porphyrin-bound metal ions, including Mn^{3+} [109, 110], Eu^{3+} [111], and Dy^{3+} [112], proved active and site-selective in either RNA or ss-DNA cleavage. Cu^{2+}-dependent, sequence-specific oxidative cleavage of RNA and both ss- and ds-DNA was obtained by a catalyst in which 1,10-phenantroline was attached to internal [113] or terminal [114–118] positions in oligonucleotides.

Although iron-bleomycin itself is well known for its sequence-specific ds-DNA cleaving abilities, it was also covalently bound to oligonucleotides, leading to cleavage of DNA [119], with the capability of performing multiple turnovers when

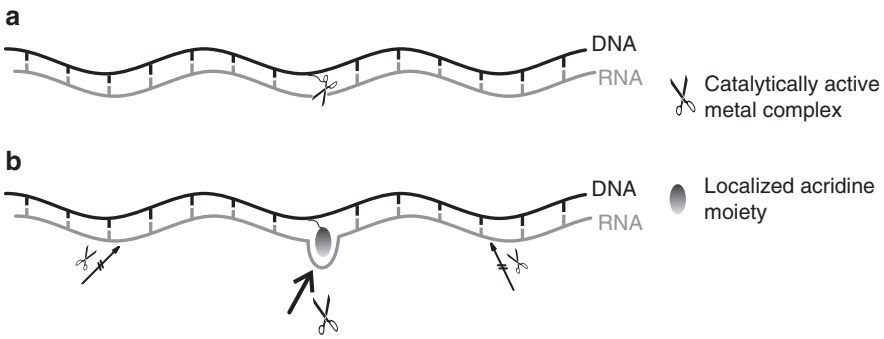

Fig. 9 Schematic representation of DNA-directed catalytic RNA scission. **a** The catalytically active metal ion is attached to the DNA via a ligand. **b** The metal ion is not localized, but site-specific cleavage is achieved by local perturbation caused by an acridine moiety covalently linked to the DNA template

the target DNA substrate was added in excess [120]. Ni-salen, introduced as nucleotide substitute in a DNA strand via template-directed synthesis, proved active in oxidative strand scission at dG sites in Watson–Crick complementary DNA [121]. After duplex formation between the catalyst and substrate strands, scission was achieved by treatment with the oxidant MMPP and piperidine. Even when dG in the substrate was not located directly opposite the Ni-salen, cleavage still occurred at dG, if it was not more than three residues away from the metal center.

Other ligands incorporated into oligonucleotides that showed cleavage activity upon addition of metal ions include bpy (2,2′-bipyridine) [122–124], tpy (2,2′:6′,2″-terpyridine) [122, 124–127], and 2,6-dicarboxypicoline or *N*,*N*-bis(2-picolyl)amine [128, 129].

An intruiging approach to site-selective RNA cleavage was reported by Kuzuya et al. [130]. In contrast to the previous examples, in this system the metal complex is free in solution (not localized). Site-selective activation for hydrolysis at single positions in a target RNA strand is achieved by covalent attachment of an acridine moiety to the template DNA strand, which causes local perturbation in the hybridized RNA strand opposite this position [131]. RNA strand scission is very site-specific for the localized perturbation (Fig. 9b). This approach was optimized for various metal ions including Ca^{2+} and Mg^{2+}, transition metal ions, and lanthanide ions [132, 133]. Two sites in a single RNA could be activated by incorporation of two acridines in the DNA template [134], and the rate of the process was further enhanced by the attachment of a ligand for Lu^{3+} in close proximity to the acridine activator [135].

3.2 DNA-Templated Catalysis

The first example of DNA-templated metal catalysis was reported by the group of Krämer [136]. In this approach, metal-catalyzed hydrolysis of an ester attached to a DNA template was performed. The catalytic system consisted of three parts: a DNA template strand, a ligand for Cu^{2+} attached to a PNA strand complementary to half of the template, and an ester substrate connected to a PNA strand complementary to the other half of the DNA template (Fig. 10). Complexation of both PNA strands to the template brings the catalytic center and the substrate in close proximity, and hydrolysis of the ester group is accelerated approximately 150-fold relative to the background hydrolysis rate, which makes it suitable as a detection method for DNA sequences [137].

Using an excess of the PNA-bound substrate, turnover numbers of up to 35 could be reached, although the background rate was substantial. Mismatches in the PNA/DNA combinations led to a considerable decrease in reaction rates, especially if the mismatch was near the site where the reaction occurred. This method was used to detect as little as 10 fmol of template DNA from a mixture of four similar DNAs that differed at a single position.

The first examples required a 2-picolyl ester for efficient cleavage because of its chelation of copper. By introducing a Cu^{2+}-binding group in the linker between the PNA strand and the target ester, it was shown that (in principle) any ester could be

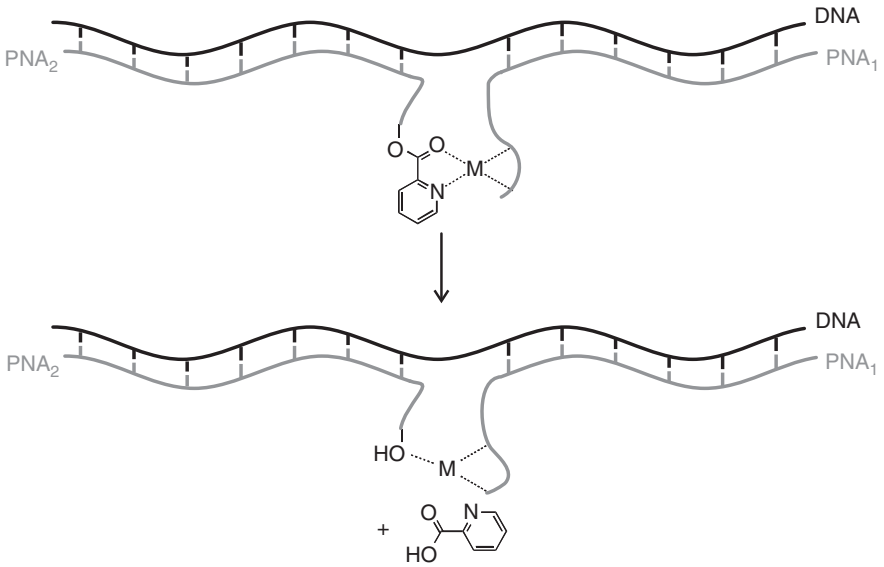

Fig. 10 Schematic representation of DNA-templated metal-catalyzed ester cleavage. Upon binding of the target DNA sequence, the PNA-bound metal complex and the PNA-bound ester substrate are brought into close proximity, resulting in hydrolysis of the ester ("signal")

cleaved [138]. The concept of DNA-templated metal catalysis is not limited to single-stranded templates. It was found that the copper-binding and ester-substrate PNAs of the previous system could locally form triple-helix structures in a sequence-specific fashion on a ds-DNA template, resulting in efficient ester hydrolysis catalyzed by the nearby Cu^{2+} center. However, turnover numbers were rather low (up to 1.65) and rate enhancement relative to the background reaction was modest with values of up to 12 [139].

A related system using DNA-templated organocatalysis rather than metal catalysis was reported in 2000, with an imidazole group linked to a DNA strand that cleaved an ester moiety on another DNA strand when both were annealed to a template DNA sequence [91]. Many other DNA-templated reactions have been described, mostly not using metal ions for catalysis [140–142].

In a different approach, a combination of metal catalysis and DNA hybridization was reported [143]. A Cu^{2+} ion tightly bound to both ends of an ss-DNA molecule via two terpyridine ligands was released upon hybridization of a complementary "signal" DNA strand, because of spatial separation of the two upon hybridization (Fig. 11). The released Cu^{2+} then bound to a 1,10-phenantroline pre-catalyst that was also present, making it an active catalyst for oxidation of a nonfluorescent substrate into a fluorescent product. Thus, binding of a signal DNA strand led to a signal transduction cascade with eventual signal amplification in the catalytic reaction. The same system was used in combination with Zn^{2+}, which activated the apoenzyme carbonic anhydrase at the end of the signal cascade [144]. The progress of the reaction was followed

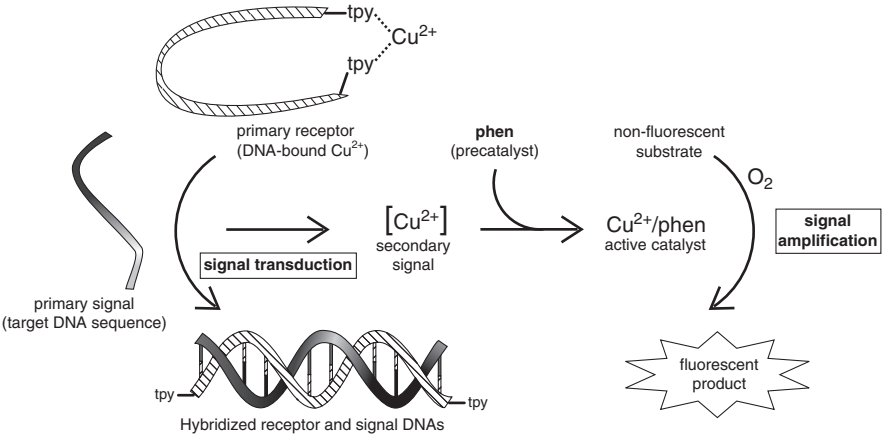

Fig. 11 Schematic representation of sequence-specific DNA detection by catalytic signal amplification. *tpy* 2,2′:6′,2″-terpyridine, *phen* 1,10-phenantroline

by colorimetric pH readout using phenol red as the indicator. The signal amplification factor was around 10^4 (one molecule of target DNA triggers the conversion of 10,000 CO_2 molecules) and response times of 28 (±5) s were reached.

4 DNA-Based Asymmetric Catalysis

In DNA-based asymmetric catalysis, DNA's role is that of a chiral scaffold, i.e., as the source of chirality for the catalyzed reaction. In this concept, it is assumed that if the catalyzed reaction takes place close to the DNA double helix, the chirality of DNA can be transferred to the reaction product, resulting in an enantiomeric excess. This can be achieved by binding of the catalyst to the DNA. Analogously to hybrid enzymes [145], two general approaches can be followed: (i) the supramolecular approach, in which the catalyst is bound using noncovalent interactions, and (ii) the covalent approach, in which the catalyst is attached to the DNA via a covalent linkage.

Double-stranded DNA represents an ideal scaffold for supramolecular anchoring of catalysts, due to the propensity of small molecules to bind to DNA with high affinity through intercalation or groove binding [146]. The concept of the supramolecular approach towards DNA-based catalysis is outlined in Fig. 12. The DNA-based catalyst is prepared via self-assembly from DNA, generally salmon testes DNA (st-DNA), and a catalyst that is based on a racemic or nonchiral ligand that is capable of binding to DNA. The advantage of this approach is that it is modular,

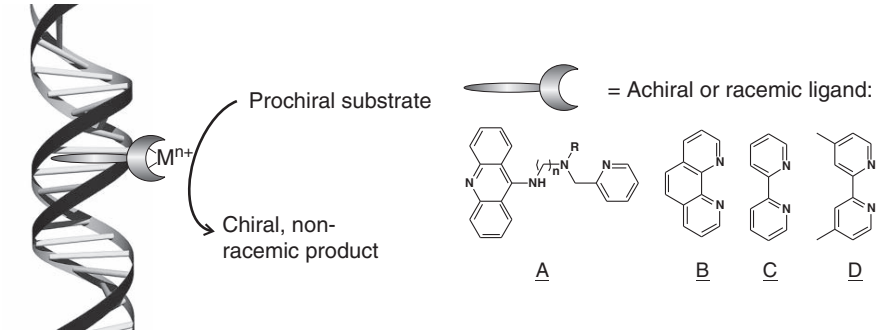

Fig. 12 Concept of DNA-based catalysis in the noncovalent approach. A Class 1 ligands. B-D Class 2 ligands

i.e., no synthesis of DNA derivatives is required and, hence, the catalyst can be optimized rapidly.

To date, two general designs of the ligand for the catalytically active metal ion have been investigated. The ligands of the first class (A in Fig. 12) contain three key structural features: (i) a metal binding domain, e.g., a bidentate chelating aminomethylpyridine, attached via (ii) a short spacer to (iii) the DNA intercalating moiety, e.g., a 9-amino acridine [147]. This design has two structural variables that can be used for optimization and fine-tuning of the catalyst: the spacer length *n*, which determines the distance of the catalyst from the DNA helix, and the side chain R, which is an important contributor to the steric environment provided by the catalyst. The corresponding DNA-based catalysts are prepared in situ by complexation of the ligand with Cu^{2+}, followed by binding to st-DNA.

The catalysts of the second generation are based on polyaromatic ligands (B–D in Fig. 12). These ligands are known to bind to DNA, although the mode of binding has not yet been established for all members of this class [148]. In this design, the DNA binding moiety is integrated into the metal binding domain. As a result, the metal center can be brought into much closer contact with the DNA helix compared to the first generation of ligands. The main difference between the ligands of the second class is the number of aromatic groups they contain; the coordination environment provided by the ligands is the same. A smaller polyaromatic moiety results in lower DNA binding strength and, most likely, a smaller distance of the metal center to the DNA helix. In this approach, the corresponding Cu^{2+} complexes were synthesized independently, followed by self-assembly of the DNA-based catalyst.

To date, the focus has been on Lewis acid catalyzed reactions in water [149, 150]. In particular, Cu^{2+}-catalyzed Diels–Alder (D–A), Michael addition, and fluorination reactions have been investigated (Fig. 13).

Using catalysts of class 1 resulted in moderate to good enantioselectivities for both stereoisomers of the product of the D–A reaction of cyclopentadiene with azachalcone. However, the results proved to be very dependent on the design of the ligand. Both the side chain R and the length of the spacer *n* were varied to optimize the catalyst.

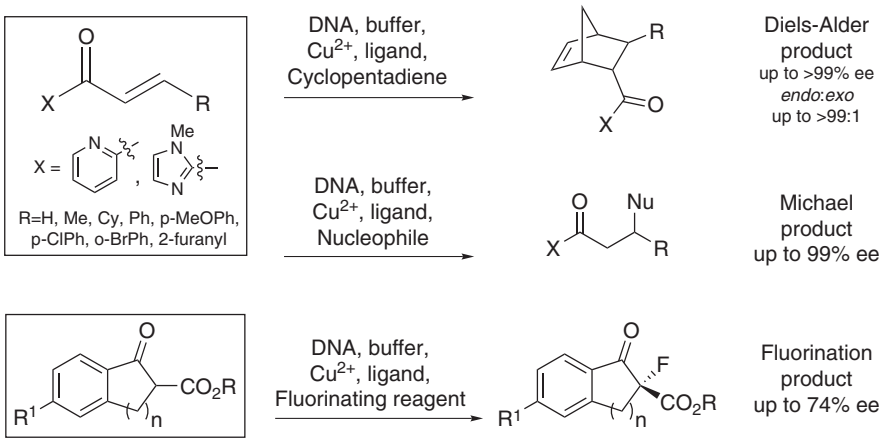

Fig. 13 DNA-based asymmetric Diels–Alder, Michael, and fluorination reactions

Screening of different R groups using a fixed spacer length of $n = 3$, revealed that R preferably is an arylmethyl group. Increasing the spacer length resulted in a rapid decrease in enantioselectivity. Interestingly, the R groups that resulted in the highest enantioselectivities (i.e., 1-naphthylmethyl and 3,5-dimethoxybenzyl) gave rise to the formation of opposite enantiomers of the D–A product. Furthermore, using a shorter spacer (i.e., $n = 2$) the (−) enantiomer of the product was obtained invariably, whereas with a ligand containing a longer spacer (i.e., $n = 3$ or more) the formation of the (+) enantiomer was observed. These findings demonstrate nicely that both enantiomers of the product are accessible by judicious design of the achiral ligand.

Catalysts of class 2 gave rise to a significant increase in enantioselectivity. Interestingly, it was observed that Cu^{2+}/ligand complexes that gave the highest enantiomeric excess had only a moderate affinity for DNA. With 2,2′-bipyridine as the ligand, >80% of the substrate was converted into the D–A product, which was obtained in a 98:2 *endo*:*exo* ratio, with the *endo* diastomer having 90% ee. A further increase in enantioselectivity up to 99% was obtained with 4,4′-dimethyl-2,2′-bipyridine as the ligand.

The use of α,β-unsaturated 2-acylimidazoles [151] as the dienophile increased the practicality of the approach, since the imidazole group can be removed readily from the product. The substrate scope is quite broad; substituents at the alkene moiety (e.g., alkyl, aryl and 2-furanyl) were very well tolerated. In all cases good to excellent enantioselectivies and diastereoselectivities were obtained, i.e., 80–98% ee for the *endo* isomer and *endo*:*exo* > 94:6, in the case of the 4,4′-dimethyl-2,2′-bipyridine ligand [152]. Moreover, the D–A reaction was successfully performed on a preparative scale (1 mmol), making it attractive from a synthetic point of view.

α,β-Unsaturated 2-acylimidazoles are not only good dienophiles, they can also undergo 1,4-addition reactions. This was applied successfully in the DNA-based asymmetric Michael addition [153]. The same catalytic system was used as for the

D–A reactions, comprising st-DNA and the Cu^{2+} complex of 4,4′-dimethyl bipyridine. Nitromethane and dimethyl malonate, both of which enolize readily, were employed as the nucleophiles. With 100 equivalents of dimethyl malonate, a clean and quantitative conversion into the Michael adduct was observed after 3 days, with an ee of 91%. The addition of nitromethane was slower; using 1000 equivalents 97% conversion and an ee of 85% were obtained in the same time. The substrate scope proved to be broad; a series of derivatives of the substrate were tested in the Michael reaction and generally gave high conversions (typically > 75%) and ees (86–99% with dimethylmalonate as the nucleophile, and 82–94% with nitromethane as the nucleophile). Only in the case of the Michael addition to the enone with R = Me instead of aryl, did the ee drop to ~60%. Again, it was shown that the reaction could be performed on a preparative scale (1 mmol), and that the catalyst solution could be recycled without loss of activity or enantioselectivity over at least two runs.

Using the same catalytic system, the electrophilic fluorination of aromatic β-ketoesters was also reported [154]. After optimization of the reaction conditions, the products could be isolated with ees up to 74%, the (*R*) enantiomer being in excess.

The absolute configurations of both the Diels–Alder and the Michael adducts with R = Ph were elucidated by transformation into known compounds. In the case of the D–A reaction, the (2*S*,3*S*) enantiomer was formed in excess, indicating that cyclopentadiene attacks from the *Si* face of the dienophile. Similarly, nucleophilic attack to the enone in the Michael reaction was shown to occur from the *Si* face. These results suggest that the *Re* face of the bound substrate is shielded efficiently by the DNA in both reaction classes (Fig. 14).

Chirality transfer from the helical DNA to the reaction can occur via two distinct mechanisms [155]. First, DNA can dictate directly the prochiral face from which the diene or nucleophile attacks, e.g., by shielding of one face of the substrate. In this case, the reaction should take place in close proximity to the chiral environment of the DNA. Therefore, this is the most likely mechanism for class 2 ligand/Cu^{2+} complexes. Alternatively, DNA can first impose a chiral conformation on the catalyst, which then directs the reaction towards one enantiomer of the product. Several observations indicate that this mechanism applies to the first-generation catalytic system. Since the copper complex of the ligand A is chiral, DNA can dictate the formation of only one of the enantiomeric complexes. Furthermore, the observation that both enantiomers of the product are accessible by only a slight variation in the design of the ligand argues for this mechanism.

The covalent approach towards DNA-based catalysis involves direct attachment of the catalytically active metal complex to the DNA via a covalent bond. The presumed advantage of this approach over the supramolecular variant is the greater control over both the geometry around the metal center and the exact microenvironments (i.e., the DNA sequence) in which the metal complex is located. So far, two reports have been published in which transition metals were anchored to deoxyribonucleotides via covalently linked phosphine ligands (Fig. 15).

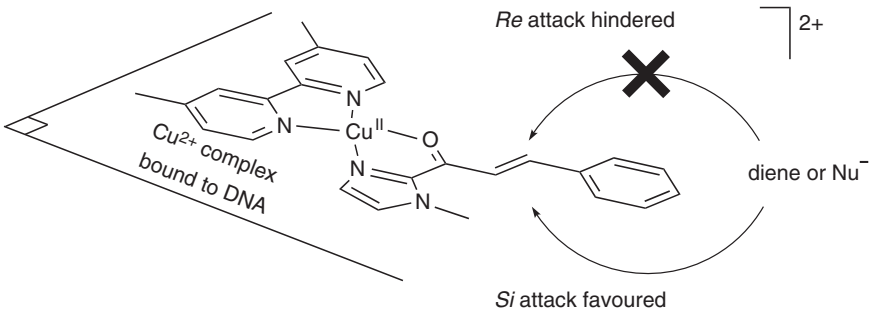

Fig. 14 Schematic representation of the stereochemistry of the attack of the diene and the nucleophile in the DNA-based catalytic asymmetric Diels–Alder and Michael reactions, respectively

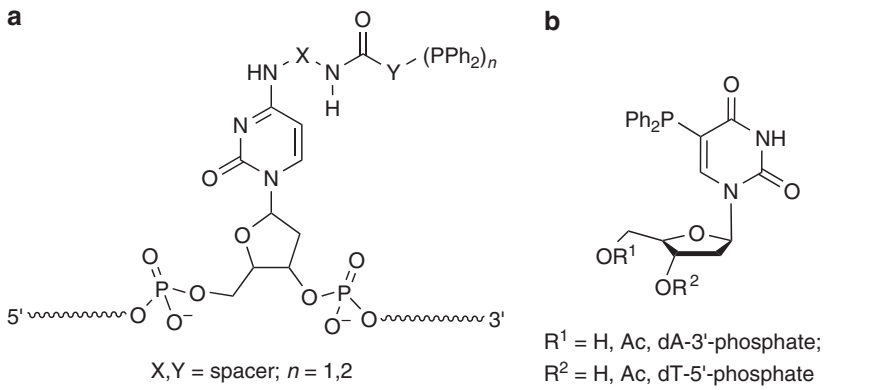

Fig. 15 **a**, **b** Phosphine-modified oligonucleotides used in the covalent approach towards DNA-based catalysis

The first example (Fig. 15a) involves post-synthetic modification of an amino-functionalized oligonucleotide by attachment of various mono- and bidentate phosphines via an amide linker [156]. No catalysis by metal complexes of the phosphines has been reported yet. In the other example (Fig. 15b), commercially available 5-iodo-2′-deoxyuridine was transformed into the 5-diphenylphosphino-2′-deoxyuridine using a palladium-catalyzed coupling [157]. Using the mononucleotide-based diphenylphosphine as a ligand in the palladium-catalyzed asymmetric allylic amination in THF, up to 80% ee was obtained. Interestingly, the opposite enantiomer of the product was obtained when a different solvent (CH_3CN-THF, DMF, or DCM) was used in the reaction. Unfortunately, incorporation of the modified nucleotide into a trinucleotide resulted in a significant drop in both the conversion and enantioselectivity for the reaction. Moreover, a further decrease in conversion was observed when the solvent was changed to water.

5 Summary and Outlook

This chapter has presented an overview of applications of DNA in metal ion catalysis. Three general approaches were outlined: metal-dependent DNAzymes, DNA-directed and templated catalysis, and DNA-based asymmetric catalysis.

DNAzymes often rely on metal ions for their activity, possibly to compensate for the limited functional diversity of DNA. The role of the metal ions can be either catalytic or structural, but in most cases this remains to be established. To date, the synthetic potential of DNAzymes is rather limited and their main application has been in nucleotide modification. However, since DNAzymes can be selected from large libraries using in vitro evolution and selection methodologies, metallo-DNAzymes for a wide range of synthetically relevant reactions (e.g., C–C bond forming reactions) will undoubtedly become available in the future.

In DNA-directed and DNA-templated synthesis, the role of DNA is to direct the catalytic metal ion towards the substrate. This implies automatically that the substrates are polynucleotides. Applications of this concept are typically found in DNA modification reactions (e.g., DNA cleavage) and sensing.

Finally, the new concept of DNA-based asymmetric catalysis in which DNA serves as a chiral scaffold for catalyst design was described. To date, DNA-based asymmetric catalysis has been applied successfully to Lewis acid catalyzed reactions in water. This concept shows much promise for application in organic synthesis as it is inexpensive, experimentally straightforward, can be performed at a synthetically relevant scale, and the catalyst can be recycled readily.

In conclusion, DNA is rapidly claiming a prominent position in the field of catalysis and due to its special properties and unique structure many new applications of DNA in catalysis can be envisioned for the future.

References

1. Lewin B (2007) Genes IX. Jones & Bartlett, Sudbury
2. Feldkamp U, Niemeyer CM (2006) Angew Chem Int Ed 45:1856
3. Clever GH, Kaul C, Carell T (2007) Angew Chem Int Ed 46:6226
4. Guerrier-Takada C, Gardiner K, Marsh T, Pace N, Altman S (1983) Cell 35: 849
5. Kruger K, Grabowski PJ, Zaug AJ, Sands J, Gottschling DE, Cech TR (1982) Cell 31:147
6. Joyce GF (2004) Annu Rev Biochem 73:791
7. Nissen P, Hansen J, Ban N, Moore PB, Steitz TA (2000) Science 289:920
8. Breaker RR (1997a) Chem Rev 97:371
9. Bartel DP, Unrau PJ (1999) Trends Biochem Sci 24:M9
10. Fiammengo R, Jäschke A (2005) Curr Opin Biotechnol 16:614
11. Sen D, Geyer CR (1998) Curr Opin Chem Biol 2:680
12. Ma Z, Taylor J-S (2000) Proc Natl Acad Sci USA 97:11159
13. Sigel RKO, Pyle AM (2007) Chem Rev 107:97
14. Kim H-K, Liu J, Li J, Nagraj N, Li M, Pavot CM-B, Lu Y (2007a) J Am Chem Soc 129:6896
15. Bonaccio M, Credali A, Peracchi A (2004) Nucleic Acids Res 32:916
16. He Q-C, Zhou J-M, Zhou D-M, Nakamatsu Y, Baba T, Taira K (2002) Biomacromolecules 3:69

17. Ota N, Warashina M, Hirano K, Hatanaka K, Taira K (1998) Nucleic Acids Res 26:3385
18. Santoro SW, Joyce GF (1998) Biochemistry 37:13330
19. Sugimoto N, Okumoto Y, Ohmichi T (1999) J Chem Soc, Perkin Trans 2 1999:1381
20. Wang Y, Silverman SK (2005a) Angew Chem Int Ed 44:5863
21. Geyer CR, Sen D (1997) Chem Biol 4:579
22. Perrin DM, Garestier T, Hélène C (2001) J Am Chem Soc 123:1556
23. Ting R, Thomas JM, Lermer L, Perrin DM (2004a) Nucleic Acids Res 32:6660
24. Bittker JA, Phillips KJ, Liu DR (2002) Curr Opin Chem Biol 6:367
25. Breaker RR (2004) Nature 432:838
26. Höbartner C, Silverman SK (2007) Biopolymers 87:279
27. Li Y, Breaker RR (1999a) Curr Opin Struct Biol 9:315
28. Lu Y (2002) Chem Eur J 8:4588
29. Peracchi A (2005) ChemBioChem 6:1316
30. Breaker RR (1997b) Nat Biotechnol 15:427
31. Breaker RR, Joyce GF (1994) Chem Biol 1:223
32. Breaker RR, Joyce GF (1995) Chem Biol 2:655
33. Santoro SW, Joyce GF (1997) Proc Natl Acad Sci USA 94:4262
34. delCardayré SB, Raines RT (1994) Biochemistry 33:6031
35. Cruz RPG, Withers JB, Li Y (2004) Chem Biol 11:57
36. Nowakowski J, Shim PJ, Prasad GS, Stout CD, Joyce GF (1999) Nat Struct Biol 6:151
37. Zaborowska , Fürste JP, Erdmann VA, Kurreck J (2002) J Biol Chem 277:40617
38. Zaborowska , Schubert S, Kurreck J, Erdmann VA (2005) FEBS Lett 579:554
39. Nawrot B, Widera K, Wojcik M, Rebowska B, Nowak G, Stec WJ (2007) FEBS J 274:1062
40. Peracchi A (2000) J Biol Chem 275:11693
41. Peracchi A, Bonaccio M, Clerici M (2005) J Mol Biol 352:783
42. Liu J, Lu Y (2002) J Am Chem Soc 124:15208
43. Kim H-K, Rasnik I, Liu J, Ha T, Lu Y (2007b) Nat Chem Biol 3:763
44. Kurreck J, Bieber B, Jahnel R, Erdmann VA (2002) J Biol Chem 277:7099
45. Lusic H, Young DD, Lively MO, Deiters A (2007) Org Lett 9:1903
46. Ting R, Lermer L, Perrin DM (2004b) J Am Chem Soc 126:12720
47. Keiper S, Vyle JS (2006) Angew Chem Int Ed 45:3306
48. Liu Y, Sen D (2004) J Mol Biol 341:887
49. Levy M, Ellington AD (2002) Chem Biol 9:417
50. Mei SHJ, Liu Z, Brennan JD, Li Y (2003) J Am Chem Soc 125:412
51. Nutiu R, Mei S, Liu Z, Li Y (2004) Pure Appl Chem 76:1547
52. Achenbach JC, Nutiu R, Li Y (2005a) Anal Chim Acta 534:41
53. Stojanovic MN, de Prada P, Landry DW (2001) ChemBioChem 2:411
54. Wang DY, Sen D (2001) J Mol Biol 310:723
55. Wang DY, Lai BHY, Feldman AR, Sen D (2002a) Nucleic Acids Res 30:1735
56. Silverman SK (2005) Nucleic Acids Res 33:6151
57. Achenbach JC, Chiuman W, Cruz RPG, Li Y (2004) Curr Pharm Biotech 5:321
58. Isaka Y (2007) Curr Opin Mol Ther 9:132
59. Li J, Zheng W, Kwon AH, Lu Y (2000) Nucleic Acids Res 28:481
60. Li J, Lu Y (2000) J Am Chem Soc 122:10466
61. Liu J, Lu Y (2007) J Am Chem Soc 129:9838
62. Liu J, Lu Y (2003) J Am Chem Soc 125:6642
63. Liu J, Lu Y (2004b) Chem Mater 16:3231
64. Liu J, Lu Y (2004d) Anal Chem 76:1627
65. Liu J, Lu Y (2004a) J Fluoresc 14:343
66. Liu J, Lu Y (2004c) J Am Chem Soc 126:12298
67. Liu J, Lu Y (2006) Org Biomol Chem 4:3435
68. Lederman H, Macdonald J, Stefanovic D, Stojanovic MN (2006) Biochemistry 45:1194
69. Stojanovic MN, Stefanovic D (2003) J Am Chem Soc 125:6673
70. Stojanovic MN, Mitchell TE, Stefanovic D (2002) J Am Chem Soc 124:3555
71. Chen Y, Wang M, Mao C (2004) Angew Chem Int Ed 43:3554

72. Tian Y, He Y, Chen Y, Yin P, Mao C (2005) Angew Chem Int Ed 44:4355
73. Carmi N, Shultz LA, Breaker RR (1996) Chem Biol 3:1039
74. Carmi N, Breaker RR (2001) Bioorg Med Chem 9:2589
75. Carmi N, Balkhi SR, Breaker RR (1998) Proc Natl Acad Sci USA 95:2233
76. Cuenoud B, Szostak JW (1995) Nature 375:611
77. Silverman AP, Kool ET (2006) Chem Rev 106:3775
78. Levy M, Ellington AD (2001) Bioorg Med Chem 9:2581
79. Li Y, Breaker RR (2001) Methods 23:179
80. Sreedhara A, Li Y, Breaker RR (2004) J Am Chem Soc 126:3454
81. Silverman SK (2004) Org Biomol Chem 2:2701
82. Flynn-Charlebois A, Wang Y, Prior TK, Rashid I, Hoadley KA, Coppins RL, Wolf AC, Silverman SK (2003a) J Am Chem Soc 125:2444
83. Flynn-Charlebois A, Prior TK, Hoadley KA, Silverman SK (2003b) J Am Chem Soc 125:5346
84. Ricca BL, Wolf AC, Silverman SK (2003) J Mol Biol 330:1015
85. Wang Y, Silverman SK (2003) J Am Chem Soc 125:6880
86. Purtha WE, Coppins RL, Smalley MK, Silverman SK (2005) J Am Chem Soc 127:13124
87. Wang Y, Silverman SK (2005b) Biochemistry 44:3017
88. Coppins RL, Silverman SK (2004) J Am Chem Soc 126:16426
89. Achenbach JC, Jeffries GA, McManus SA, Billen LP, Li Y (2005b) Biochemistry 44:3765
90. Li Y, Breaker RR (1999b) Proc Natl Acad Sci USA 96:2746
91. McManus SA, Li Y (2007) Biochemistry 46:2198
92. Wang W, Billen LP, Li Y (2002b) Chem Biol 9:507
93. Li Y, Liu Y, Breaker RR (2000) Biochemistry 39:3106
94. Sheppard TL, Ordoukhanian P, Joyce GF (2000) Proc Natl Acad Sci USA 97:7802
95. Baum DA, Silverman SK (2007) Angew Chem Int Ed 46:3502
96. Li Y, Sen D (1996) Nat Struct Biol 3:743
97. Travascio P, Li Y, Sen D (1998) Chem Biol 5:505
98. Cochran AG, Schultz PG (1990) Science 249:781
99. Li Y, Sen D (1997) Biochemistry 36:5589
100. Li Y, Sen D (1998) Chem Biol 5:1
101. Sugimoto N, Toda T, Ohmichi T (1998) Chem Commun 1998:1533
102. Rojas AM, Gonzalez PA, Antipov E, Klibanov AM (2007) Biotechnol Lett 29:227
103. Boutorin AS, Vlassov VV, Kazakov SA, Kutiavin IV, Podyminogin MA (1984) FEBS Lett 172:43
104. Chu BCF, Orgel LE (1985) Proc Natl Acad Sci USA 82:963
105. Dreyer GB, Dervan PB (1985) Proc Natl Acad Sci USA 82:968
106. Moser HE, Dervan PB (1987) Science 238:645
107. Le Doan T, Perrouault L, Hélène C, Chassignol M, Thuong NT (1986) Biochemistry 25:6736
108. Le Doan T, Perrouault L, Chassignol M, Thuong NT, Hélène C (1987) Nucleic Acids Res 15:8643
109. Dubey I, Pratviel G, Meunier B (2000) J Chem Soc, Perk Trans 1 2000:3088
110. Pitié M, Casas C, Lacey CJ, Pratviel G, Bernadou J, Meunier B (1993) Angew Chem Int Ed Engl 32:557
111. Magda D, Miller RA, Sessler JL, Iverson BL (1994) J Am Chem Soc 116:7439
112. Magda D, Crofts S, Lin A, Miles D, Wright M, Sessler JL (1997) J Am Chem Soc 119:2293
113. Bergstrom DE, Gerry NP (1994) J Am Chem Soc 116:12067
114. Chen C-HB, Sigman D (1986) Proc Natl Acad Sci USA 83:7147
115. Chen C-HB, Sigman D (1988) J Am Chem Soc 110:6570
116. François J-C, Saison-Behmoaras T, Chassignol M, Thuong NT, Sun J-S, Hélène C (1988) Biochemistry 27:2272
117. François J-C, Saison-Behmoaras T, Chassignol M, Thuong NT, Hélène C (1989a) J Biol Chem 264:5891
118. François J-C, Saison-Behmoaras T, Barbier C, Chassignol M, Thuong NT, Hélène C (1989b) Proc Natl Acad Sci USA 86:9702
119. Sergeyev DS, Godovikova TS, Zarytova VF (1991) FEBS Lett 280:271
120. Sergeyev DS, Godovikova TS, Zarytova VF (1995) Nucleic Acids Res 23:4400
121. Czlapinski JL, Sheppard TL (2004) Chem Commun 2004:2468

122. Bashkin JK, Xie J, Daniher AT, Sampath U, Kao JL-F (1996) J Org Chem 61:2314
123. Bergstrom DE, Chen J (1996) Bioorg Med Chem Lett 6:2211
124. Putnam WC, Daniher AT, Trawick BN, Bashkin JK (2001) Nucleic Acids Res 29:2199
125. Bashkin JK, Frolova EI, Sampath U (1994) J Am Chem Soc 116:5981
126. Daniher AT, Bashkin JK (1998) Chem Commun 1998:1077
127. Sakamoto S, Tamura T, Furukawa T, Komatsu Y, Ohtsuka E, Kitamura M, Inoue H (2003) Nucleic Acids Res 31:1416
128. Groves JT, Kady IO (1993) Inorg Chem 32:3868
129. Kady IO, Groves JT (1993) Bioorg Med Chem Lett 3:1367
130. Kuzuya A, Mizoguchi R, Komiyama M (2001) Chem Lett 30:584
131. Komiyama M, Kuzuya A, Mizoguchi R (2002) Bull Chem Soc Jpn 75:2547
132. Kuzuya A, Mizoguchi R, Morisawa F, Machida K, Komiyama M (2002a) J Am Chem Soc 124:6887
133. Kuzuya A, Machida K, Mizoguchi R, Komiyama M (2002b) Bioconjugate Chem 13:365
134. Kuzuya A, Mizoguchi R, Sasayama T, Zhou J-M, Komiyama M (2004) J Am Chem Soc 126:1430
135. Kuzuya A, Shi Y, Sasayama T, Komiyama M (2005) J Biol Inorg Chem 10:270
136. Brunner J, Mokhir A, Krämer R (2003) J Am Chem Soc 125:12410
137. Boll I, Krämer R, Brunner J, Mokhir A (2005) J Am Chem Soc 127:7849
138. Zelder FH, Brunner J, Krämer R (2004) Chem Commun 2004:902
139. Boll I, Jentzsch E, Krämer R, Mokhir A (2006) Chem Commun 2006:3447
140. Gartner ZJ, Liu DR (2001) J Am Chem Soc 123:6961
141. Gartner ZJ, Tse BN, Grubina R, Doyon JB, Snyder TM, Liu DR (2004) Science 305:1601
142. Li X, Liu DR (2004) Angew Chem Int Ed 43:4848
143. Graf N, Göritz M, Krämer R (2006) Angew Chem Int Ed 45:4013
144. Graf N, Krämer R (2006) Chem Commun 2006:4375
145. Ward TR (2005) Chem Eur J 11:3798
146. Erkkila KE, Odom DT, Barton JK (1999) Chem Rev 99:2777
147. Roelfes G, Feringa BL (2005) Angew Chem Int Ed 44:3230
148. Roelfes G, Boersma AJ, Feringa BL (2006) Chem Commun 2006:635
149. Grieco PA(ed) 1998 Organic synthesis in water, 1st edn. Blackie, London
150. Lindström UM 2007 (ed) Organic reactions in water: principles, strategies and applications, 1st edn. Blackwell, Oxford
151. Evans DA, Fandrick KR, Song H-J (2005) J Am Chem Soc 127:8942
152. Boersma AJ, Feringa BL, Roelfes G (2007) Org Lett 9:3647
153. Coquière D, Feringa BL, Roelfes G (2007) Angew Chem Int Ed 46:9308
154. Shibata N, Yasui H, Nakamura S, Toru T (2007) Synlett 2007:1153
155. Roelfes G (2007) Mol Biosyst 3:126
156. Caprioara M, Fiammengo R, Engeser M, Jäschke A (2007) Chem Eur J 13:2089
157. Ropartz L, Meeuwenoord NJ, van der Marel GA, van Leeuwen PWNM, Slawin AMZ, Kamer PCJ (2007) Chem Commun 2007:1556

Top Organomet Chem (2009) 25: 25–43
DOI:10.1007/3418_2008_4

Artificial Metalloproteins Exploiting Vacant Space: Preparation, Structures, and Functions

Satoshi Abe, Takafumi Ueno, and Yoshihito Watanabe

Abstract Molecular design of artificial metalloproteins is one of the most attractive subjects in bioinorganic chemistry. Protein vacant space has been utilized to prepare artificial metalloproteins because it provides a unique chemical environment for application to catalysts and to biomaterials bearing electronic, magnetic, and medical properties. Recently, X-ray crystal structural analysis has increased in this research area because it is a powerful tool for understanding the interactions of metal complexes and protein scaffolds, and for providing rational design of these composites. This chapter reviews the recent studies on the preparation methods and X-ray crystal structural analyses of metal/protein composites, and their functions as catalysts, metal-drugs, etc.

Key words Catalytic reaction, Metal-drugs, Metal materials, Nanocage, Protein, X-ray crystal structure

S. Abe and T. Ueno
Department of Chemistry, Graduate School of Science, Nagoya University, Nagoya 464-8602, Japan
Current address: Institute for Integrated Cell-Material Sciences (iCeMS), Kyoto University, Kyoto 615-8510, Japan

T. Ueno
PRESTO, Japan Science and Technology Agency (JST), Saitama 332-0012, Japan

Y. Wantanabe(✉)
Research Center for Materials Science, Nagoya University, Nagoya 464-8602, Japan
e-mail: yoshi@nucc.cc.nagoya-u.ac.jp

Contents

1 Introduction

Construction of artificial metalloproteins has been intensively studied and applied to catalysts and biomaterials bearing electronic, magnetic, and medical properties [1–6]. In particular, topics on the composites of metal complexes or materials in protein vacant space are becoming the most important subjects in the field of bioinspired materials. In early works of this research area, Akabori et al. reported that the artificial metalloenzyme constructed by the deposition of Pd particles on silk protein fibers was able to catalyze asymmetric hydrogenation of oximes and oxazolones [7]. Whiteside et al. prepared the first artificial organometalloenzyme, which catalyzed asymmetric olefin hydrogenations using an avidin–biotin interaction [8]. However, at that time, it was difficult to characterize and improve the catalytic activities of the composites due to the lack of structural information and the limitations on molecular design using computational methods.

Recently, protein mutagenesis and X-ray structural analysis of proteins have become familiar tools for inorganic chemists in constructing artificial metalloproteins. Thus, the number of reports on the preparation and crystal structures of metal complex/protein hybrids have been increasing since 2000 [1, 3, 5, 6, 9–20]. Proteins and metal complexes utilized intensively for artificial metalloproteins are listed in Table 1. In these studies, the main subject is conjugation of metal complex catalysts with protein scaffolds for catalytic reactions [1, 3, 5]. On the other hand, some researchers have utilized nanoscaled protein cages for deposition of metal nanoparticles and encapsulation of functional nanomaterials [4, 5]. For the last few years, the direction of this research has been shifting toward biomineralization, design of metal-drugs, and fine-tuning of artificial enzymes.

In this chapter, the key topics of artificial metalloproteins utilizing protein vacant space are reviewed, outlining recent studies since 2000. Section 3 shows the approaches for construction of the metal complex/protein composites and their crystal structures and, further, describes the interactions between metal-drugs and proteins. Section 4

Table 1 Summary of proteins and metal complexes for the preparation of artificial metalloproteins and their functions

Protein	Metal complexes	Function	References
Myoglobin	Heme derivatives	Catalyst/O_2 storage/ electron transfer	[13, 21, 22]
	Cr and Mn Schiff base complexes	Catalyst	[17, 23, 24]
Avidin	Biotinated Rh and Ru complexes	Catalyst	[8, 25, 26]
Albumin	Heme, Cu, and Rh complexes	Catalyst/O_2 storage	[27–30]
Lysozyme	Ru and Cu complexes	Metal drug	[14, 31]
Kinase	Ru complex	Inhibitor	[12]
Ferritin	Pd, Ag, CdS, Fe_3O_4, ZnSe clusters and Gd complex	Catalyst/material	[32–37]
Virus	Au, CoPt, and FePt clusters	Material	[38–41]

provides the coordination structures of metal multinuclear clusters binding on protein scaffolds. Section 5 shows the direct observation of reaction intermediates in the active sites of some oxygenases. Section 6 describes how the self-assembled nanoprotein cages are utilized for deposition of metal nanoclusters and metal complexes for their application to catalysts, and to magnetic and medical materials.

2 Protein Structures Utilized for Artificial Metalloproteins

For the construction of artificial metalloproteins, protein scaffolds should be stable, both over a wide range of pH and organic solvents, and at high temperature. In addition, crystal structures of protein scaffolds are crucial for their rational design. The proteins reported so far for the conjugation of metal complexes are listed in Fig. 1. Lysozyme (Ly) is a small enzyme that catalyzes hydrolysis of polysaccharides and is well known as a protein easily crystallized (Fig. 1a). Thus, lysozyme has been used as a model protein for studying interactions between metal compounds and proteins [13, 14, 42, 43]. For example, $[Ru(p\text{-cymene})]^{2+}$, $[Mn(CO)_3]^+$, and cisplatin are regiospecifically coordinated to the N^{ε} atom of His15 in hen egg white lysozyme [14, 42, 43]. Serum albumin (SA) is one of the most abundant blood proteins, and exhibits an ability to accommodate a variety of hydrophobic compounds such as fatty acids, bilirubin, and hemin (Fig. 1b). Thus, SA has been used to bind several metal complexes such as Rh(*acac*)$(CO)_2$, Fe- and Mn-corroles, and Cu-phthalocyanine and the composites applied to asymmetric catalytic reactions [20, 28–30].

Avidin is a glycoprotein and consists of four identical subunits. Avidin shows a very strong affinity to biotin with a K_a of approximately 10^{15} M^{-1} (Fig. 1c). The affinity of avidin for biotin can be utilized to introduce metal complexes into the avidin cavity by a covalent bond with biotin. In fact, hybrids of avidin and biotin conjugated with Rh diphosphine and Ru diamine moieties have been shown to allow asymmetric hydrogenations of olefin and ketone substrates [8, 25, 26].

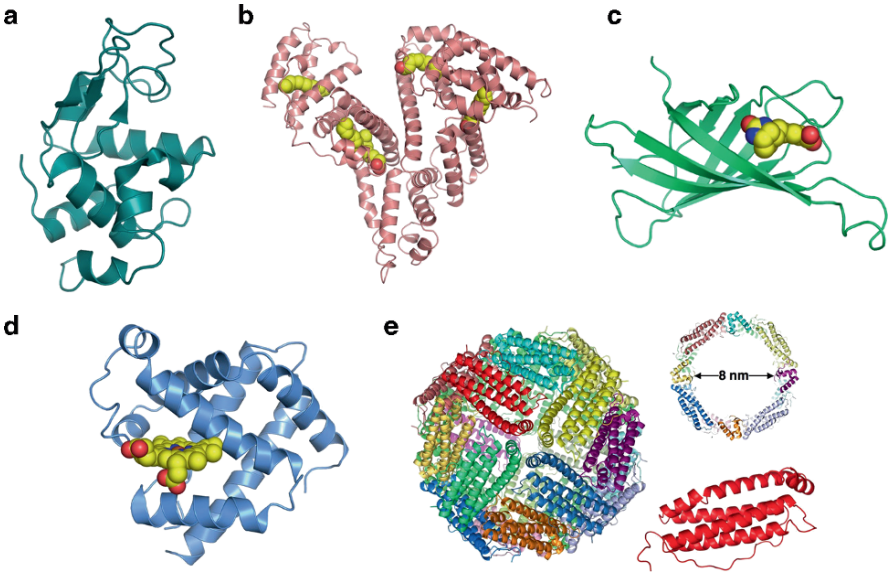

Fig. 1 Ribbon diagrams of protein architectures: **a** lysozyme, **b** serum albumin, **c** avidin, **d** myoglobin, and **e** ferritin taken from PDB ID: 2VB1, 1BJ5, 1AVD, 4MBN, and 1DAT, respectively

Myoglobin (Mb) is a small hemoprotein that functions as an oxygen storage, and has been used as a model for many heme enzymes by modifying the heme prosthetic group and/or replacing some amino acids near the heme (Fig. 1d) [44–46]. Thus, Mb is a good candidate for a host protein scaffold to incorporate synthetic metal complexes such as M^{III}(Schiff base) (M = Fe, Cr, and Mn) and iron porphycene [22–24]. Ly, SA, avidin, and Mb have been used to fix a single metal complex in their cavities. On the other hand, self-assembled protein cages are capable of accommodating many metallic compounds and inorganic materials [4, 5, 47, 48].

Ferritin (Fr) is a spherical protein composed of 24 subunits with a cavity where iron atoms are accumulated as a cluster of ferric oxyhydroxide (Fig. 1e) [49]. Some metal ions and organic molecules are able to penetrate through the hydrophilic channels of the threefold axis to the inside of Fr, which has an internal diameter of 8 nm [50]. Fr is stable both at high temperature (<80°C) and in a pH range of 3–11. Fr has been used for the deposition of monodisperse metal particles such as FeS, CdS, CdSe, Pd, and Ag in the cage [35, 37, 40, 48, 51–55]. Thus, it is possible to use the Fr cage to incorporate and fix many metal complexes [32, 56, 57]. Self-assembled supermolecular proteins have different size of cages, such as cowpea chlorotic mottle virus (CCMV) with 28 nm diameter cages, small heat shock protein (sHsp) with 12 nm, and DNA binding protein (Dps) with 9 nm. Huge supermolecular assemblies such as tobacco mosaic virus, M-13 bacteriophage, and chaperonins have also been utilized as well-defined spaces for the encapsulation of metal compounds and organic materials [4, 33, 47, 58–65].

3 Functions and Structures of Metal Complexes in Protein Cavities

3.1 Preparation of Artificial Metalloproteins

There have been many reports that described protein composites containing metal complexes [1–3, 5, 6]. Three different approaches for the incorporation of synthetic metal complexes into protein cavities have been reported: (i) modification of natural substrates, (ii) covalent anchoring, and (iii) non-covalent insertion. For example, Whiteside et al. constructed artificial metalloenzymes by the conjugation of a Rh diphosphine complex with biotin, which strongly binds to avidin [8]. Ward et al. have improved this method to increase the reaction activities [25]. They optimized the reaction conditions by screening the structures of metal complexes and protein environments. Finally, optimized composites catalyzed asymmetric hydrogenation with up to 97% ee (Fig. 2a) [2, 3, 26].

Covalent anchoring is an attractive approach for conjugation of metal complexes directly to specific sites of protein scaffolds. Several metal complexes such as Cu, Pd, and Rh complexes have been incorporated into protein cavities by covalent anchoring of the thiol group of Cys or the amine group of Lys with metal complexes [66–68]. On the other hand, Lu et al. have succeeded in dual covalent attachment of a Mn(salen) complex bearing two thiosulfonate moieties to apo-myoglobin (apo-Mb) mutant L72C/Y103C Mb to restrict the conformational freedom of the metal complex in the cavity [23]. The dual covalent attachment also improved the enantioselectivity of thioanisole sulfoxidation up to 51% ee while a single attachment exhibited only 12% ee (Fig. 2b) [23].

Non-covalent insertion of several modified metal cofactors and synthetic metal complexes into protein cavities such as serum albumin (SA) and Mb has been reported [5, 24, 28, 30, 69]. If synthetic metal complexes, whose structures are very different from native cofactors, can be introduced into protein cages, the bioconjugation of metal complexes will be applicable to many proteins and metal complexes. Mn(corrole) and Cu(phthalocyanine) are inserted into SA by non-covalent interactions and the composites catalyze asymmetric sulfoxidation and Diels-Alder reactions with up to 74 and 98% ee, respectively (Fig. 2c) [28, 30]. Since the heme is coordinated to Tyr161 in the albumin cavity, determined by X-ray crystal structure [20], it is expected that both Mn(corrole) and Cu(phtalocyanine) are also bound to albumin with the same coordination. The incorporation of synthetic metal complexes in protein cavities using these methods is a powerful approach for asymmetric catalytic reactions. However, there are still some difficulties in further design of the composites for improving reactivities and understanding reaction mechanisms because detailed structural analyses are not available for most of the composites.

Successful structural analyses of artificial metalloproteins have been reported [5, 6, 17, 22]. Hayashi et al. have determined the crystal structure of a reconstituted apo-Mb with the iron porphycene derivative 13,16-dicarboxyethyl-2,7-diethyl-3,6,12,17-tetramethylporphycenato-Fe^{III} (iron porphycene) [22]. The structure shows

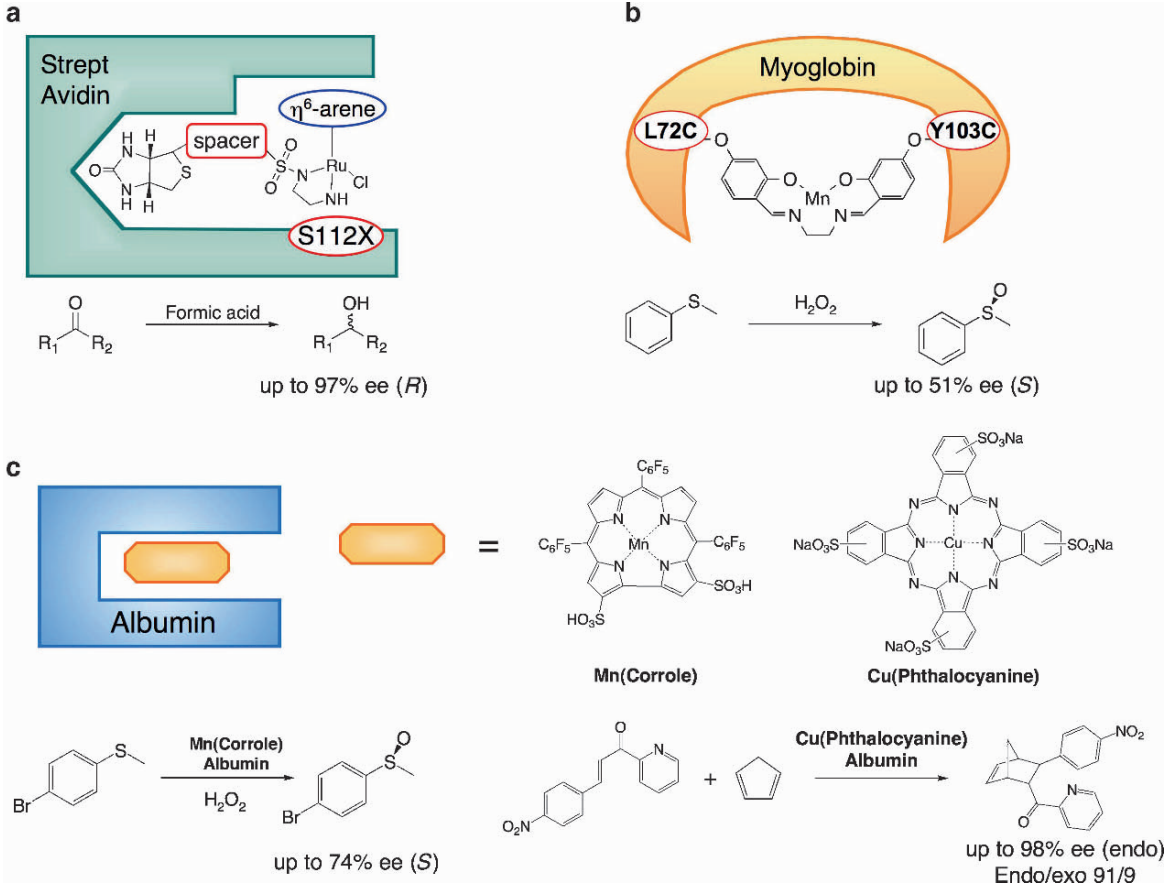

Fig. 2 Artificial metalloenzymes and asymmetric reactions catalyzed by them. Metal cofactors are introduced by **a** covalent modification of biotin, **b** double anchoring to myoglobin, and **c** non-covalent insertion to serum albumin

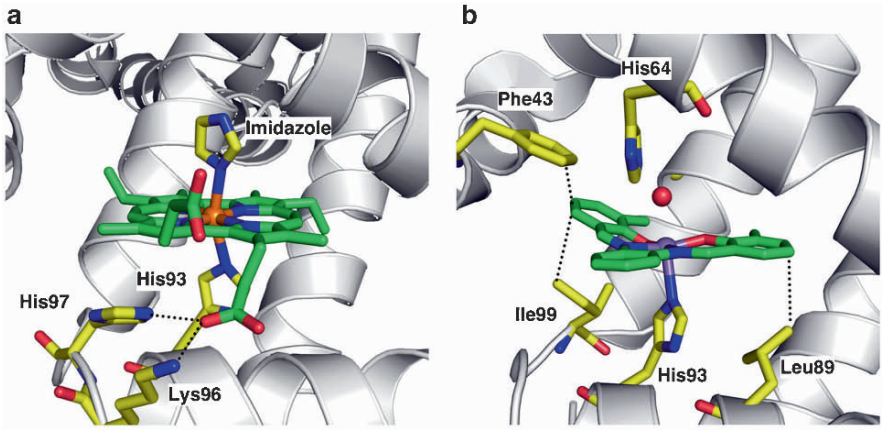

Fig. 3 Crystal structures of active site of artificial metalloproteins: **a** Fe(Porphycene)•apo-Mb, and **b** Cr(Schiffbase)•apo-A71G Mb taken from PDB ID: 2D6C, and 1V9Q, respectively

that the iron porphycene is located in the apo-Mb cavity by coordinating to N^{ε} of His93 and an external imidazole ligand. The specific interactions such as hydrogen bonding with Lys96 and His97 are also observed (Fig. 3a). The composite showed higher peroxidase and peroxygenase activities than native Mb due to stronger coordination of iron porphycene to His93 than that of heme.

Crystal structures of a series of metal Schiff base complexes in the apo-Mb cavity have been determined by Watanabe et al. [16, 17]. The crystal structures of apo-Mb reconstituted with M^{III}(3,3′-salophen) (salophen = *N*,*N*′-bis(salicylidene)-1,2-phenylenediamine, M = Cr, Mn, Fe) complexes show that the metal salophen complexes are tightly ligated to the N^{ε} atom of His93 in the apo-Mb cavity with the same coordination geometry as that of heme, i.e., planar four coordinate ligands and the use of proximal histidine as an axial ligand (Figs. 3b and Fig. 4) [16, 17]. The metal salophen complexes fixed in the apo-Mb cavity are further stabilized by several π–π and CH–π interactions with surrounding amino acid residues (Fig. 3b). Ueno et al. also succeeded in controlling the enantioselectivity of sulfoxidation by design of metal complexes based on the crystal structures [17, 69]. They have extended this method to other metal complexes with different coordination geometries from heme and salophen complexes.

The group reported two novel coordination structures of Cu^{II}(Sal-X) (Sal-X = *N*-salicylideneaminoacidato) and organometallic rhodium 2,6-bis(2-oxazolinyl)-phenyl (Rh•Phebox) complexes, whose structures are completely different from heme, in the Mb cavity (Fig. 4). The crystal structure of Cu^{II}(Sal-Phe)•apo-Mb shows that the Cu^{II} complexes are coordinated to the nitrogen of His64 with a square-planar coordination geometry with the assistance of CH–π and π–π interactions between a benzene ring in the salicylidene moiety of the ligand and the surrounding hydrophobic amino acid

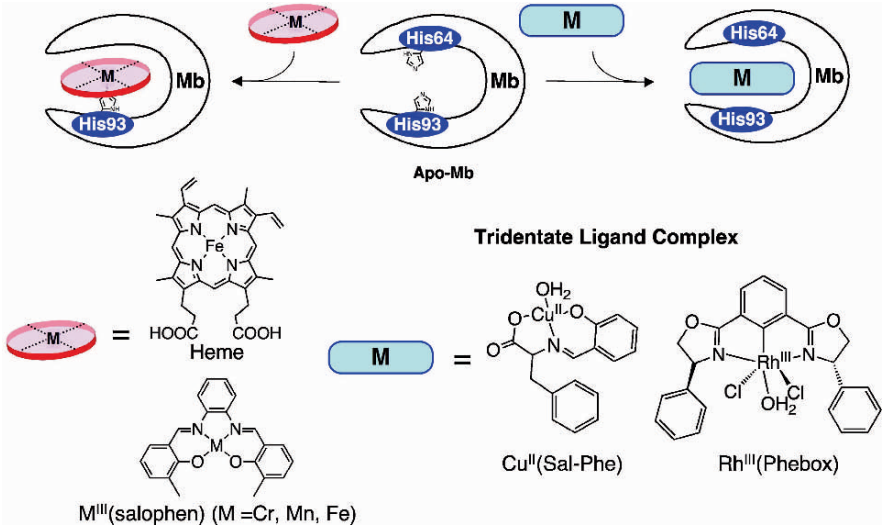

Fig. 4 Various binding geometries of incorporated metal complexes in the apo-Mb cavity

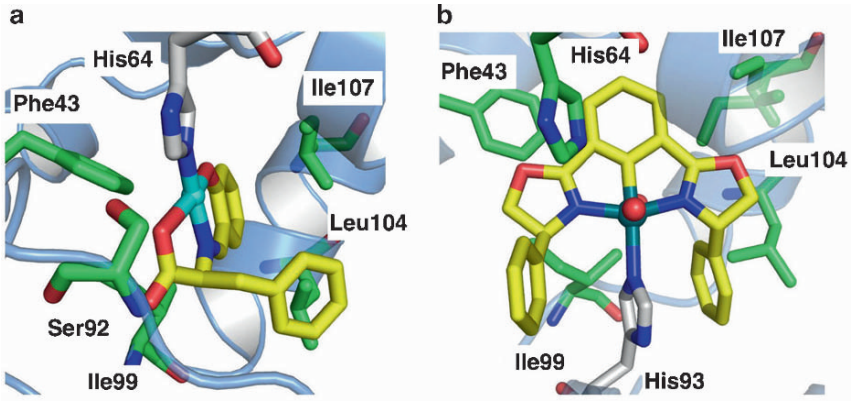

Fig. 5 Crystal structures of active site of artificial metalloproteins: **a** Cu(Sal-Phe)•apo-Mb, and **b** Rh•Phebox•apo-A71G Mb taken from PDB ID: 2EB8, and 2EF2, respectively

residues (Fig. 5a). The crystal structure of Rh^{III}•Phebox•apo-A71G Mb reveals that the Rh•Phebox complex is fixed in the apo-Mb cavity with an unprecedented arrangement that is almost perpendicular to the heme (Fig. 5b). These results suggest that apo-Mb is capable of accommodating various metal complexes having different coordination structures and functions from the native metal cofactors.

3.2 *Interaction of Metal-Drugs with Proteins*

There is increasing importance of metal-based drugs in the field of medicinal chemistry. Structural study of metal-drug/protein interactions is of upmost importance for understanding the molecular fragments interacting with proteins, their locations, and their binding affinities. There have been an increasing number of reports describing the X-ray crystal structures of metal-drug/protein composites in recent years [11–13, 42]. For example, the interactions of cisplatin, known as an anticancer drug, with proteins such as copper–zinc superoxide dismutase (SOD) and lysozyme have been reported [11, 42]. The crystal structure of SOD interacting with cisplatin shows that the Pt atom is selectively bound to N^{ε} of His19. Two chloride atoms also ligate to the Pt atom with a distorted square-planar geometry (Fig. 6a) [11]. The crystal structure of cisplatin and lysozyme adducts reveals selective platination of N^{δ} of His15 [42], which is also found to ligate to the organometallic complexes Ru(*p*-cymene) and $Mn(CO)_3$ (Fig. 6b) [14, 43]. Meggers et al. have designed an organometallic RuCp(CO) complex as a protein

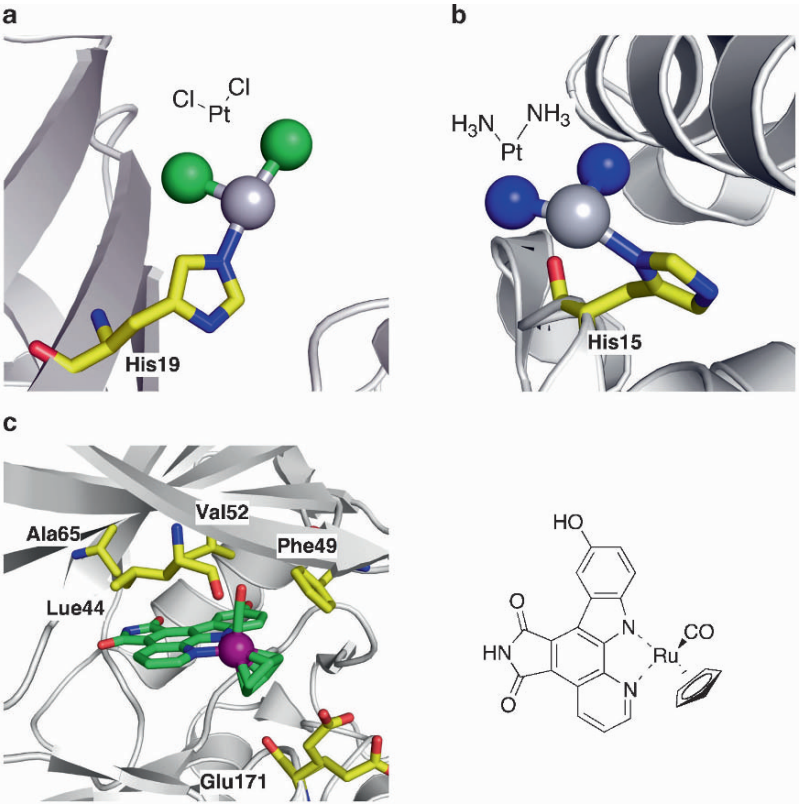

Fig. 6 Crystal structures of metal-drug/protein composites. **a** cisplatin/SOD, **b** cisplatin/lysozyme, and **c** Ru complex/Pim-1 taken from PDB ID: 2AEO, 2I6Z, and 2BZI, respectively

kinase inhibitor on the basis of the structure of staurosporine, a well-known organic inhibitor of protein kinases. The RuCp(CO) complex exhibits more than two orders of magnitude higher activity than that of staurosporine for Pim-1 (Human serine/threonine protein kinase), which is one of the protein kinases. The crystal structure of the RuCp(CO) complex and Pim-1 adduct shows the binding mode of the Ru complex to be completely identical to that of staurosporine (Fig. 6c) [12].

4 Direct Observation of Metal Accumulation on Protein Surfaces

To understand the molecular mechanism of biomineralization, it is very important to study the initial metal binding process as well as the process of metal cluster formation. However, little is known so far on the interactions between amino acids and metal clusters. Ferritin and other ferritin-like spherical proteins are known to catalyze biomineralization in the protein cages [4, 49]. For example, Fe^{II} ions incorporated in these protein cages are oxidized to Fe^{III} at the ferroxidase center and deposited in the protein large cavities as iron oxides [49].

Zeth et al. have reported biomineralization processes by crystallographic analysis of Dps-like (Dps, DNA-protecting protein during starvation) ferritin proteins containing various amounts of Fe^{II} ions [65]. Fe^{II} ions penetrate channels composed of acidic amino acid residues (Glu13, Glu15, Asp18, Glu167, Glu171, and Asp173), which are expected to act as an electrostatic guide for incorporating Fe^{II}, and travel to three translocation sites within the DpsA pore (Fig. 7a). Fe^{II} is oxidized to Fe^{III} at the ferroxidase center and iron oxide clusters are formed at two nucleation sites. Five iron atoms are accommodated at one of the nucleation sites and [4Fe–3O] clusters are created using glutamic acid (Fig. 7b).

Sadler et al. have shown multinuclear Hf and Zr clusters formed in a ferric-ion-binding protein, Fbp [10, 19]. The crystal structure of Fbp containing Hf atoms shows that three types of Hf clusters are formed by utilizing a di-tyrosyl cluster nucleation motif (Tyr195-Tyr196) in an interdomain cleft. Two types of trinuclear clusters and one pentanuclear oxo-Hf cluster are generated at this site (Fig. 7c, Fig. 7d) [10]. These results show that a Tyr–Tyr motif is very important for the metal mineralization.

Müller and Ermler et al. have observed various types of polynuclear tungsten oxide clusters in the cavity of a Mo/W-storage (Mo/WSto) protein [70], i.e., five types of polyoxotungstates such as W_3, W_6, W_7, W_2, and, W_{7+x} are formed in the pockets of Mo/WSto protein. The W_3 cluster shown in Fig. 7e consists of ten O atoms and N atoms of three His139 in different subunits, described as $W_3O_{10}H_3N_3$.

Although we are able to observe coordination structures in metal accumulation processes on the protein surfaces, it is still difficult to design the coordination structures and functions of artificial metal clusters formed in protein scaffolds. If we are able to overcome the problems, we could construct metal clusters having desired coordination structures and functions. Furthermore, it may help us in understanding the formation processes of metal clusters prepared in natural proteins such as FeMoco, Fe–S clusters, and Mn clusters in nitrogenase, ferredoxins, and photosystem II [71–73].

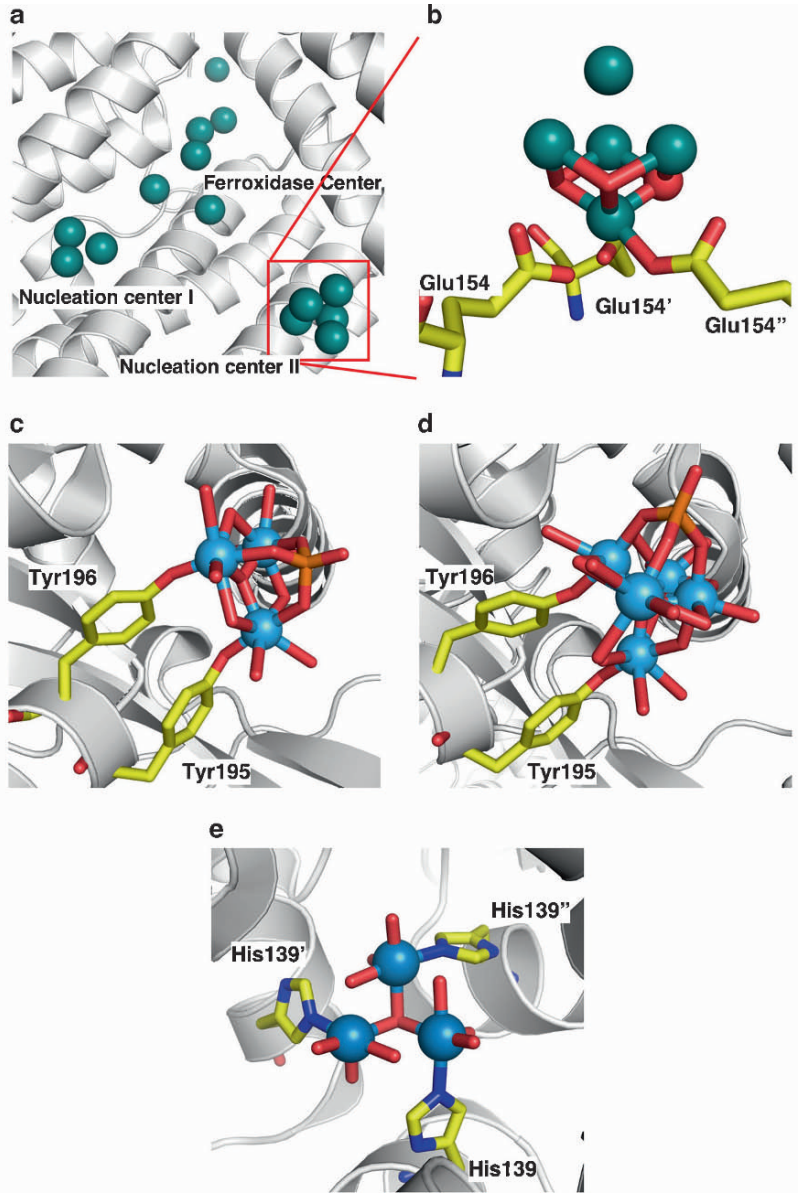

Fig. 7 Crystal structures of proteins that interact with metal minerals. **a** iron-oxide clusters on the interior surface of DpsA, **b** close up view of the nucleation center II, **c** tri Hf-oxo cluster, and **d** penta Hf-oxo cluster at the di-tyrosyl nucleation motif of ferric-ion-binding protein, Fbp. **e** W_3 cluster at an intersection of subunits in Mo/WSto protein

5 Direct Observation of Enzymatic Reaction Processes

Direct observation of enzymatic reaction processes by X-ray crystallographic analysis is very important because the resulting structures are direct evidence for the intermediates of the reactions. There are a series of independent studies showing intermediates of enzymatic reactions of some oxygenases elucidated by X-ray crystallographic analyses [74–78]. For instance, the intermediate structures in hydroxylation of *d*-camphor by cytochrome P450cam show the ferrous dioxygen adduct and oxyferryl species [77]. The crystal structures of naphthalene dioxygenase (NDO) show that a molecular oxygen is bound to the mononuclear iron atom in a side-on fashion in the active site (Fig. 8a) [74]. The structure containing a substrate (indole) and molecular oxygen in the NDO active site shows that the dioxygen molecule bound to the iron atom is at an appropriate position to attack the double bond of the substrate. The structure clearly shows how the enzyme oxidizes the substrate with high stereospecificity (Fig. 8b). The crystal structures of Fe^{2+} containing 2,3-homoprotocatechuate dioxygenase show three intermediate states in the O_2 activation and oxygen insertion reaction by the dioxygenase [76]. Figure 8c shows the dioxygen molecule bound to iron in a side-on fashion at the active site, having the substrate near to the oxygen. The dioxygen bound to the iron then attacks the substrate to afford an iron-peroxide-substrate intermediate (Fig. 8d) followed by formation of an aromatic ring-opened product (Fig. 8e). These crystal structures provide the actual reaction mechanisms, including the origin of high selectivity. By considering these structures, we could design artificial metalloenzymes having high activities.

6 Introduction of Functional Metal Materials in Protein Nanocages

Self-assembled protein cages have been utilized for the introduction of functional materials on interior or exterior surfaces of spherical proteins since they are thermally stable and it is easy for us to chemically and genetically modify the protein interior and exterior surfaces [4, 69]. For example, Fr, a small heat shock protein (sHsp), and cowpea chlorotic mottle virus (CCMV) are available for the deposition and modification of inorganic metal particles and organic materials [4, 35, 37, 39, 40, 47, 48, 51–55, 58, 64]. sHsp consists of 24 subunits and affords an interior cavity of 6.5 nm in diameter. sHsp has large pores (3 nm) at the intersections of subunits, which permit easy access into the cavity [40, 64]. CCMV is an RNA-containing plant virus composed of 180 coat protein subunits and provides an outer diameter of 28 nm and an interior cavity of 18–24 nm. CCMV exhibits an ability both to encapsulate organic polymers and metalloenzymes and to regulate metal incorporation in the cavity by controlling the pH-dependent gating behavior of its pores or dissociation of the viral assembly [47, 58]. Tobacco mosaic virus (TMV) [59, 63],

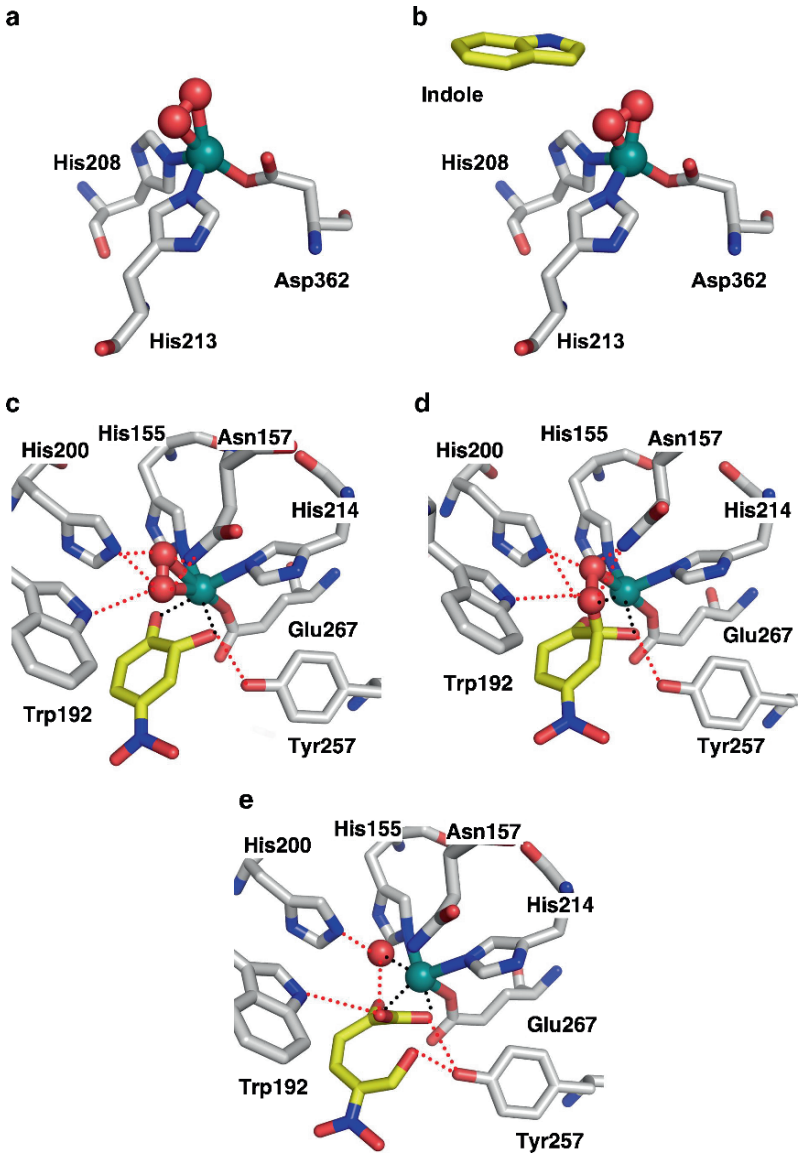

Fig. 8 Active site structures of O_2 adducts of NDO and HPCD. The O_2 adducts of NDO in the absence (**a**) and in the presence (**b**) of indole. The O_2 and 4-NC bound structures of HPCD are shown before the oxygen insertion (**c**), the C-O-O-Fe formation (**d**), and the product formation (**e**). These structures are taken from PDB ID: **a** 1O7M, **b** 1O7N, **c**–**e** 2IGA. *Red dashed lines* show hydrogen-bonds. *Black lines* indicate bonds or potential bonds to iron

chaperonins composed of two stacked supermolecular protein cages [33, 61], and the gene product 27–gene product 5 component from bacteriophage T4 [79, 80] have also been utilized as biological templates for preparation, deposition, and encapsulation of metal nanoparticles in their vacant spaces.

6.1 Preparation of Metal Particles in Protein Cages

Naik et al. and Douglas et al. have prepared Ag and CoPt clusters having a precise crystal phase in the Fr and sHsp cages, respectively, by the introduction of metal binding peptides identified from phage-display screening on protein interior surfaces [35, 40]. The AG4 peptide introduced in the ferritin interior acts as a binding site of silver ions and helps to reduce them to Ag^0 nanoparticles whose size and crystal phase are highly restricted (Fig. 9a) [35]. A CoPt bimetallic particle was also prepared by the reduction of Co and Pt ions incorporated in the sHsp interior cavity having the CoPt binding peptide. The peptide provided the growth of a tetragonal L10 phase of a CoPt particle in the Hsp cage (Fig. 9b). The particle shows a ferromagnetic property at room temperature [40].

6.2 Application to Biomedicines

Protein nanocages are utilized not only for the deposition of metal nanoparticles, but also for the entrapment of chemotherapeutic agents. For example, Gd-HPDO3A (gadlinium-[10-(2-hydroxypropyl)-1,4,7,10-tetraazacyclododecane-1,4,7-triacetic acid]), which is known to be a magnetic resonance imaging (MRI) contrast agent, is entrapped in the apo-ferritin (apo-Fr) cage by an acid-dissociation method (Fig. 10) [32]. The Gd complexes entrapped in the apo-Fr cage exhibit high relaxivity of water protons, thus, the complex is a potent candidate for its use in MRI.

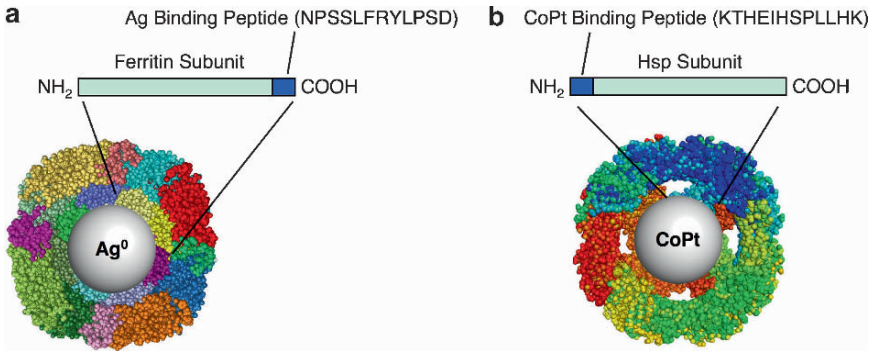

Fig. 9 Representative structures of **a** Ag particle in L-ferritin captured by the Ag binding peptide, and **b** CoPt particle in Hsp on the CoPt binding peptide

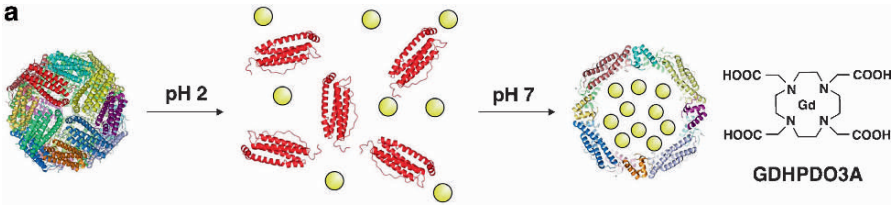

Fig. 10 Schematic drawing of incorporation of a GDHPDO3A complex into apo-ferritin by an acid-dissociation method

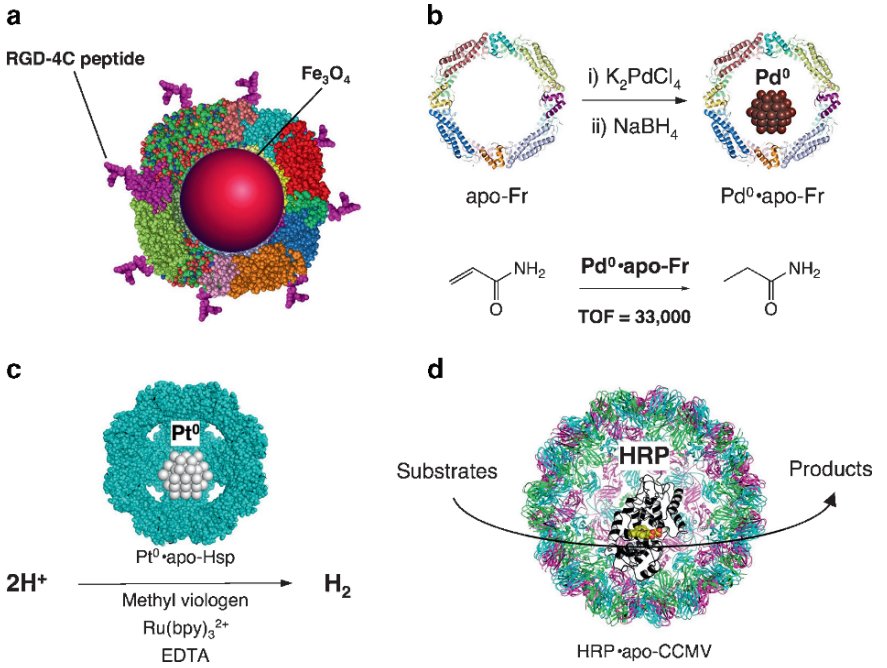

Fig. 11 Schematic representation of **a** preparation of cell targeted ferritin with the binding RGD-4C peptide on the exterior surface of apo-Fr including Fe_3O_4, **b** preparation of a Pd nanoparticle in apo-Fr and olefin hydrogenation, **c** hydrogen production reaction using Pt^0•apo-Hsp, and **d** encapsulation of horseradish peroxidase (HRP) in the cavity of CCMV and an enzymatic reaction

Douglas et al. have reported the introduction of multifunctional molecules to apo-Fr. They introduced a cell-specific targeting peptide, RGD-4C on the exterior surface of apo-Fr, where the peptide is capable of binding particular tumor proteins [81]. Indeed, the transmission electron microscopic images of RGD-4C Fr containing a magnetite nanoparticle of Fe_3O_4 show that electron-dense particles corresponding to Fe_3O_4 were observed on the surface of the C32 melanoma cells (Fig. 11a). These results show how nanoscale protein containers serve to accommodate a variety of functional metal complexes and metal clusters.

6.3 Application to Catalysts

Protein nanocages can be used as a catalytic reaction space of metal particles [54, 64]. For example, Ueno et al. have succeeded in the preparation of monodispersed Pd nanoparticles and the size-selective olefin hydrogenation catalyzed by the composite (Fig. 11b) [54]. Olefin substrates must penetrate the threefold channels of apo-Fr to react with the Pd particle, thus, larger substrates are less reactive than smaller substrates.

Varpness et al. prepared a biomimetic material, aiming for artificial hydrogenase, by employing small heat shock protein (sHsp) including Pt particles [64]. The composite catalyzes hydrogen production in the presence of EDTA, Ru(2,2 -bioyridine)$_3^{2+}$, methyl viologen as a reductant, photocatalyst, and electron-transfer mediator, respectively (Fig. 11c). The system in the protein cage architecture can provide a new concept for hydrogen production [64].

Engelkamp et al. have reported the incorporation of horseradish peroxidase in the interior cage of CCMV by using its disassembly/assembly property to elucidate a single molecule study of enzyme behaviors (Fig. 11d). They showed that CCMV permits easy access of substrates and products through the pores of CCMV and that this permeability can be controlled by pH [58]. These results show that protein nanocages are very useful templates for the entrapment of functional materials and provide chemical reaction space.

7 Summary

The recent examples described in this chapter demonstrate that the construction of artificial metalloproteins is an active field in bioinorganic chemistry. We are able to use small protein cavities as well as large protein cages such as ferritin and virus molecules as molecular templates for incorporating synthetic metal complexes and materials into the scaffolds. The metal complex/protein composites are able to function as asymmetric catalysts, electron transfer materials, and magnetic and electronic materials. It is possible to modify the functions of the composites by changing the metal complexes and/or protein cavities. This progress has been achieved by cooperation of molecular and structural biology and inorganic chemistry. In particular, X-ray crystal structure analyses of the composites provide coordination structures and non-covalent interactions between metal complexes and protein scaffolds. Structural information is very important for improving catalytic activities, to understand their reaction mechanisms, and to design novel metal-drugs and metal inhibitors. Furthermore, dynamic processes of mineralization and catalytic reactions on the metal binding sites through structural studies of intermediates have just started. We believe that these results will provide intriguing implications for their application in catalysts, sensors, electronics devices, and so on.

References

1. Lu Y (2006) Angew Chem Int Ed 45:5588–5601
2. Steinreiber J, Ward TR (2008) Coord Chem Rev 252:751–766
3. Thomas CM, Ward TR (2005) Chem Soc Rev 34:337–346
4. Uchida M, Klem MT, Allen M, Suci P, Flenniken M, Gillitzer E, Varpness Z, Liepold LO, Young M, Douglas T (2007) Adv Mater 19:1025–1042
5. Ueno T, Abe S, Yokoi N, Watanabe Y (2007) Coord Chem Rev 251:2717
6. Ueno T, Yokoi N, Abe S, Watanabe Y (2007) J Inorg Biochem 101:1667
7. Akabori S, Sakurai S, Izumi Y, Fujii Y (1956) Nature 178:323–324
8. Wilson ME, Whitesides GM (1978) J Am Chem Soc 100:306–307
9. Abe S, Ueno T, Reddy PAN, Okazaki S, Hikage T, Suzuki A, Yamane T, Nakajima H, Watanabe Y (2007) Inorg Chem 46:5137–5139
10. Alexeev D, Zhu HZ, Guo ML, Zhong WQ, Hunter DJB, Yang WP, Campopiano DJ, Sadler PJ (2003) Nat Struct Biol 10:297–302
11. Calderone V, Casini A, Mangani S, Messori L, Orioli PL (2006) Angew Chem Int Ed 45:1267–1269
12. Debreczeni JE, Bullock AN, Atilla GE, Williams DS, Bregman H, Knapp S, Meggers E (2006) Angew Chem Int Ed 45:1580–1585
13. Hu YZ, Tsukiji S, Shinkai S, Oishi S, Hamachi I (2000) J Am Chem Soc 122:241–253
14. McNae IW, Fishburne K, Habtemariam A, Hunter TM, Melchart M, Wang FY, Walkinshaw MD, Sadler PJ (2004) Chem Commun 2004:1786–1787
15. Satake Y, Abe S, Okazaki S, Ban N, Hikage T, Ueno T, Nakajima H, Suzuki A, Yamane T, Nishiyama H, Watanabe Y (2007) Organometallics 26:4904–4908
16. Ueno T, Ohashi M, Kono M, Kondo K, Suzuki A, Yamane T, Watanabe Y (2004) Inorg Chem 43:2852–2858
17. Ueno T, Koshiyama T, Ohashi M, Kondo K, Kono M, Suzuki A, Yamane T, Watanabe Y (2005) J Am Chem Soc 127:6556–6562
18. Ueno T, Yokoi N, Unno M, Matsui T, Tokita Y, Yamada M, Ikeda-Saito M, Nakajima H, Watanabe Y (2006) Proc Natl Acad Sci USA 103:9416–9421
19. Zhong WQ, Alexeev D, Harvey I, Guo ML, Hunter DJB, Zhu HZ, Campopiano DJ, Sadler PJ (2004) Angew Chem Int Ed 43:5914–5918
20. Zunszain PA, Ghuman J, Komatsu T, Tsuchida E, Curry S (2003) BMC Struct Biol 3:6–14
21. Hayashi T, Hitomi Y, Ando T, Mizutani T, Hisaeda Y, Kitagawa S, Ogoshi H (1999) J Am Chem Soc 121:7747–7750
22. Hayashi T, Murata D, Makino M, Sugimoto H, Matsuo T, Sato H, Shiro Y, Hisaeda Y (2006) Inorg Chem 45:10530–10536
23. Carey JR, Ma SK, Pfister TD, Garner DK, Kim HK, Abramite JA, Wang Z, Guo Z, Lu Y (2004) J Am Chem Soc 126:10812–10813
24. Ohashi M, Koshiyama T, Ueno T, Yanase M, Fujii H, Watanabe Y (2003) Angew Chem Int Ed 42:1005–1008
25. Collot J, Gradinaru J, Humbert N, Skander M, Zocchi A, Ward TR (2003) J Am Chem Soc 125:9030–9031
26. Letondor C, Humbert N, Ward TR (2005) Proc Natl Acad Sci USA 102:4683–4687
27. Komatsu T, Ohmichi N, Zunszain PA, Curry S, Tsuchida E (2004) J Am Chem Soc 126:14304–14305
28. Mahammed A, Gross Z (2005) J Am Chem Soc 127:2883–2887
29. Marchetti M, Mangano G, Paganelli S, Botteghi C (2000) Tetrahedron Lett 41:3717–3720
30. Reetz MT, Jiao N (2006) Angew Chem Int Ed 45:2416–2419
31. Hunter TM, McNae IW, Liang XY, Bella J, Parsons S, Walkinshaw MD, Sadler PJ (2005) Proc Natl Acad Sci USA 102:2288–2292
32. Aime S, Frullano L, Crich SG (2002) Angew Chem Int Ed 41:1017–1019
33. Ishii D, Kinbara K, Ishida Y, Ishii N, Okochi M, Yohda M, Aida T (2003) Nature 423:628–632

34. Iwahori K, Yoshizawa K, Muraoka M, Yamashita I (2005) Inorg Chem 44:6393–6400
35. Kramer RM, Li C, Carter DC, Stone MO, Naik RR (2004) J Am Chem Soc 126:13282–13286
36. Meldrum FC, Heywood BR, Mann S (1992) Science 257:522–523
37. Wong KKW, Mann S (1996) Adv Mater 8:928
38. Blum AS, Soto CM, Wilson CD, Cole JD, Kim M, Gnade B, Chatterji A, Ochoa WF, Lin TW, Johnson JE, Ratna BR (2004) Nano Lett 4:867–870
39. Douglas T, Strable E, Willits D, Aitouchen A, Libera M, Young M (2002) Adv Mater 14:415–418
40. Klem MT, Willits D, Solis DJ, Belcher AM, Young M, Douglas T (2005) Adv Funct Mater 15:1489–1494
41. Mao CB, Solis DJ, Reiss BD, Kottmann ST, Sweeney RY, Hayhurst A, Georgiou G, Iverson B, Belcher AM (2004) Science 303:213–217
42. Casini A, Mastrobuoni G, Temperini C, Gabbiani C, Francese S, Moneti G, Supuran CT, Scozzafava A, Messori L (2007) Chem Commun 156–158
43. Razavet M, Artero V, Cavazza C, Oudart Y, Lebrun C, Fontecilla-Camps JC, Fontecave M (2007) Chem Commun 2007:2805–2807
44. Hayashi T, Hisaeda Y (2002) Acc Chem Res 35:35–43
45. Ozaki SI, Roach MP, Matsui T, Watanabe Y (2001) Acc Chem Res 34:818–825
46. Watanabe Y, Nakajima H, Ueno T (2007) Acc Chem Res 40:554–562
47. Douglas T, Young M (1998) Nature 393:152–155
48. Douglas T, Dickson DPE, Betteridge S, Charnock J, Garner CD, Mann S (1995) Science 269:54–57
49. Liu XF, Theil EC (2005) Acc Chem Res 38:167–175
50. Yang XK, Chasteen ND (1996) Biophys J 71:1587–1595
51. Mackle P, Charnock JM, Garner CD, Meldrum FC, Mann S (1993) J Am Chem Soc 115:8471–8472
52. Mann S, Meldrum FC (1991) Adv Mater 3:316–318
53. Tsukamoto R, Iwahor K, Muraoka M, Yamashita I (2005) Bull Chem Soc Jpn 78:2075–2081
54. Ueno T, Suzuki M, Goto T, Matsumoto T, Nagayama K, Watanabe Y (2004) Angew Chem Int Ed 43:2527–2530
55. Yamashita I, Hayashi J, Hara M (2004) Chem Lett 33:1158–1159
56. Dominguez-Vera JM, Colacio E (2003) Inorg Chem 42:6983–6985
57. Yang Z, Wang XY, Diao HJ, Zhang JF, Li HY, Sun HZ, Guo ZJ (2007) Chem Commun 3453–3455
58. Comellas-Aragones M, Engelkamp H, Claessen VI, Sommerdijk N, Rowan AE, Christianen PCM, Maan JC, Verduin BJM, Cornelissen J, Nolte RJM (2007) Nat Nanotechol 2:635–639
59. Dujardin E, Peet C, Stubbs G, Culver JN, Mann S (2003) Nano Lett 3:413–417
60. Lee SW, Mao CB, Flynn CE, Belcher AM (2002) Science 296:892–895
61. McMillan RA, Paavola CD, Howard J, Chan SL, Zaluzec NJ, Trent JD (2002) Nat Mater 1:247–252
62. Nam KT, Kim DW, Yoo PJ, Chiang CY, Meethong N, Hammond PT, Chiang YM, Belcher AM (2006) Science 312:885–888
63. Shenton W, Douglas T, Young M, Stubbs G, Mann S (1999) Adv Mater 11:253–256
64. Varpness Z, Peters JW, Young M, Douglas T (2005) Nano Lett 5:2306–2309
65. Zeth K, Offermann S, Essen LO, Oesterhelt D (2004) Proc Natl Acad Sci USA 101:13780–13785
66. Davies RR, Distefano MD (1997) J Am Chem Soc 119:11643–11652
67. Kruithof CA, Casado MA, Guillena G, Egmond MR, van der Kerk-van Hoof A, Heck AJR, Gebbink R, van Koten G (2005) Chem Eur J 11:6869–6877
68. Panella L, Broos J, Jin JF, Fraaije MW, Janssen DB, Jeronimus-Stratingh M, Feringa BL, Minnaard AJ, de Vries JG (2005) Chem Commun 2005:5656–5658
69. Ueno T, Koshiyama T, Abe S, Yokoi N, Ohashi M, Nakajima H, Watanabe Y (2007) J Organomet Chem 692:142–147

70. Schemberg J, Schneider K, Demmer U, Warkentin E, Muller A, Ermler U (2007) Angew Chem Int Ed 46:2408–2413
71. Ferreira KN, Iverson TM, Maghlaoui K, Barber J, Iwata S (2004) Science 303:1831–1838
72. Loll B, Kern J, Saenger W, Zouni A, Biesiadka J (2005) Nature 438:1040–1044
73. Messerschmidt A, Huber R, Poulos T, Wieghardt K (eds) (2001) Handbook of metalloproteins, vol 1. Wiley, Chichester
74. Karlsson A, Parales JV, Parales RE, Gibson DT, Eklund H, Ramaswamy S (2003) Science 299:1039–1042
75. Katona G, Carpentier P, Niviere V, Amara P, Adam V, Ohana J, Tsanov N, Bourgeois D (2007) Science 316:449–453
76. Kovaleva EG, Lipscomb JD (2007) Science 316:453–457
77. Schlichting I, Berendzen J, Chu K, Stock AM, Maves SA, Benson DE, Sweet BM, Ringe D, Petsko GA, Sligar SG (2000) Science 287:1615–1622
78. Unno M, Chen H, Kusama S, Shaik S, Ikeda-Saito M (2007) J Am Chem Soc 129:13394–13395
79. Koshiyama T, Yokoi N, Ueno T, Kanamaru S, Nagano S, Shiro Y, Arisaka F, Watanabe Y (2008) Small 4:50–54
80. Ueno T, Koshiyama T, Tsuruga T, Goto T, Kanamaru S, Arisaka F, Watanabe Y (2006) Angew Chem Int Ed 45:4508–4512
81. Uchida M, Flenniken ML, Allen M, Willits DA, Crowley BE, Brumfield S, Willis AF, Jackiw L, Jutila M, Young MJ, Douglas T (2006) J Am Chem Soc 128:16626–16633

Top Organomet Chem (2009) 25: 45–61
DOI:10.1007/3418_2008_1

Manganese-Substituted α-Carbonic Anhydrase as an Enantioselective Peroxidase

Qing Jing, Krzysztof Okrasa, and Romas J. Kazlauskas

Abstract Carbonic anhydrase binds a zinc ion in a hydrophobic active site using the imidazole groups of three histidine residues. The natural role of carbonic anhydrase is to catalyze the reversible hydration of carbon dioxide to bicarbonate, but it also catalyzes hydrolysis of esters with moderate enantioselectivity. Replacing the active-site zinc with manganese yielded manganese-substituted carbonic anhydrase (CA[Mn]), which shows peroxidase activity with a bicarbonate-dependent mechanism. In the presence of bicarbonate and hydrogen peroxide, CA[Mn] catalyzed the efficient oxidation of *o*-dianisidine with $k_{cat}/K_M = 1.4 \times 10^6\ M^{-1}s^{-1}$, which is comparable to that for horseradish peroxidase, $k_{cat}/K_M = 57 \times 10^6\ M^{-1}s^{-1}$. CA[Mn] also catalyzed the moderately enantioselective epoxidation of olefins to epoxides ($E = 5$ for *p*-chlorostyrene). This enantioselectivity is similar to that for natural heme-based peroxidases, but has the advantage that CA[Mn] avoids formation of aldehyde side products. CA[Mn] degrades during the epoxidation, limiting the yield of the epoxidations to <12%. Replacement of active-site residues Asn62, His64, Asn67, Gln92, or Thr200 with alanine by site-directed mutagenesis decreased the enantioselectivity showing that the active site controls enantioselectivity of the epoxidation.

Key Words Carbonic anhydrase, Enantioselective epoxidation, Hydrogen peroxide, Manganese, Peroxidase

Contents

Q. Jing, K. Okrasa, and R.J. Kazlauskas (✉)
Department of Biochemistry, Molecular Biology & Biophysics and the Biotechnology Institute,University of Minnesota, 1479 Gortner Avenue, Saint Paul, MN 55108, USA
e-mail: rjk@umn.edu

Abbreviations

Ala	Alanine
Asn	Asparagine
Asp	Aspartic acid
BES	*N,N*-bis(2-hydroxyethyl)-2-aminoethanesulfonic acid
CA	Carbonic anhydrase
CA[Mn]	Manganese-substituted bovine carbonic anhydrase mixture of isozymes
CAII[Mn]	Manganese-substituted bovine carbonic anhydrase isoenzyme II
CiP	Peroxidase from *Coprinus cinereus*
CPO	Chloroperoxidase from *Caldariomyces fumago*
Mn	Manganese
E	Enantioselectivity
ee	Enantiomeric excess
ESI-MS	Electrospray ionization mass spectrometry
Gln	Glutamine
Glu	Glutamic acid
hCAII	Human carbonic anhydrase isozyme II
His	Histidine
HRP	Horseradish peroxidase
ICP-AES	Inductively coupled plasma atomic emission spectrometry
k_{cat}	Catalytic constant
K_M	Michaelis constant
Leu	Leucine
PNPA	*P*-Nitrophenyl acetate
Ser	Serine
Trp	Tryptophan
Thr	Threonine
TOF	Turnover frequency
TTN	Total turnover number
Val	Valine
VClPO	Vanadium chloroperoxidase

1 Introduction

Combining proteins with metals creates catalysts not likely to be found in nature.

The ligands bound to a catalytic metal control that metal's reactivity by adjusting the electron density at the metal, opening and closing coordination sites for the substrates and creating a shape to orient the substrate. Organic ligands often require complex syntheses and are difficult to optimize.

Nature's ligands for catalytic metals are proteins. Although proteins are hundreds of times larger and more complex than organic ligands, proteins are easy to prepare by fermentation and modern methods of molecular biology allow creation of hundreds, even millions, of variants for rapid optimization of proteins. Proteins create complex chiral surfaces that can orient unfunctionalized substrates and impart high stereoselectivity, including enantioselectivity. This review will focus on using one protein as a ligand, α-carbonic anhydrase.

But why make this artificial combination of protein and metal catalyst? Doesn't nature already contain all the catalysts we need? Couldn't we just search nature for the one we want? Although nature contains a vast array of catalysts, there are many catalysts that would be useful for organic synthesis, but are unlikely to be found in nature.

Nature's catalysts solve biochemical problems using biochemical building blocks, but the problems in organic synthesis may differ. For example, hydrogen peroxide is an ideal oxidant because it has high active oxygen content and produces water as the reduction product [1, 2]. Nature rarely encounters hydrogen peroxide so it did not evolve catalysts that use it as the oxidant. (Peroxidases seem to be an exception to this statement, but the natural role of peroxidases remains uncertain. At least some peroxidase-catalyzed reactions are likely examples of catalytic promiscuity and do not represent the biochemical function of the enzymes.) Nature further links redox reactions via cofactors so that an oxidation in one metabolic pathway can be linked to a reduction elsewhere. In contrast, organic synthesis prefers direct oxidation or reduction of the substrate without using complex and unstable cofactors. Nature also prefers solutions using abundant materials, i.e., using existing metabolic intermediates for synthesis and avoiding rare metals that may be hard to find in nature.

The combination of proteins as nature's versatile ligands with chemistry's catalytic metals, including metals not abundant in nature, has the potential to solve current problems in advanced organic synthesis (for a recent review see [3]).

1.1 Metal with Ligands Attached to Protein

The first approach to combine proteins and metal catalysts was to covalently link a protein with a metal–organic ligand complex (for reviews see [4, 5]). For example, three research groups created hybrid hydrogenation catalysts by covalently attaching a phosphorus ligand to biotin, which binds tightly to the protein avidin. In 1978

Wilson and Whitesides first embedded an achiral biotinylated rhodium–diphosphine moiety within the protein avidin [6]. This protein–phosphine–rhodium construct catalyzed the asymmetric hydrogenation of *N*-acetamindoacrylate with quantitative conversion and 41% ee. In 1999, Chan used an enantiopure biotinylated pyrphos–Rh(I) complex with avidin to catalyze enantioselective hydrogenation of itaconic acid with up to 48% ee [7]. In 2003 Ward and coworkers optimized this system and achieved high enantioselectivity (94% ee) [8]. They changed from avidin to strepavidin, which binds the biotin in a deeper pocket, and optimized the chemical linker to biotin. Ward and coworkers demonstrated the hydrogenation of α-acetamidoacrylic acid and α-acetamidocinnamic acid [9–11] and the enantioselective transfer hydrogenation of ketones with a different rhodium complex [12, 13]. Ward and coworkers also showed that mutagensis of the strepavidin could increase the activity and enantioselectivity of the catalyst [14]. While these experiments clearly demonstrate that attaching metal complexes to proteins can extend the catalytic range of enzymes, this approach still requires a phosphorus ligand and extensive optimization.

Complexes of metal + ligand + protein or DNA can also catalyze the Diels Alder cycloaddition or oxidations with hydrogen peroxide. Copper complexes bound to DNA catalyzed the Diels–Alder cycloaddition with up to 99% ee [15, 16]. Cu(phthalocyanine) complexed to serum albumin also catalyzed the enantioselective (98% ee) Diels–Alder reaction, but only with very high catalyst loading (10 mol%) and only with pyridine-bearing dienophiles (presumably to complex the copper) [17]. Achiral Cr(III) complexes or Mn(Schiff-base) complexes inserted into the active site of apomyoglobin variants catalyzed the sulfoxidation of thioanisole with up to 13 and 51% ee, respectively [18, 19]. A copper phenanthroline complex attached to the adipocyte lipid-binding protein catalyzed the enantioselective hydrolysis of esters and amides [20].

1.2 Proteins as Direct Ligands for Catalytic Metal Ions

In principle, binding a catalytic metal ion directly to a protein places it closer to the protein so that the protein can better control selectivity. In practice, binding a catalytic metal ion directly to a protein has rarely yielded an enantioselective catalyst. Rhodium complexed nonspecifically to human serum albumin (likely through the histidine side chains) catalyzed efficient hydroformylation (>500,000 turnovers), but without mention of enantioselectivity [21]. A Pd cluster trapped into the cavity of apo-ferritin (a complex of 24 subunits forming a hollow cage-like structure 12 nm in diameter that normally stores iron) catalyzed the size-selective hydrogenation of acrylamide derivatives, but was not enantioselective [22]. Yamamura and Kaiser replaced the zinc in carboxypeptidase with copper(II) to catalyze the slow air oxidation of ascorbate [23]. Da Silva and Ming replaced the two zinc ions in an aminopeptidase with copper ions to yield a good catalyst ($k_{cat} \sim 1\ s^{-1}$) for the air oxidation of 3,5-di-*tert*-butylcatechol [24]. No enantioselective reactions were reported.

Bakker et al. [25] replaced the zinc in thermolysin with anions such as molybdate, selenate, or tungstate to give an enzyme that catalyzed the nonenantioselective oxidation of thioanisoles with hydrogen peroxide. Van de Velde et al. [26] added a vanadate ion to the active site of phytase to create a catalyst for enantioselective oxididation of thioanisole to the sulfoxide in 66% ee. Selenosubtilisin (protease subtilisin where a selenoserine replaces the active-site serine) catalyzes the enantioselective reduction of hydroperoxides [27] with enantioselectivity >100 for one substrate.

Nature has also replaced a catalytic metal to create a new function. For example, rubredoxin oxidase contains an iron in the active site and catalyzes electron transfer. The amino acid sequence of β-lactamase is related to that of rubredoxin oxidase, indicating that they evolved from a common ancestor. β-Lactamase contains a zinc ion in the active site and detoxifies β-lactam antibiotics by hydrolysis of the β-lactam ring. Evolutionary pressure from the use of β-lactam antibiotics likely caused rubredoxin oxidase to bind a different metal to create a new function [28].

2 Carbonic Anhydrase

2.1 Structure

Carbonic anhydrases, also known as carbonate dehydratase and placed in enzyme classification 4.2.1.1, are zinc metalloproteins that catalyze the reversible hydration of carbon dioxide to bicarbonate (Eq. 1):

$$CO_2 + H_2O \overset{CA}{\rightleftharpoons} HCO_3^- + H^+ \quad (1)$$

The zinc ion activates a water molecule that reacts with carbon dioxide, or destabilizes bicarbonate in the reverse reaction. A hydrogen bond donor near the zinc ion positions the substrate water or bicarbonate ion.

Convergent evolution has yielded three different classes of carbonic anhydrases. Mammals contain α-CA, plants and certain bacterial contain β-CA, while archea contain γ-CA. The three classes of carbonic anhydrases differ in amino acid sequence and in their protein fold. Nevertheless, the active sites all contain a zinc ion (held by three histidine residues in the α- and γ-CA, and by one histidine and two cysteines in the β-CA) and a hydrogen bond donor near the zinc and presumably catalyze the reaction in a similar manner.

The best-studied carbonic anhydrases are the bovine and human α-carbonic anhydrases. They exist as isozymes (enzymes with the same function, but slightly different amino acid sequence) and the focus is on the most abundant one – isozyme II, abbreviated α-CAII. The bovine enzyme, isolated from red blood cells, is a byproduct of the meat industry. The human enzyme is a current drug target for glaucoma and a possible target for several other diseases (for a review see [29]). Fierke and coworkers cloned human α-CAII and expressed it in *E. coli*. Numerous mutants

have been created in the effort to dissect the role of the amino acid residues forming the active site.

α-CAII is a stable zinc metalloprotein containing no cysteine residues in a mostly β-sheet structure with a three-histidine binding site for the zinc ion (Fig. 1).

The active site of α-CAII is larger (~15 Å wide) than carbon dioxide (~4 Å) and contains a hydrophobic patch that binds a range of aromatic inhibitors as well as ester substrates (see below). The hydrophobic patches contribute 100- to1000-fold to the binding of hydrophobic ligands, regardless of their structure [32].

2.2 *Catalytic Promiscuity: Enantioselective Hydrolysis of Esters*

hCAII also shows a catalytically promiscuous activity – hydrolysis of activated esters such as *P*-nitrophenyl acetate (PNPA). The hydrolysis shows low enantioselectivity toward some esters, but high enantioselectivity ($E > 100$) toward *N*-acetyl

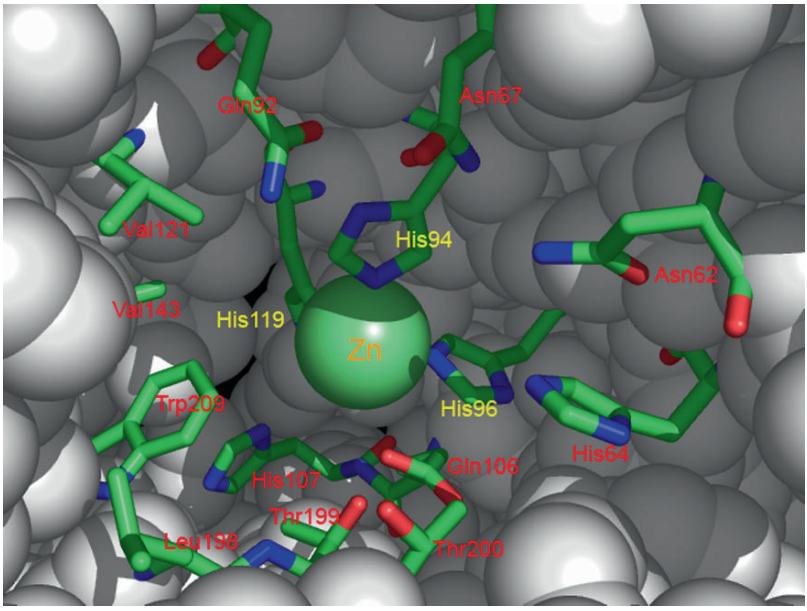

Fig. 1 Structure of the active site of human carbonic anhydrase isozyme II (hCAII) as revealed by X-ray crystallography [30]. Three histidine residues (His119, His94, His96) bind the zinc ion (*green ball*). Selected residues in the active site are shown as *sticks*, while the rest of protein is shown as *gray balls*. The hydrophobic patch lies on the *bottom left*, formed by Leu198, Trp209, Val143, and Val121. The X-ray structure of the CA[Mn] is similar [31]. Mutations at Asn62, His64, Thr200, or Thr199 (*bottom right*) decreased the enantioselectivity of hCAII[Mn]-catalyzed epoxidations of styrene or *p*-chlorostyrene, suggesting that the olefin and/or peroxybicarbonate may bind in these regions

phenylalanine methyl ester and several related compounds [33, 34]. This promiscuous esterase activity probably stems from the mechanistic similarity between hydration of carbon dioxide and hydrolysis of an ester (i.e., nucleophilic attack by a zinc-coordinated OH^- ion and the stabilization of the resulting oxyanionic intermediate). Indeed, many amidases and peptidase are zinc metallohydrolases with catalytic centers similar to carbonic anhydrase.

This ability of carbonic anhydrase to bind larger substrates and catalyze non-physiological reactions makes it likely that a carbonic anhydrase with a new metal ion could also bind substrates and catalyze new chemical reactions.

3 Replacement of the Active-Site Zinc in Carbonic Anhydrase with Manganese

3.1 Removal of the Active-Site Zinc Ion

Dialysis of carbonic anhydrase against a zinc chelate, 2,6-pyridinedicarboxylate, removes the active-site zinc leaving apo-carbonic anhydrase (Scheme 1) [35–37]. In our experiments [38], dialysis of carbonic anhydrase from bovine erythrocytes (a mixture of isoenzymes) against 2,6-pyridinedicarboxylate in acetate buffer at pH 5.5 removed 90–95 mol% of the zinc as shown by inductively coupled plasma atomic emission spectrometry (ICP-AES). This amount is similar to that removed previously for bovine [35–37] and human [39] carbonic anhydrase. Consistent with this removal of the active-site zinc, the apo-carbonic anhydrase lost 93–97% of the original catalytic activity for the hydrolysis of *p*-nitrophenyl acetate. Similar treatment of bovine carbonic anhydrase isoenzyme II (available commercially) and human carbonic anhydrase isoenzyme II gave the corresponding apo-enzymes.

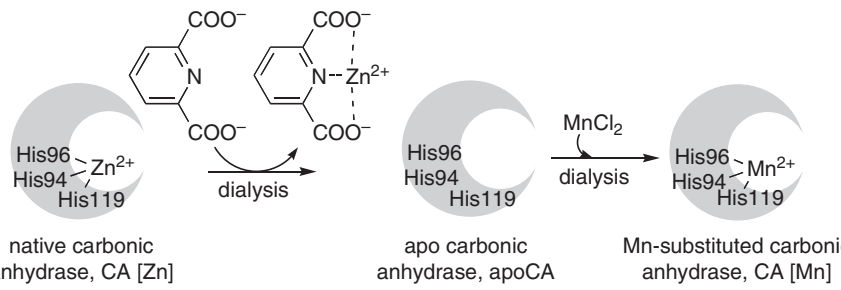

Scheme 1 Dialysis of carbonic anhydrase against a zinc chelate (2,6-pyridinedicarboxylate) removed 90–95% of the active-site zinc. Subsequent dialysis against Mn(II) yielded manganese-substituted carbonic anhydrase, CA[Mn]. Similar procedures yielded manganese-substituted carbonic anhydrase isoenzyme II (CAII[Mn]) and manganese-substituted human carbonic anhydrase isoenzyme II (hCAII[Mn])

The zinc ion does not contribute to protein folding or to protein stability of carbonic anhydrase.

3.2 Binding Manganese Ion to apo-Carbonic Anhydrase

Adding metal ions to apo-carbonic anhydrase creates a metal-substituted carbonic anhydrase. We focused on manganese-substituted carbonic anhydrase (CA[Mn] or CAII[Mn] for isoenzyme II and hCAII[Mn] for human carbonic anhydrase).

Metal analysis showed that manganese-substituted carbonic anhydrase contained up to 80 mol% manganese and 5–10 mol% zinc. The remaining 10–15 mol% was likely apo-carbonic anhydrase since manganese binds to apo-carbonic anhydrase less tightly than zinc (pK_D =< 3.4–4.0 for Mn(II) vs. 12.0 for Zn(II)) [39] and dissociates rapidly in the presence of zinc ($t_{1/2}$ = 27 min at pH 6.8) [35]. The samples showed 10–15% of original hydrolytic activity toward *p*-nitrophenyl acetate, likely due both to the remaining zinc and to hydrolytic activity of CA[Mn], which is 7–8% of the native carbonic anhydrase [40].

The X-ray crystal structure of native carbonic anhydrase shows a tetrahedral arrangement of ligand around the zinc ion – three histidines and one water molecule. In contrast, the X-ray crystal structure of hCAII[Mn] shows an octahedral coordination geometry with a bound water and sulfate ion [31].

4 Oxidation Reactions Catalyzed by Manganese-Substituted Carbonic Anhydrase

4.1 Oxidations Catalyzed by Free Manganese Ions in Solution

Manganese(II) salts catalyze a bicarbonate-mediated epoxidation of olefins with hydrogen peroxide [41–44]. No chiral ligands are involved, so the reactions are not enantioselective. The proposed mechanism is formation of peroxybicarbonate, followed by a manganese-catalyzed reaction with olefins to form epoxides. Support for this mechanism includes the analogous reaction of peroxycarboxylic acids with olefins to form epoxides. Manganese salts in bicarbonate buffer can also form hydroxyl and other radicals from hydrogen peroxide [45], but these are not believed to be prevalent in these epoxidations. The concentration of Mn(II) is approximately tenfold higher than the concentration of manganese-substituted carbonic anhydrase used in the experiments below.

The apo-carbonic anhydrase, as well as other manganese-chelating agents, inhibit this epoxidation. Adding apo-carbonic anhydrase to a manganese-catalyzed epoxidation of 4-vinylbenzoic acid inhibited the reaction [46]. This observation is consistent with the binding of free manganese by the apo-enzyme and a slower epoxidation

by CA[Mn] (440-fold slower, see below). The inhibition corresponded to an apparent dissociation constant of 6.5×10^{-7} M, which is approximately 100-fold tighter binding than reported previously for Mn(II) ions (pK_D ~ 3.4–4.0 according to [40]). Hydrogen peroxide may oxidize the manganese to a higher oxidation state during the epoxidation, thereby leading to tighter binding of the manganese.

4.2 Oxidation of the Dyes with Hydrogen Peroxide with CA[Mn]

CA[Mn] efficiently catalyzed the oxidation of *o*-dianisidine to the red quinonediimine with hydrogen peroxide (Scheme 2). This *o*-dianisidine oxidation is a common assay for peroxidase [47–50] or for peroxidase-based detection of hydrogen peroxide [51]. As control reactions, native zinc carbonic anhydrase showed <1% of the activity of CA[Mn], while the same concentrations of manganese(II) chloride and bicarbonate alone showed only 5% of the activity of CA[Mn]. Unlike other peroxidases [47–50], the CA[Mn]-catalyzed oxidation of *o*-dianisidine required bicarbonate and showed only 1.5% of the activity in the absence of bicarbonate.

Solutions of CA[Mn] inevitably contain some free manganese. At the same concentrations, CA[Mn] oxidizes *o*-dianisidine faster than free manganese, likely because carbonic anhydrase holds both reactants together. Adding up to ten equivalents of free manganese to solutions of CA[Mn] did not change the reaction rate or the product distribution.

This oxidation of *o*-dianisidine by hydrogen peroxide catalyzed by CA[Mn] is only 60- to 75-fold less efficient than the hydration of carbon dioxide catalyzed by native carbonic anhydrase (Table 1). The kinetic constants for the oxidation show an unexceptional catalytic constant (k_{cat}) of 17 s^{-1}, but a low apparent Michaelis constant (K_M) of 15 μM. These values give an apparent specificity constant (k_{cat}/K_M) of 1.1×10^6 $M^{-1}s^{-1}$. Similarly CAII[Mn] showed a k_{cat} of 140 s^{-1}, and a K_M of

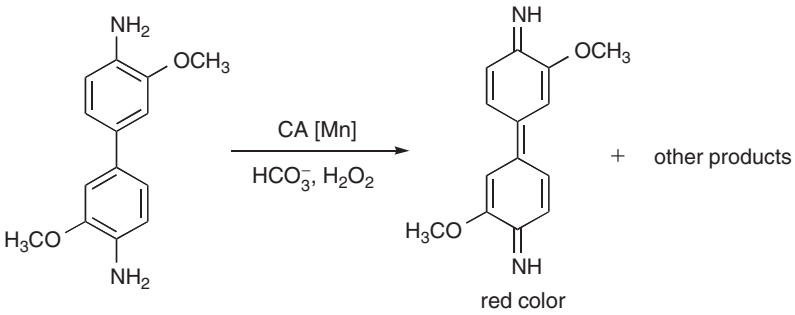

Scheme 2 CA[Mn] catalyzes the oxidation of *o*-dianisidine by hydrogen peroxide. Reaction conditions: 25 °C, BES buffer (0.1 M, pH 7.2), CA[Mn] (20 μM), sodium bicarbonate (8 mM), *o*-dianisidine (43 μM) and H_2O_2 (400 μM). The red color was monitored at 460 nm and is apparent by eye after a few seconds

Table 1 Kinetic constant for reactions catalyzed by carbonic anhydrase and peroxidases

Enzyme	Substrate	K_M (mM)	k_{cat} (s^{-1})	k_{cat}/K_M (M^{-1} s^{-1} × 10^6)
CA	CO_2	12,000	1,000,000	83
CA	HCO_3^-	26,000	400,000	15
CA[Mn]	*o*-Dianisidine[a]	15	17	1.1
CAII[Mn]	*o*-Dianisidine[a]	98	140	1.4
HRP	*o*-Dianisidine	11	630	57

CA carbonic anhydrase, *HRP* horseradish peroxidase

[a]Apparent kinetic constants for *o*-dianisidine were measured at fixed concentrations of 0.4 mM hydrogen peroxide for CA[Mn] (1.2 mM H_2O_2 for CAII[Mn]) and 8 mM sodium bicarbonate

98 μM, which corresponds to a specificity constant of 1.4×10^6 $M^{-1}s^{-1}$. For comparison, carbonic anhydrase shows a high catalytic constant for hydration of carbon dioxide (10^6 s^{-1}), but a low affinity for carbon dioxide (K_M = 12 mM) [51]. These values correspond to a specificity constant of 83×10^6 $M^{-1}s^{-1}$, which is only 60- to 75-fold higher than the value for the CA[Mn] or CAII[Mn]-catalyzed oxidation of *o*-dianisidine. In the reverse direction (dehydration of bicarbonate), the specificity constant is lower at 15×10^6 $M^{-1}s^{-1}$ [52]. This is only 11–14 times higher than the value for the CA[Mn] or CAII[Mn]-catalyzed oxidation of *o*-dianisidine. The tight binding of *o*-anisidine is likely due to the hydrophobic patch in the active site. Carbon dioxide is a much smaller and more polar molecule so it interacts more weakly with this hydrophobic patch.

The peroxidase activity of CA[Mn] is comparable to that for true peroxidases. For horseradish peroxidase (HRP)-catalyzed oxidation of *o*-dianisidine [49], k_{cat} = 630 s^{-1} and $k_{cat}/K_M = 57 \times 10^6$ $M^{-1}s^{-1}$, which is approximately 50-fold higher than for the CA[Mn]-catalyzed reaction. Another peroxidase, vanadium chloroperoxidase (VClPO), showed a lower k_{cat}/K_M of 0.31×10^6 $M^{-1}s^{-1}$ (approximately threefold lower than for CA[Mn]), but this comparison is imperfect since the VCIPO data is for a different substrate, 2,2 -azino-bis-(3-ethylbenzthiazoline-6-sulfonic acid) [53].

A related example of a hydrolase that also show redox activity is arginase. Arginase contains two manganese ions in the active site and catalyzes hydrolysis of the guanidinium group of arginine to ornithine and urea. Arginase also catalyzes a redox reaction – the disproportionation of hydrogen peroxide to water and oxygen [54]. This example does not require changing the metal ion since the hydrolase already contained manganese.

5 Enantioselective Epoxidation of Olefins with Hydrogen Peroxide with CA[Mn]

In 2006, two groups reported the enantioselective epoxidation of olefins by manganese-substituted carbonic anhydrase [38, 46]. In the presence of bicarbonate, hydrogen peroxide, and BES buffer, CA[Mn] also catalyzed the enantioselective

epoxidation of *p*-chlorostyrene (Scheme 3). This epoxidation was moderately enantioselective (E = 5 favoring the (*R*)-enantiomer) suggesting that oxygen transfer occurs in the active site. Like the oxidation of *o*-dianisidine above, the epoxidation required bicarbonate.

Replacing sodium bicarbonate with sodium phosphate or sodium acetate gave no epoxidation. Native zinc carbonic anhydrase containing zinc also showed no epoxidation. On the other hand, with a tenfold higher concentration of manganese(II) chloride than CA[Mn], about 1% conversion to racemic epoxide was observed after 16 h (see Table 2).

CA[Mn] also catalyzes the enantioselective epoxidation of other olefins (not shown in Table 2). Expoxidation of styrene (56% ee), 5-bromobutene (45% ee), and *trans*-β-methyl styrene (46% ee) was less enantioselective than epoxidation of *p*-chlorostyrene (67% ee) [38]. Epoxidation with CAII[Mn] (pure isoenzyme CAII instead of a mixture of isozymes) gave slightly higher enantioselectivity for 5-bromobutene (52% ee) and *trans*-β-methyl styrene (50.5% ee), but no change for styrene (57% ee) and *p*-chlorostyrene (66.5% ee).

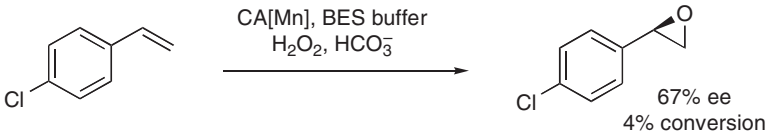

Scheme 3 Epoxidation of *p*-chlorostyrene catalyzed by CA[Mn]. Reaction conditions: 30 °C, 16 h, 0.1 M BES buffer, pH 7.2, 41 μM CA[Mn], 147 mM sodium bicarbonate, 7.4 mM *p*-chlorostyrene, and 7.4 mM H_2O_2

Table 2 Epoxidation of styrene and *p*-chlorostyrene by manganese-substituted carbonic anhydrases[a]

Substrate	Catalyst	Time (h)	ee (config.) (%)	Conversion (%)	TTN[b]
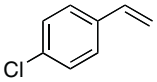	–	16	0	0	–
	$MnCl_2$[c]	16	0	1	–
	CA[Zn] + $MnCl_2$[c]	16	0	2	3.5
	CA[Mn]	4	66.5 (*R*)	1.8	4
	CA[Mn]	16	67 (*R*)	4	7
	CAII[Mn]	16	66.5 (*R*)	12.5	22
	hCAII[Mn][d]	16	55 (*R*)	6.5	9.5
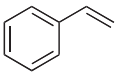	Cip [55, 56]	16	21 (*S*)	43	21.5
	CA[Mn]	16	56 (*R*)	6	10.5
	CAII[Mn]	16	57.5 (*R*)	12	21
	Cip [53]	16	35 (*S*)	18	9
	CPO [56, 57]	5	49 (*R*)	40	1,500

Cip peroxidase from *Coprinus cinereus*, *CPO* chloroperoxidase from *Caldariomyces fumago*

[a] Reaction conditions as in Scheme 3

[b] Total turnover is number of micromoles of epoxide formed per micromole of enzyme

[c] 412 μM $MnCl_2$

[d] 50 μM hCAII[Mn]

Two advantages of CA[Mn] are a broader substrate range and the lack of aldehyde side products. CA[Mn] catalyzed epoxidation of *trans*-β-methyl styrene (46% ee), but this substrate was not oxidized by CPO [57]. We did not detect any aldehyde side products in the CA[Mn] catalyzed epoxidations. In contrast, the CPO and CiP-catalyzed epoxidation of styrene formed 24% [57] and 52% [55] benzaldehyde side product. These aldehyde side products form simultaneously with epoxide during styrene epoxidation catalyzed by heme peroxidases [55]. Although the mechanism of aldehyde formation is unknown, this simultaneous formation of aldehyde suggests that it forms from a reaction intermediate of epoxidation. Since the mechanism of epoxidation for the CA[Mn] percarbonate reaction differs from that for the heme peroxidases, this different mechanism may account for the lack of aldehyde side products.

The two groups reported different effects of buffer on enantioselectivity. Fernández-Gacio et al. found no effect of buffer on enantioselectivity [46], but our group found that epoxidation was enantioselective only with an amino alcohol buffer [38]. A possible explanation is that our preparations contained traces of free manganese that catalyzed a nonenantioselective epoxidation. (Fernández-Gacio et al. used only half an equivalent of manganese relative to apo-carbonic anhydrase, while we used a full equivalent.) The amino alcohol could bind the free manganese and inhibit the nonenantioselective epoxidation. This hypothesis has not been tested.

An alternative hypothesis is that the amino alcohol induces enantioselectivity by binding to the active site and changing its shape. An X-ray structure shows that Tris buffer (an amino alcohol) binds to the hydrophobic patch in the active site of carbonic anhydrase [58]. Similar binding of other amino alcohols could restrict the orientation of *p*-chlorostyrene in the active site. This second hypothesis does not explain why Fernández-Gacio et al. found no effect of buffer on enantioselectivity.

The slower initial rate of epoxidation suggests that protein hinders access to manganese. The initial rate of the CA[Mn]-catalyzed epoxidation of *p*-chlorostyrene was slower than that for nonenzymatic manganese-dependent epoxidation catalysts (Table 3). The CA[Mn]-catalyzed formation of *p*-chlorostyrene epoxide is constant initially (time$\leq$4 h) and corresponds to a turnover frequency (TOF) of 0.013 min^{-1}. This value is 440-fold lower than the corresponding manganese/bicarbonate catalyst without the carbonic anhydrase ligand (5.7 min^{-1}). This slower reaction of the CA[Mn] catalyst is consistent with the notion that the protein hinders access of the olefin to the manganese reaction center, thereby imparting enantioselectivity to the epoxidation. Jacobsen's enantioselective epoxidation catalyst is also slower than free manganese/bicarbonate, 0.06 min^{-1} [59], but about 4.6 times faster than CA[Mn].

The conversion of all the CA[Mn]-catalyzed epoxidations were disappointingly low, with a maximum of 12.5%, which corresponds to a turnover number of 22 (22 moles of *p*-chlorostyrene epoxide formed per mole of CAII[Mn]). These turnover numbers are similar or higher than peroxidase from *Coprinus cinereus* (Cip) (*p*-chlorstyrene TTN = 21.5; styrene TTN = 9) [55], but not as high as those for chloroperoxidase from *Caldariomyces fumago* (CPO) (styrene TTN = 1500) [57]. Importantly, we did not observe any aldehyde byproducts during epoxidation, but heme peroxidases Cip and CPO formed up to 50% aldehyde byproducts.

Table 3 Turnover frequency during epoxidation of styrenes catalyzed by different catalysts with hydrogen peroxide as a source of oxygen

Substrate	Catalyst	TOF[a] (min^{-1})
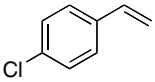	CA[Mn]/bicarbonate	0.013
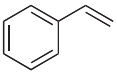	Chiral complex Mn(III)–salen	0.06[b]
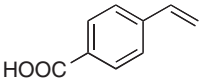	Mn(II)/bicarbonate	5.7[c]

[a]Turnover frequency is number of millimoles of epoxide formed per millimole of enzyme per minute

[b]From Kureshy et al. [59]

[c]Calculated from data in Lane and Burgess [41], Lane et al. [43], Tong et al. [44] and Yim et al. [45]; reaction conditions: 0.2 mM $MnSO_4$, 20 mM 4-vinylbenzoic acid, 100 mM bicarbonate, 10 equiv of H_2O_2

The timecourse of the CA[Mn]-catalyzed epoxidation of olefins showed good activity over the first 4 h, followed by a rapid decrease. For example, the turnover number of CA[Mn] was 4 over the first 4 h, but increased to only 7 over the next 12 h. This result and the mass spectral analysis suggest that CA[Mn] degrades during epoxidation.

5.1 Possible Mechanism of Epoxidation

The likely mechanism of the CA[Mn]-catalyzed epoxidation of olefins is similar to that proposed by Burgess for free manganese involving peroxycarbonate as the key intermediate [41, 43–45]. CA[Mn] forms a stable manganese–bicarbonate complex in the active-site [60]. Hydrogen peroxide may add to carbonyl of this bicarbonate complex and displace water thereby forming a peroxycarbonate, which then may epoxidize a bound olefin. In contrast, heme peroxidases catalyze epoxidations either by a radical mechanism or by a ferryl-oxygen transfer mechanism [55].

Site-directed mutagenesis supports the proposal that epoxidation occurs in the active site of hCAII[Mn]. Changing three amino acid residues in the active site to a smaller amino acid residue (alanine) decreased the enantioselectivity of epoxidation. hCAII[Mn] variants containing an Asn62Ala, His64Ala or a Thr200Ala substitution showed lower enantioselectivity (0–13% ee) than the wild type (55% ee). This drop in enantioselectivity suggests that these three residues may orient *p*-chlorostyrene during catalysis. Mutations at Thr199 either decreased catalytic activity (Thr199Glu, Thr199Asp) or decreased enantioselectivity (Thre199Ser, Thr199Ala).

Computer modeling shows that both the olefin and peroxycarbonate can fit into the active site of carbonic anhydrase in an orientation consistent with the observed enantioselectivity [38]. Thus, the working hypothesis is that peroxybicarbonate forms from hydrogen peroxide and bicarbonate in the active site of CA[Mn] and then the manganese-bound peroxybicarbonate transfers an oxygen to the olefin bound in the active site.

6 Limitations and New Directions

6.1 Oxidative Degradation Limits the Turnover Number

As the epoxidation proceeds, the ESI-MS spectrum of CA[Mn] broadens and after 16 h shows no clear protein peak [38]. This disappearance suggests oxidation of the protein during epoxidation. CA[Mn] was stable to added *m*-chloroperoxybenzoic acid or hydrogen peroxide (0.01 M, 8 h) and showed no mass increase corresponding to added oxygen atoms. This concentration of oxidants was twice as high as during epoxidation. This stability to added oxidant suggests that intermediates generated during catalysis, possibly radicals, cause the degradation of bovine carbonic anhydrase.

Soluble manganese complexes are powerful bleaching agents using hydrogen peroxide and may involve radical intermediates [61, 62]. Such radical intermediates may also form in the CA[Mn]-catalyzed epoxidation and damage the protein. It may be possible to eliminate this degradation using protein engineering, since protein engineering yielded a more than 100-fold stabilization of a heme peroxidase toward oxidative degradation [63].

Because of this catalyst degradation, organometallic catalysts are currently the best synthetic reagents for enantioselective epoxidation of olefins. Chiral Mn(III)-salen complexes yield up to 99% ee for *cis*-disubstituted, tri- and tetra-substituted alkenes [62], but the best results require less desirable oxidants – iodosyl benzene or hypochlorite. Other catalysts accept a more limited substrate range: the Sharpless–Katsuki titanium-tartrate ester [65] for allylic alcohols and the Juliá–Colonna epoxidation for α,β-unsaturated ketones [66].

6.2 Potential to Bind Second and Third Row Transition Metals

Although the atomic number of second and third row transition metals is much higher than zinc, the atomic radii are remarkably similar. Zinc has an atomic radius of 1.35 Å, while the second row transition elements ruthenium, rhodium, and palladium have atomic radii of 1.30, 1.35, and 1.40 Å, respectively. The third row transition element iridium has an atomic radius of 1.35 Å. These similar atomic radii suggest that a binding site that binds a zinc ion will also bind some second and third row transition metals. In comparison, manganese has an atomic radius

of 1.40 Å. Second and third row transition metal catalyze a wide range of reactions including hydrogenation, hydroformylation, and olefin metathesis.

Preliminary results indeed show that ruthenium, rhodium, and iridium bind to apo-carbonic anhydrase, but they bind to many sites on the protein since we measured a metal-to-protein ratio of approximately seven. We hypothesize that the metals bind both to the active site and to the protein surface. Removing amino acids with electron donor atoms in the side chain (e.g., histidine) may restrict the binding to the active site and permit stereoselective catalysis [67].

6.3 Other Carbonic Anhydrases

The other structural classes of carbonic anhydrases may also serve as protein ligands. The active site of the β-CA is the approximate mirror image of that for α-CA. Nature's substrates, carbon dioxide and biocarbonate, are achiral so this mirror-image relationship is only an accident of convergent evolution. However, for enantioselective reactions, these two enzymes may form an enantiocomplementary pair and may catalyze reactions with opposite enantioselectivity.

Other metalloenzyme proteins are also candidates for metal substitutions to create new catalytic activities.

References

1. Bäckvall J-E (ed) (2004) Modern oxidation methods. Wiley-VCH, New York, p 295
2. Strukul G (ed) (1992) Catalytic oxidation with hydrogen peroxide as oxidant. Springer, Boston
3. Lu Y (2005) Curr Opin Chem Biol 9:118
4. Letondor C, Ward TR (2006) ChemBioChem 7:1845
5. Thomas CM, Ward TR (2005) Chem Soc Rev 34:337
6. Wilson ME, Whitesides GM (1978) J Am Chem Soc 100:306
7. Lin CC, Lin CW, Chan ASC (1999) Tetrahedron: Asymmetry 10:1887
8. Collot J, Gradinaru J, Humbert N, Skander M, Zocchi A, Ward TR (2003) J Am Chem Soc 125:9030
9. Skander M, Humbert N, Collot J, Gradinaru J, Klein G, Loosli A, Sauser J, Zocchi A, Gilardoni F, Ward TR (2004) J Am Chem Soc 126:1441
10. Skander M, Malan C, Ivanova A, Ward TR (2005) Chem Commun 2005:4815
11. Ward TR (2005) Chem Eur J 11:3798
12. Letondor C, Humbert N, Ward TR (2005) Proc Natl Acad Sci USA 102:4683
13. Letondor C, Pordea A, Humbert N, Ivanova A, Mazurek S, Novic M, Ward TR (2006) J Am Chem Soc 128:8320
14. Klein G, Humbert N, Gradinaru J, Ivanova A, Gilardoni F, Rusbandi UE, Ward TR (2005) Angew Chem Int Ed 44:7764
15. Roelfes G, Feringa BL (2005) Angew Chem Int Ed 44:3230
16. Roelfes G, Boersma AJ, Feringa BL (2006) Chem Commun 2006:635
17. Reetz MT, Jiao N (2006) Angew Chem Int Ed 45:2416
18. Carey JR, Ma SK, Pfister TD, Garner DK, Kim HK, Abramite JA, Whang Z, Guo Z, Lu Y (2004) J Am Chem Soc 126:10812

19. Ohashi M, Koshiyama T, Ueno T, Yanase M, Fujii H, Watanabe Y (2003) Angew Chem Int Ed 42:1005
20. Ory JJ, Mazhary A, Kuang H, Davies RR, Distefano MD, Banaszak LJ (1998) Prot Eng 11:253
21. Bertucci C, Botteghi C, Giunta D, Marchetti M, Paganelli S (2002) Adv Synth Catal 344:556
22. Ueno T, Suzuki M, Goto T, Matsumoto T, Nagayama K, Watanabe Y (2004) Angew Chem Int Ed 4:2527
23. Yamamura K, Kaiser ET (1976) J Chem Soc Chem Commun 1976:830
24. da Silva GFZ, Ming L-J (2005) J Am Chem Soc 127:16380
25. Bakker M, van Rantwijk F, Sheldon RA (2002) Can J Chem 80:622
26. van de Velde F, Könemann L, van Rantwijk F, Sheldon RA (1998) Chem Commun 1998:1891
27. Haering D, Schueler E, Adam W, Saha-Moeller CR, Schreier P (1999) J Org Chem 64:832
28. Gomes CM, Frazão C, Xavier AV, Legall J, Teixeira M (2002) Prot Sci 11:707
29. Supuran CT (2007) Curr Topics Med Chem 7:825
30. Eriksson AE, Kylsten PM, Jones TA, Liljas A (1998) Proteins 4:283
31. Håkansson K, Wehnert A, Liljas A (1994) Acta Crystallogr D Biol Crystallogr 50:93
32. Jain A, Whitesides GM, Alexander RS, Christianson DW (1994) J Med Chem 37:2100
33. Chênevert R, Letourneau M (1990) Can J Chem 68:314
34. Gould SM, Tawfik DS (2005) Biochemistry 44:5444
35. Kidani Y, Hirose J (1976) J Biochem 79:43
36. Kidani Y, Hirose J (1977) J Biochem 81:1383
37. Wilkins RG, Williams KR (1974) J Am Chem Soc 96:2241
38. Okrasa K, Kazlauskas RJ (2006) Chem Eur J 12:1587
39. McCall KA, Fierke CA (2004) Biochemistry 43:3979
40. Lanir A, Gradstajn S, Navon G (1975) Biochemistry 14:242
41. Lane BS, Burgess K (2001) J Am Chem Soc 123:2933
42. Lane BS, Burgess K (2003) Chem Rev 103:2457
43. Lane BS, Vogt M, DeRose VJ, Burgess K (2002) J Am Chem Soc 124:11946
44. Tong K-H, Wong K-Y, Chan TH (2003) Org Lett 5:3423
45. Yim MB, Berlett BS, Chock PB, Stadtman ER (1990) Proc Natl Acad Sci USA 87:394
46. Fernández-Gacio A, Codina A, Fastrez J, Riant O, Soumillion P (2006) ChemBioChem 7:1013
47. Claiborne A, Fridovich I (1979) Biochemistry 18:2324
48. Keyhani J, Keyhani E, Zarchipour S, Tayefi-Nasrabadi H, Einollahi N (2005) Biochim Biophys Acta 1722:312
49. Ugarova NN, Lebedeva OV, Berezin V (1981) J Mol Catal 13:215
50. Zou P, Schrempf H (2000) Eur J Biochem 267:2840
51. Gabler M, Hensel M, Fisher L (2000) Enzym Microb Technol 27:605
52. Kernohan JC (1965) Biochim Biophys Acta 96:304
53. ten Brink HB, Dekker HL, Schoemaker HE, Wever R (2000) J Inorg Biochem 80:91
54. Sossong TM, Khangulov SV, Cavalli RC, Soprano DR, Dismukes GC, Ash DE (1997) J Biol Inorg Chem 2:433
55. Tuynman A, Spelberg JL, Kooter IM, Schoemaker HE, Wever R (2000) J Biol Chem 275:3025
56. Patel R (ed) (2000) Stereoselective biocatalysis. Marcel Dekker, New York
57. Zaks A, Dodds DR (1995) J Am Chem Soc 117:10419
58. Green MK, Vestling MM, Johnston MV, Larsen BS (1998) Anal Biochem 260:204
59. Kureshy RI, Khan NH, Abdi SHR, Singh S, Ahmed I, Shukla RS, Jasra RV (2003) J Catal 219:1
60. Led JJ, Neesgaard E, Johansen J (1982) FEBS Lett 147:74
61. Hage R, Iburg JE, Kerschner J, Koek JH, Lempers ELM, Martens RJ, Racherla US, Russell SW, Swarthoff T (1994) Nature 369:637
62. Kuhne L, Odermatt J, Wachter T (2000) Holzforschung 54:407

63. Cherry JR, Lamsa MH, Schneider P, Vind J, Svendsen A, Jones A, Pedersen AH (1999) Nature Biotechnol 17:379
64. Abel EW, Stone FGA, Wilkinson G (ed) (1995) Comprehensive organometallic chemistry II, vol 12. Pergamon, New York, p 1097
65. Ojima I (ed) (2000) Catalytic asymmetric synthesis, 2nd edn, vol 6A. Wiley-VCH, New York, p 231
66. Carrea G, Colonna S, Kelly DR, Lazcano A, Ottolina G, Roberts SM (2005) Trends Biotechnol 23:507
67. Jing Q, Okrasa K, Kazlauskas RJ (2008) Chem Eur J, accepted.

Top Organomet Chem (2009) 25: 63–92
DOI:10.1007/3418_2008_12

Directed Evolution of Stereoselective Hybrid Catalysts

Manfred T. Reetz

Abstract Whereas the directed evolution of stereoselective enzymes provides a useful tool in asymmetric catalysis, generality cannot be claimed because enzymes as catalysts are restricted to a limited set of reaction types. Therefore, a new concept has been proposed, namely directed evolution of hybrid catalysts in which proteins serve as hosts for anchoring ligand/transition metal entities. Accordingly, appropriate genetic mutagenesis methods are applied to the gene of a given protein host, providing after expression a library of mutant proteins. These are purified and a ligand/transition metal anchored site-specifically. Following en masse *ee*-screening, the best hit is identified, and the corresponding mutant gene is used as a template for another round of mutagenesis, expression, purification, bioconjugation, and screening. This allows for a Darwinian optimization of transition metal catalysts.

Key words Bioconjugation, Directed evolution, Enantioselectivity, Hybrid catalysts, Hydrogenation, Transition metal catalysis

Contents

M.T. Reetz(✉)
Max-Planck-Institut für Kohlenforschung, Kaiser-Wilhelm-Platz 1, 45470 Mülheim/Ruhr, Germany
e-mail: reetz@mpi-muelheim.mpg.de

Abbreviations

BINOL	Binaphthol
BSA	Bovine serum albumin
CAST	Combinatorial active-site saturation test
cod	1,5-Cyclooctadiene *ee* Enantiomeric excess
epPCR	Error-prone polymerase chain reaction
ESI-MS	Electro-spray ionization mass spectrometry
ESI-TOF MS	Electro-spray ionization time of flight mass spectrometry
HSA	Human serum albumin
IPTG	Isopropyl-β-D-thiogalactopyranoside
ISM	Iterative saturation mutagenesis
L-BAPNA	*N*-Benzoyl-l-arginine-*p*-nitroanilide
LB-medium	Luria–Bertani medium
MALDI-TOF-MS	Matrix assisted laser desorption ionization time of flight mass spectrometry
MS	Mass spectrometry
PCR	Polymerase chain reaction
SDS PAGE	Sodium dodecylsulfate polyacrylamide gel electrophoresis
TB-medium	Terrific broth
WT	Wild-type

1 Introduction

Asymmetric catalysis is a challenging field of research in synthetic organic chemistry. When applying this form of catalysis, chemists have several options, namely transition metal catalysis [1–5], organocatalysis [6–10] or biocatalysis [11–14]. The best choice depends on a number of factors, including the nature of the immediate goal, cost of catalysts, catalyst activity, enantioselectivity, and stability under operating conditions as well as recyclability. When engaging in the challenging research directed towards developing *new* synthetic chiral catalysts, success depends upon the quality of design, but also on experience, trial-and-error, and serendipity. Combinatorial asymmetric catalysis, based on the design and use of modular ligands, has been implemented experimentally with some degree of success [15–23], including the use of mixtures of monodentate P-ligands [24–26]. This approach was reviewed recently [25].

The exploitation of enzymes in synthetic organic chemistry, both in academic and industrial laboratories, has increased dramatically during the past 20 years [11–14]. The realization that many of them can be used in organic solvents is one of the important advances [27]. Moreover, rapid progress in biotechnological engineering and microbiology has contributed heavily to success in making biocatalysis practical, and more progress can be expected in the near future [28]. Nevertheless, the traditional problem in applied enzymology was not solved until the 1990s,

namely the limited substrate scope and poor enantioselectivity that enzymes often display. Rational design based on site-specific mutagenesis had been shown to be successful in some cases, but the process is far from general due to the structural complexity of proteins [29–33].

In 1997, a fundamentally new approach to asymmetric catalysis was proposed and implemented experimentally, namely the directed evolution of enantioselective enzymes for use in synthetic organic chemistry [34–37]. It is based on the appropriate combination of random gene mutagenesis, expression, and high-throughput screening. Previous efforts in directed evolution had focused on engineering thermostability and stability toward hostile solvents [38–44]. In the case of directed evolution of enantioselective enzymes, high-throughput *ee*-assays had to be developed first [19, 45–47]. Using the known molecular biological methods such as error-prone polymerase chain reaction (epPCR), saturation mutagenesis, and/or DNA shuffling, the hits of the initial mutant libraries are used as templates for another round of mutagenesis/expression/screening. The process can be repeated as many times as necessary until the desired degree of enantioselectivity has been reached (Fig. 1) [34–37]. Typically, in each cycle several thousand mutants are generated, but larger libraries are possible.

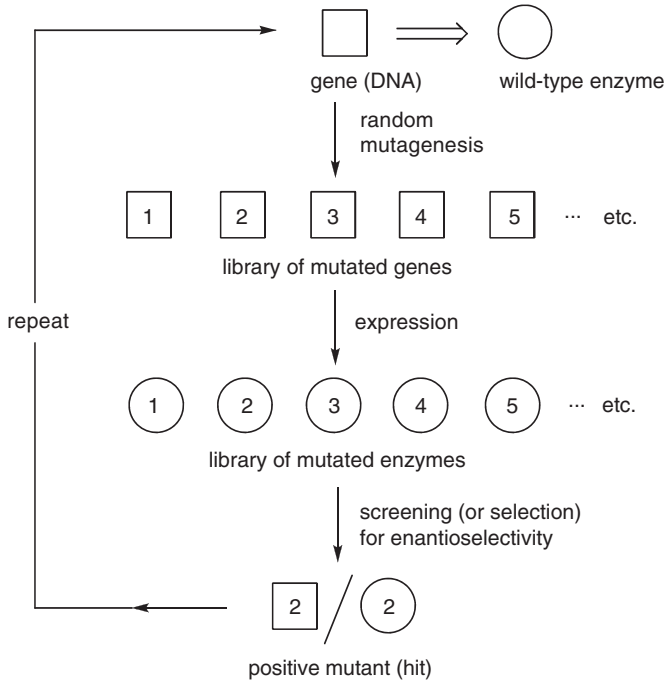

Fig. 1 Strategy for directed evolution of an enantioselective enzyme [34–37]

This new approach to asymmetric catalysis was applied to a variety of enzymes, including lipases, esterases, epoxide hydrolases, nitrilases, hydantoinases, aldolases, and monooxygenases, as summarized in a recent review [37]. However, it became apparent that the efficiency in probing protein sequence space had to be improved, as in the directed evolution of other catalyst properties such as stability [38–44]. A recent development is iterative saturation mutagenesis (ISM) [48, 49], which is a symbiosis of rational design and combinatorial saturation mutagenesis. Accordingly, a Cartesian view of the protein is considered in which predetermined sites composed of one, two, or three amino acid positions are chosen for saturation mutagenesis, based on rational considerations using structural information (X-ray or homology model) [48, 49]. Saturation mutagenesis is a molecular biological method with which amino acid randomization at one, two, three, or more positions is induced simultaneously, meaning the introduction of all 20 proteinogenic amino acids [38–44]. The principle of ISM is illustrated schematically in Fig. 2, in which four sites A, B, C, and D are shown (arbitrarily). Each site may be composed of one, two, or three (or more) amino acid positions. Following the generation of the original saturation mutagenesis libraries, the upward climb in the fitness landscape can proceed in several pathways by using the gene of a given hit from one library as a template to perform another cycle of saturation mutagenesis at the other sites, and so on. The nature of the to-be-improved catalytic property determines the criterion for choosing the appropriate sites A, B, C, D etc.

The crucial criterion for choosing the saturation mutagenesis sites in the case of enantioselectivity or substrate scope is the so-called combinatorial active-site saturation test (CAST) [48, 50]. Accordingly, all sites having amino acids with side-chains next to the binding pocket are considered, not just one or two sites as in previous studies regarding focused libraries [35, 38–44]. Thus, *CASTing is the systematic generation of focused libraries around the complete binding pocket.* Consequently, iterative CASTing is an embodiment of ISM that is useful for enhancing enantioselectivity and influencing the substrate scope of enzymes. CASTing has been used to evolve enantioselective hydrolases [48, 49] and mono-oxygenases [50].

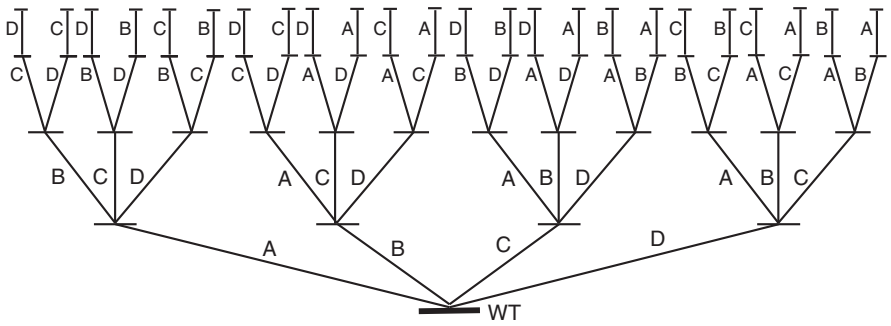

Fig. 2 Iterative saturation mutagenesis (ISM) employing four sites *A*, *B*, *C*, and *D*, each site in a given upward pathway being visited only once [48, 49]

Nowadays directed evolution of enantioselective enzymes is well established as a method to create biocatalysts for asymmetric organic transformations [34–37, 48–50]. Numerous academic and industrial studies have appeared. Nevertheless, this novel approach has clear limitations, the most important one being the fact that enzymes cannot catalyze numerous synthetically important transformations known to be possible by transition metal catalysis [1–5, 51, 52]. Due to these limitations, the notion of directed evolution of hybrid catalysts was proposed in 2001/2002 [53–61] (Fig. 3). It had been known for decades that achiral ligand/metal moieties can be anchored covalently or non-covalently to proteins acting as a host [62–77]. Accordingly, a given system provides a single chiral catalyst, the wild-type (WT) protein providing a defined local environment around the synthetic catalytically active transition metal center.

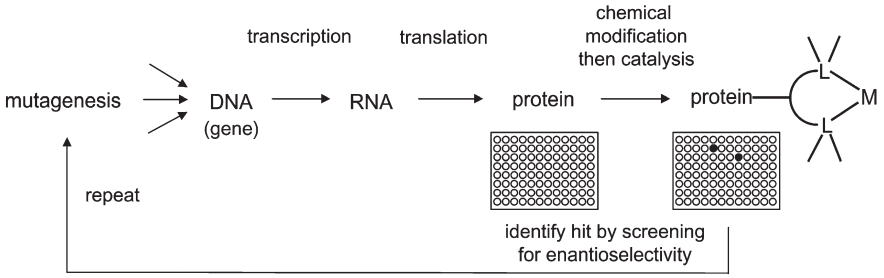

Fig. 3 Concept of directed evolution of hybrid catalysts showing the flow of genetic information from the gene to transition metal hybrid catalysts [53–61]

There are three ways to introduce an appropriate transition metal center into a host protein, which can be an enzyme or a protein having no catalytic function (Fig. 4):

1. Covalent attachment utilizing an appropriate ligand/metal moiety, usually at a cysteine thiol function by S_N2-reaction or Michael addition, which are known bioconjugation techniques [78, 79]
2. Non-covalent anchoring ,as for example in the Whitesides system utilizing avidin (or streptavidin) and a biotinylated Rh/diphosphine moiety [80, 81]
3. Direct interaction of a transition metal salt with a designed binding site composed of appropriate amino acid side-chains in a host protein (Reetz et al., unpublished results).

The general concept of directed evolution of hybrid catalysts as illustrated schematically in Fig. 3 offers exciting perspectives, but also entails challenges when attempting to implement it experimentally. Among the perspectives is not only the control of enantio-, diastereo-, and/or regioselectivity, but also the possibility of enhancing the activity of a transition metal catalyst as such. Relevant is Pauling's postulate that the appropriate protein environment stabilizes the transition state of enzyme-catalyzed transformations. Among the serious challenges (problems!) inherent in applying the concept in Fig. 3 is the need to choose a host protein that can be expressed in large amounts. In contrast to classical directed evolution, which requires only

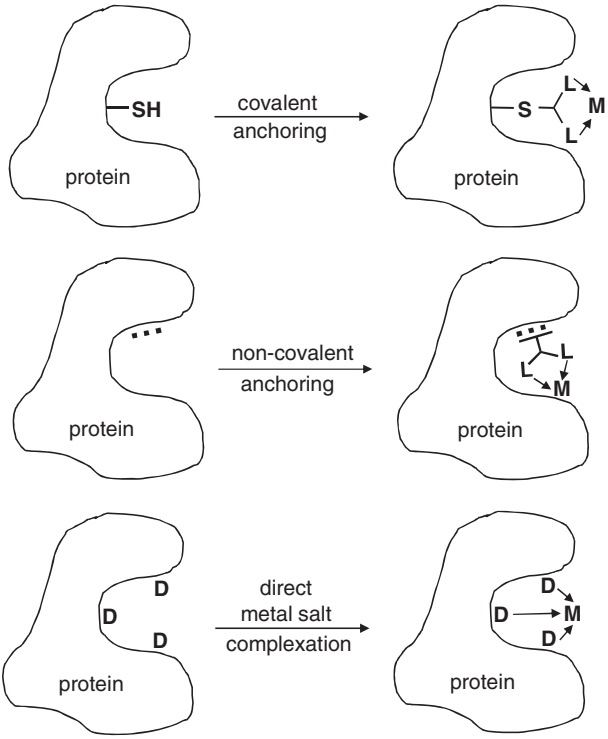

Fig. 4 Three strategies for introducing transition metals (M) site-specifically in protein hosts

small amounts of enzymes in the 1–2 mL wells of microtiter plates [34–44], much larger amounts of protein are needed in the hybrid protein system because synthetic catalysts are much less active than enzymes. Moreover, a purification step prior to bioconjugation is necessary, because foreign protein is present in the supernatants. Finally, bioconjugation should be a smooth and (ideally) quantitative step. Due to these problems, it has taken 5 years from the date of conception [53, 54] to the first example of proof-of-principle [82]. Most of the research has been devoted to establishing appropriate platforms for applying the process of directed evolution. This chapter reviews the recent efforts in this new area of catalysis.

2 Covalent Anchoring of Ligands/Transition Metals in the Cavities of Proteins

As already pointed out, prior to the suggestion of directed evolution of enantioselective hybrid catalysts (Fig. 4) [53–61], numerous studies regarding the introduction of cofactors in foreign proteins had already appeared [62–77]. The most popular

anchoring point is the nucleophilic thiol function of cysteine, as shown by the seminal studies of Kaiser [70], Hilvert [71], Distefano [62] and others, generally using wild-type (WT) papain, which is a cystein-protease. This and similar important work has been reviewed earlier [62], and only new developments relevant to the directed evolution concept will be treated here. However, the older papain-based systems as well as other proteins that have previously been shown to be scaffolds for bioconjugation with ligands/metals [62] can also be considered for directed evolution, the intriguing systems of Watanabe [75] and of Lu [83–86] being one of several possibilities.

2.1 Papain as the Host Protein

Papain is a commercially available cysteine-protease isolated from the papaya fruit *Carica papaya* [87]. The crystal structure of papain is shown in Fig. 5, featuring the catalytic triad Cys25, His159, and Asn175 as well as the C- and N-termini [87]. Mechanistically, Asn175 activates His159, which in turn activates Cys25 by deprotonation via a proton shuttle. The activated Cys25 then attacks the amide bonds of proteins with formation of the respective oxyanion, which is followed by cleavage of the protein chain. In addition to Cys25, papain harbors six other cysteines that are not catalytically active. Thus, appropriate electrophiles react exclusively at Cys25, as shown by older publications. When working with papain, it is important

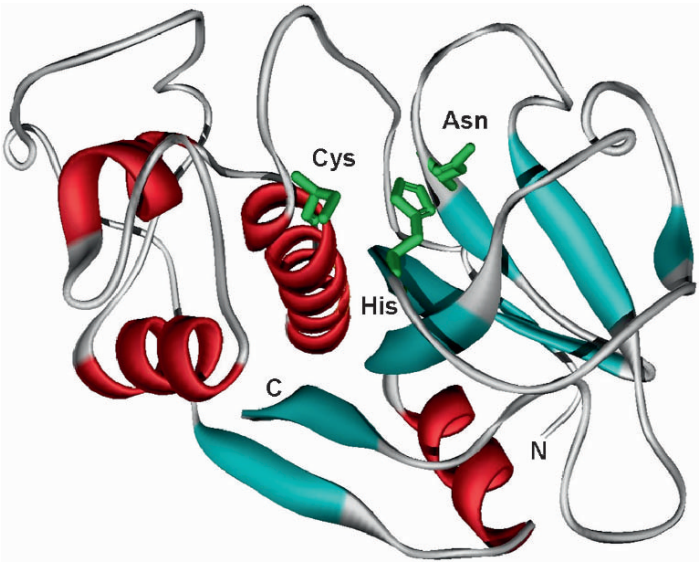

Fig. 5 Crystal structure of papain [87], showing the catalytic triad composed of cysteine 25 (Cys), histidine 159 (His) und asparagine 175 (Asn) as well as the C-and N-termini

to remember that most commercial forms occur as a mixture of two forms. Cys25 can either occur as a free thiol or in the disulfide form (dimer). Therefore, the material needs to be activated, e.g., by the addition of an excess of a water-soluble thiol such as cystein, which cleaves the disulfide bond. Gel filtration or affinity chromatography then delivers active papain in pure form. In order to check whether the desired bioconjugation is effective, a simple photometric test for proteolytic activity using *N*-benzoyl-l-arginine-*p*-nitroanilide (l-BAPNA) can be applied [53–61].

Two recent examples of papain bioconjugation with formation of potential hybrid catalysts are shown in Figs. 6 and 7, featuring a manganese salen catalyst and dipyridyl complexes of copper, palladium, and rhodium, respectively [53, 58].

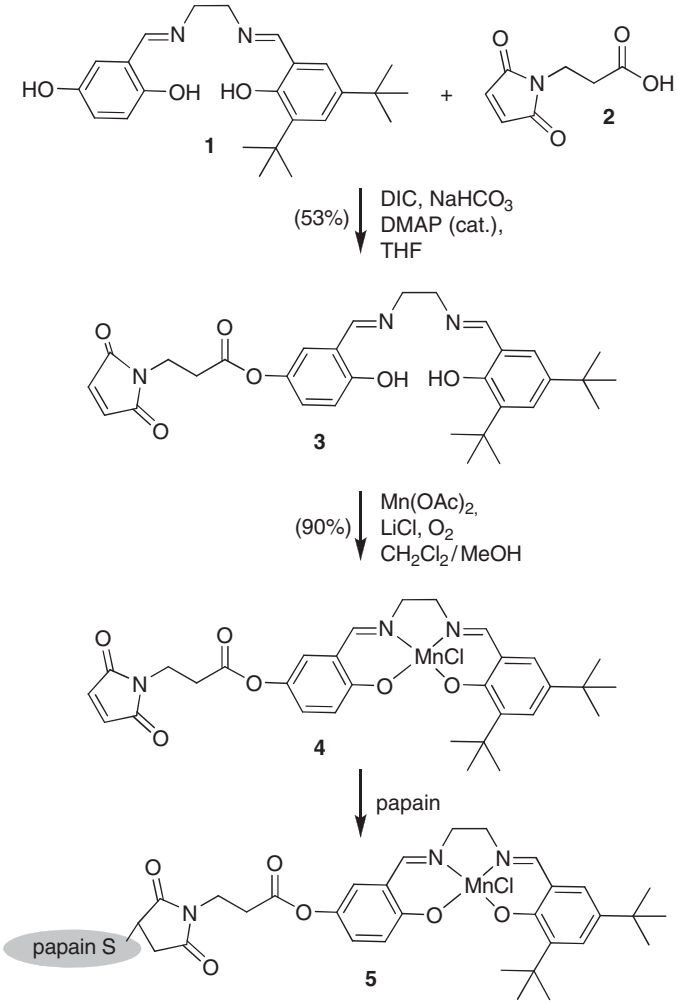

Fig. 6 Papain-based bioconjugation involving a Mn-salen complex [53, 60]

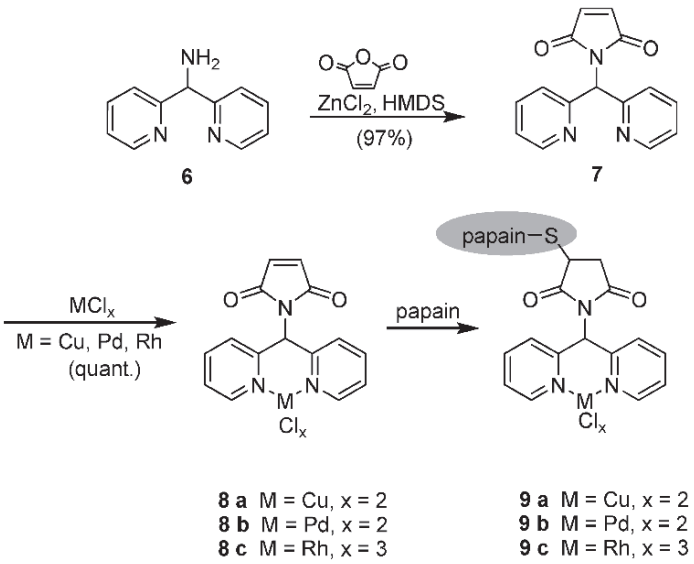

Fig. 7 Papain-based bioconjugation involving Cu-, Pd-, and Rh-dipyridyl complexes [53, 58]

In all cases it was demonstrated that reaction at Cys25 had occurred essentially quantitatively, as proven by the photometric l-BAPNA test. However, this does not prove that bioconjugation has occurred in the expected form. For example, it is conceivable that cysteine attacks the metal directly. Thus, further characterization, especially of the manganese salen hybrid catalyst (Fig. 6), was performed carefully using ESI-MS, UV/Vis spectroscopy and capillary electrophoresis, which proved to be successful [58].

The manganese salen hybrid catalyst was then tested in the sulfoxidation of thio-ether **10** and epoxidation of olefin **12** employing dilute aqueous H_2O_2 [57].

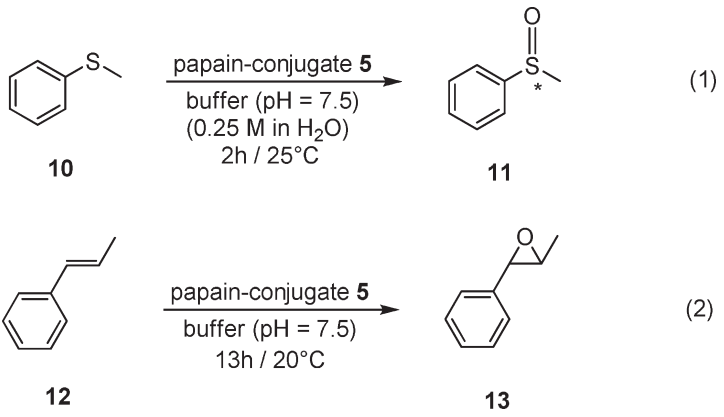

In both cases conversions of about 30% were observed under set conditions, which were not optimized, the products **11** and **13** showing no significant enantiomeric enrichment (*ee* <10%) [57]. The lack of significant *ee* does not surprise, because there is no reason to expect the WT papain to provide the proper local environment for high enantioselectivity in these reactions. However, it was shown that the respective bioconjugates are in fact active catalysts. For example, a control experiment in which the saturated succinyl analog of **4** was added to papain and the mixture used as a catalyst showed that only 12% conversion occurs in a slower reaction [57]. Apparently the Mn-salen complex positioned site selectively via covalent bioconjugation constitutes a more active catalyst than a freely moving analog. Thus, several reasons speak for the potential use of papain as a host protein for the concept of directed evolution of hybrid catalysts (Fig. 3), including the availability of an adequate expression system. However, a system for en masse purification needs to be developed before libraries of mutant hybrid catalysts can be produced by bioconjugation of mutant papains.

Irrespective of the latter problem, papain has been used recently as a host for a Rh-complex (Fig. 8) [88]. The complex comprises a monophosphite, a type of ligand that had previously been shown to be well suited for asymmetric Rh-catalyzed olefin-hydrogenation (as BINOL derivatives) [24, 89, 90]. Bioconjugate **15** was characterized by ESI-MS, and then treated with an excess (8 equivalents) of $Rh(cod)_2BF_4$ to form complex **16** as indicated by ESI-MS analysis [88]. However, other products were also shown to be present. Indeed, an excess of rhodium was used because it had been reported earlier that histidine, methionine, tryptophan, and cysteine bind Rh(II). This state of affairs underlines the potential problems that may arise when working with hybrid catalysts. The ligand system chosen should bind the metal so strongly that other donor sites in the protein cannot compete. In the present case an active hydrogenation system was created, but it was not unambiguously shown that a single Rh-species is in fact present (even after purification). Moreover, once the second cod-ligand has been cleaved by H_2 leading to the actual active catalyst, further Rh migration may occur. It was reported that racemic product is formed when hydrogenating a prochiral olefin [88].

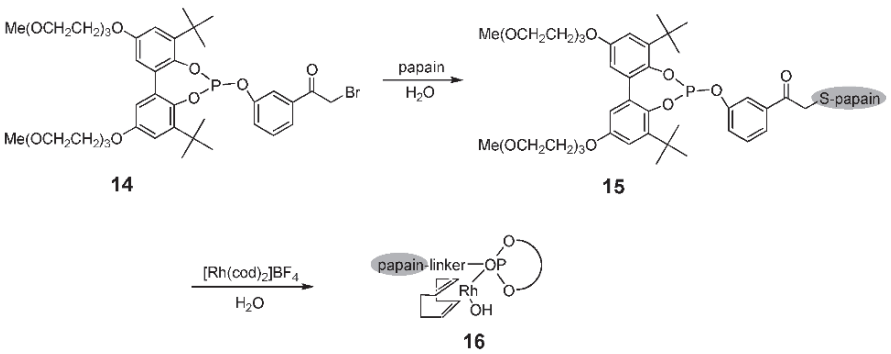

Fig. 8 Bioconjugation of papain with formation of an Rh-based hybrid catalyst [88]

2.2 Lipases as Host Proteins

A different and potentially likewise attractive strategy for bioconjugation was originally proposed in 2002, based on the use of lipases as host proteins [53]. Site-specific conjugation to ligand/metal moieties can be achieved by appropriate enzyme inhibitors. Activated phosphonates (or sulfonates) are known to be effective lipase inhibitors, reacting specifically at serine of the catalytically active triad Ser/His/Asp with formation of covalently bonded phosphonates [78, 79, 91]. In this covalent form they mimic the transition state of lipase-catalyzed hydrolysis of esters. Keeping the concept of Fig. 3 in mind, activated phosphonate **17** was reacted with several lipases (Fig. 9), including the lipase from *Bacillus subtilis* (LipA) [53, 59].

It was demonstrated that the envisioned site-specific bioconjugation had occured quantitatively as proven by a lipase-activity test based on the reaction of *p*-nitrophenyl acetate. No release of *p*-nitrophenolate was observed. However, within one day lipase activity was slowly restored, signaling that the covalently bound inhibitor in **18** was "washed" out [53, 59]. Such effects are known in some systems, and in the present case it is due to the presence of a good leaving group in **18**, namely the second *p*-nitrophenol moiety. Therefore, it was concluded that phosphonate **17** is not the optimal building block, and that one of the *p*-nitrophenol groups needs to be replaced by a less active leaving group such as ethanolate [59].

Later, this strategy was put into practice using another lipase [92], namely cutinase, a 21 kDa lipase isolated from the fungus *Fusarium solani pisi* lacking the usual lid found in most other lipases. The active site is accessible for hydrophilic or

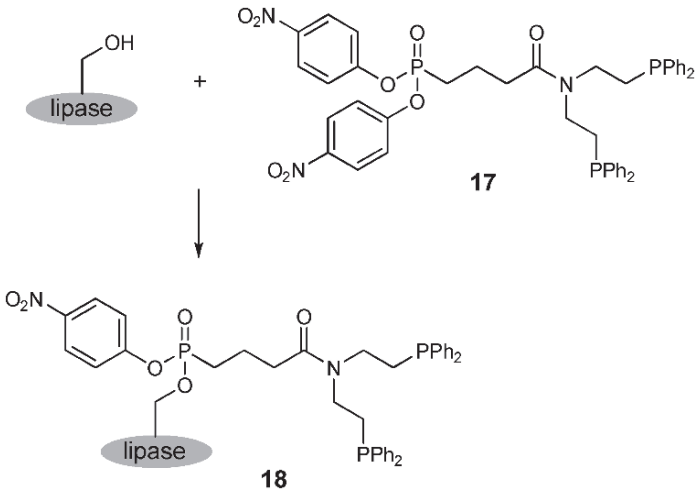

Fig. 9 Site-specific bioconjugation of a diphosphine-modified phosphonate **17** with a lipase acting as an enzyme inhibitor at the serine of the catalytic triad Ser/His/Asp [53, 59, 60]

hydrophobic substrates in aqueous medium, making this protein scaffold attractive for the purpose at hand. Metallopincer complexes **19**, **20**, and **21** were anchored covalently to cutinase at Ser120 (Fig. 10). The bioconjugates were carefully characterized by ESI-MS and shown to be stable with respect to undesired hydrolysis and release of the phosphonate functionality [92]. Thus, the stage is set for catalysis and perhaps directed evolution, provided en masse purification and bioconjugation can be implemented.

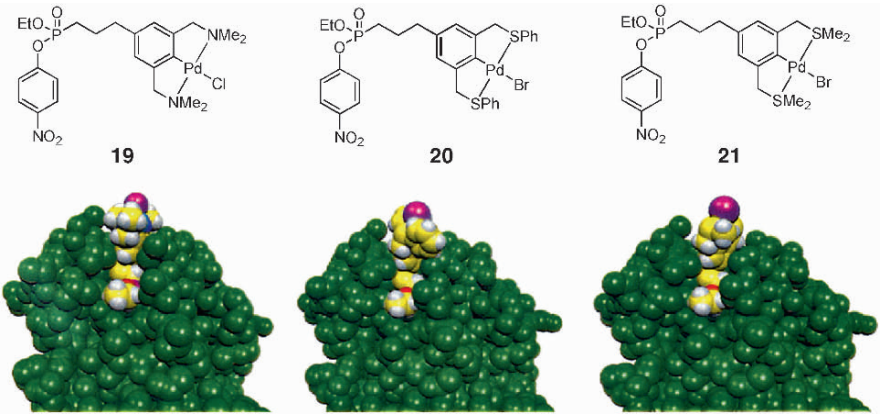

Fig. 10 *Upper*: Organometal-adapted lipase inhibitors. *Lower*: Space-filling models of the respective bioconjugates of cutinase [92]

2.3 Thermostable Enzyme tHisF as the Host Protein

Since progress in developing an appropriate platform for performing directed evolution of hybrid catalysts was slow, specifically based on the proteins featured in Sects. 2.1 and 2.2, alternatives were sought [53–61]. In doing so, one of the foci of research was solving the problem of en masse purification and bioconjugation of the mutant proteins (Fig. 3). As already pointed out in the Introduction, the presence of "foreign" proteins in addition to the chosen scaffold cannot be tolerated, because bioconjugation can then occur with many different proteins, leading to an undesired mixture of hybrid catalysts.

The thermostable enzyme tHisF from *Thermotoga maritima* [93–98] seems to fulfill these requirements. Recent research using this host protein is reviewed here more closely, because the details offer some insight into what factors need to be considered in general when developing platforms for directed evolution of hybrid catalysts. The enzyme tHisF constitutes the synthase subunit of the glutaminase-synthase bi-enzyme complex, which catalyzes the formation of imidazole glycerol phosphate in histidine biosynthesis [93, 94]. Monomeric tHisF contains 253 amino

acid residues, corresponding to a molecular mass of 27.7 kDa. In the canonical $(\beta\alpha)_8$-barrel fold, the eight strands form a central parallel β-sheet, the barrel, which is surrounded by the eight α-helices (Fig. 11). In all known $(\beta\alpha)_8$-barrels, the active site residues are located at the C-terminal ends of the β-strands and in the βα-loops that connect the strands with the following α-helices ("catalytic face"). In contrast, the αβ-loops connecting the α-helices with the following β-strands form the "stability face" of the barrel.

There are several reasons why this protein is an appropriate candidate for hosting synthetic catalysts such as ligand/metal entities or organocatalysts [57–59, 61]. Firstly, protein expression in *E. coli* in a 38-L fermenter has already been established [93–98], delivering approximately 12 mg of pure monomeric protein per liter of culture medium following purification [98]. An alternative procedure optimized in 3-L shaking flasks produces 100 mg of protein per liter of culture medium [98]. Secondly, the pronounced thermostability of tHisF allows a heat treatment as a straightforward way to parallelize purification, because such a process leads to the denaturation and precipitation of undesired proteins [57, 98]. Thirdly, the X-ray structure of tHisF [95] suggests the wide upper rim at the catalytic face of the enzyme as a convenient site for covalent anchoring of synthetic transition metal catalysts or organocatalysts (see next section). Site-specific introduction of cysteine at appropriate sites allows the predictable positioning of such catalytic entities.

As an initial step toward establishing a platform for performing directed evolution of hybrid catalysts based on tHisF, laboratory-scale fermentation of the WT protein was optimized [57]. State-of-the-art fermentation protocols allowed the production of 400–500 mg of essentially pure tHisF within 1.5 days using a 5-L fermentation unit. Subsequent miniaturization and parallelization, first in a 19-fold fermentation unit and then in 24-deep-well plate format, was successfully

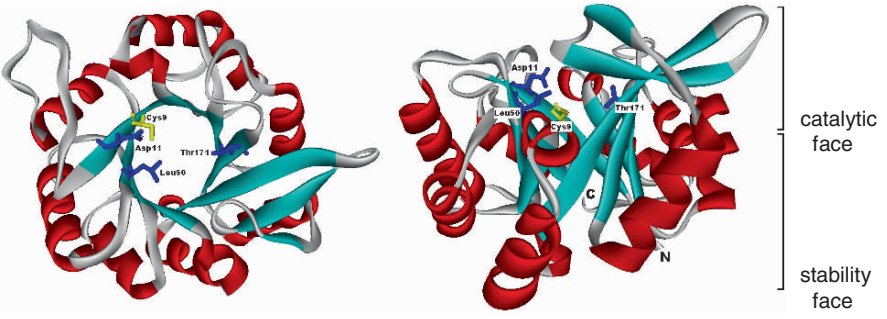

Fig. 11 X-ray structure of tHisF [95]. *Left*: top view onto the C-terminal face of the central β-barrel containing the active site; *right*: side view. The central β-barrel is depicted in *cyan*, and the surrounding α-helices are depicted in *red*. In the bioconjugation study [61], the positions suitable for potential bioconjugation following the introduction of cysteine are 11, 50, and 171 (*blue*), whereas Cys9 (*yellow*) was mutated to Ala. In the *side view*, the N- and C-termini of the polypeptide chain are marked

performed in addition to a simple but efficient purification step [57, 58]. Since tHisF is unusually robust, heat treatment of the well plates for 30 min at 72 °C, preferably in a PCR-block, leads to complete denaturing of all foreign proteins while not decomposing the desired tHisF host (Fig. 12).

The OD_{600} range in which induction with IPTG in LB-medium results in good levels of expression turned out to be narrow (see Fig. 12). The individual wells were unlikely to reach this range simultaneously, making the procedure less suitable for high-throughput. Previously, Studier reported facile and reproducible expression of proteins encoded on a pET vector (by making use of catabolite repression) [99]. Indeed, in the case of tHisF, this auto-induction system allowed high-density parallel fermentation without the additional induction step. However, the resulting tHisF preparation contained significant amounts of impurities even after prolonged heat treatment, which cannot be tolerated. This serious problem was finally solved by inducing protein expression permanently from the beginning of the fermentation (instead of the more tedious induction at a certain cell density using a buffered medium supplemented with additional glycerol TB-medium instead of LB-medium). The workup after protein expression was performed according to the procedure shown in Fig. 12, except that the ammonium sulfate precipitation was deleted because the protein was already essentially pure (~95% as judged by SDS PAGE). It turned out that this very straightforward parallel fermentation on 12.8-mL scale (4 × 3.2 mL) in 24-deep-well plates provides an average of 1.2 mg (0.044 mmol) of pure tHisF. Thus, reproducible expression and purification can be achieved by this improved protocol [61].

It can be concluded by this recent work that the development of the optimized 24-well fermentation unit and the successful parallelized purification procedure taken together constitute a potential platform for performing directed evolution of selective hybrid catalysts [61] (Fig. 3). Indeed, the parallelization on 24-well plates offers the possibility of using robotics in order to achieve higher throughput. Moreover, further parallelization following the fermentation step, for example in a 96-well format, can be achieved easily by the use of pipetting robots. These details are included in this review because the tHisF study provides a guideline for developing other platforms that may be equally viable or even better suited [61].

Following this important work, bioconjugation studies of tHisF were carried out [61], specifically by S_N2 or Michael reactions at the thiol function of an appropriate cysteine. The WT tHisF contains only one cysteine at amino acid position 9, which is located deep inside the barrel structure (Fig. 11). Exploratory experiments had shown that chemical reactions at the respective thiol function occur sluggishly, if at all [57]. Therefore, this cysteine residue was exchanged for alanine (Cys9Ala) in the WT and, guided by the crystal structure of tHisF [93, 95], a different cysteine was introduced at various positions that could be expected to be spatially accessible. One option was to perform site-directed mutagenesis with introduction of cysteine at positions in the region of the lower (narrow) rim at the so-called “stability face” of the central β-barrel, where the flexible C- and N-termini are located (Fig. 11) [95]. However, the other option was chosen, namely to focus on the upper (relatively wide) rim at the “catalytic face” of the barrel where the natural cyclization reaction

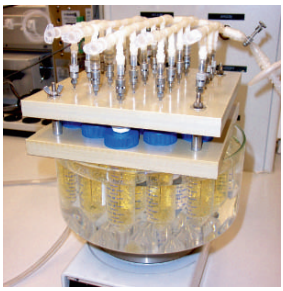

19-fold fermentation unit

- 19 × 40 mL sterile LB-medium
- Inoculation with 0.5 mL preculture, incubation at 37 °C
- Induction with 40 µL 1 M IPTG at OD_{600} = 0.4 - 0.7
- Centrifugation after 6 h at 3200 *g* / 10 min / 4 °C in rotor for 30 tubes
- Rinsing of cell pellet with 1 mL phosphate buffer (100 mM, pH = 7.8)
- Resuspension in 400 µL phosphate buffer (10 mM, pH = 7.8 containing 2 mM DTT and 12.5 units / mL benzonase)

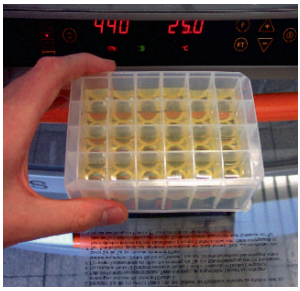

24-deep-well plate

- 24 × 5 mL sterile LB-medium
- Corresponds to 576 cultures per incubator
- Inoculation with 0.1 mL preculture, incubation at 37 °C
- Induction with 5 µL 1 M IPTG at OD_{600} = 0.4 - 0.7
- Centrifugation after 6 h at 3200 *g* / 40 min / 4 °C using rotor for 4 plates
- Rinsing of cell pellet with 200 µL phosphate buffer (100 mM, pH = 7.8)
- Resuspension in 100 µL phosphate buffer (10 mM, pH = 7.8 containing 2 mM DTT and 12.5 units / mL benzonase)

↓

- Transfer into 96-well plates suitable for PCR-block
- 30 min heat treatment at 72 °C in PCR-block (combined cell lysis and thermoprecipitation of *E. coli* host proteins)
- Centrifugation at 3200 *g* / 120 min / 4 °C in rotor for plates
- Collecting supernatant and freezing at –78 °C for storage

- Yield: approx. 3 mg in 200 µL Buffer
- Yield: approx. 0.3 mg in 40 µL Buffer

- Immediately before chemical modification: precipitation with 400 / 80 µL sat. ammonium sulfate, centrifugation, 2 × rinsing with 200 / 40 µL ammonium sulfate, resuspension of protein precipitate in phosphate buffer (10 mM, pH = 7.0).

Fig. 12 Parallelized fermentation and purification of tHisF. Comparison of the 19-fold fermentation and purification unit and the 24-deep well plate format, which connects to 96-well plate units [57, 61]

catalyzed by tHisF is known to occur. Consequently, positions 11, 50, and 171 were thought to be appropriate sites for the introduction of cysteine (Fig. 11). Three tHisF mutants were generated as potential proteins for bioconjugation, namely Cys9Ala/Asp11Cys, Cys9Ala/Leu50Cys, and Cys9Ala/Thr171Cys [57]. Most of the efforts were concentrated on the mutant Cys9Ala/Asp11Cys as the host protein to which synthetic catalysts were then anchored by Michael additions to chemically modified maleimides or S_N2-reactions of α–halo ketones (Fig. 13).

A collection of maleimides **22**–**30** harboring ligands, ligand/metals, or organocatalysts were chosen for Michael additions [57–59, 61]. In the case of bioconjugation based on appropriately modified α-halo ketones, compound **31** was synthesized. Ligands **22**, **25**, and **31** were designed for potential transition metal coordination (see also complex **23**), whereas **24** constitutes a potential flavin-dependent organocatalyst for possible Baeyer–Villiger reactions [100–107] (also sulfoxidation and/or oxidation of dihydro-nicotinamides). Finally, **26**–**30** pave the way to potential organocatalysis in benzoin reactions similar to those catalyzed by pyruvate decarboxylase and/or Stetter-type reactions [108–112].

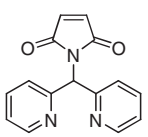

22

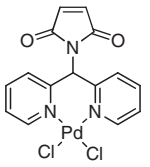

23

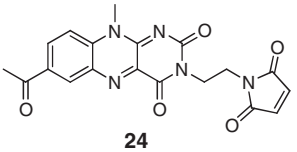

24

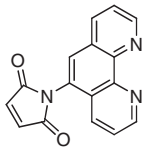

25

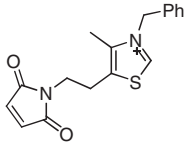

26

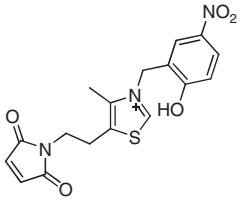

27

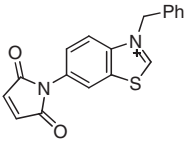

28

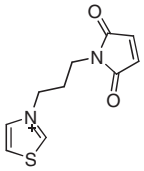

29

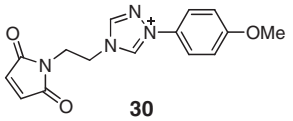

30

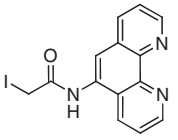

31

Mutant Cys9Ala/Asp11Cys was then employed as a host protein, bioconjugation being performed with compounds **22**–**31** under standard conditions described in the literature for other systems [78, 79]. The bioconjugates were characterized by mass spectrometry (MS) and in some cases by limited proteolysis using trypsin followed

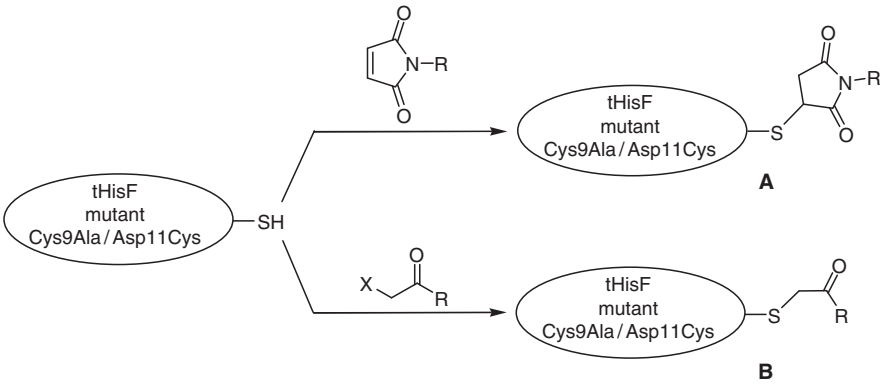

Fig. 13 Chemical modification of the tHisF mutant Cys9Ala/Asp11Cys by means of Michael additions leading to bioconjugates ***A*** and by S_N2-reactions providing bioconjugates ***B*** [57, 61]

by MS analysis [61]. For example, the bioconjugate derived from tHisF mutant Cys9Ala/Asp11Cys and 5-iodoacetamide-1,10-phenanthroline (**31**) was characterized by a combination of ESI-TOF MS and limited proteolysis with trypsin. Trypsin is a serine protease that cleaves peptide bonds only on the C-terminal side of the basic amino acids lysine and arginine, thereby allowing for predictable selectivity. The amino acid sequence of tHisF comprises 7% lysine and 5% arginine [93–98]. In a denaturated or highly flexible protein one would expect complete digestion by trypsin. However, it was previously shown that tHisF is accessible to trypsin digestion only at two positions due to its pronounced stability [94]. Therefore, a combination of limited tryptic digestion and MS analysis was performed in order to demonstrate that the chemical modification occurs in the desired part of the host protein. The reported cleavage positions are located at Arg27 and Lys58, the reaction occurring much faster at Arg27. The cysteine in position 11, which was modified with a variety of ligands, is part of the N-terminal region that was cleaved off, and the remaining protein was analyzed by MS. The results correspond to the expectations. Similar analyses were performed for bioconjugates of the other mutants Cys9Ala/Leu50Cys and Cys9Ala/Thr171Cys [57–59, 61].

It was also shown that the chemical modification of the host protein does not alter its behavior towards trypsin, a conclusion that is corroborated by following the progress of the tryptic digestion by SDS-PAGE [57, 61] (Fig. 14). Had undesired denaturation of the host protein occurred upon chemical modification, more extensive fragmentation in the tryptic digestion would have resulted. In further experiments, the other bioconjugation reactions were also shown to proceed in the expected way with the host protein. In addition to the tHisF mutant, Cys9Ala/Asp11Cys, variants Cys9Ala/Leu50Cys, and Cys9Ala/Thr171Cys also proved to be suitable for selective modification [57, 61].

In bioconjugation experiments followed by tryptic digestion, it was found in the case of mutant Cys9Ala/Asp11Cys, for example, that the mass of the resulting

high molecular weight fragment is the same as for the unmodified protein. This shows that chemical modification occurs within the first 27 amino acids. In the case of the mutant Cys9Ala/Leu50Cys, the bioconjugate derived from maleimide **22** shows after tryptic digestion a higher mass than the digested unmodified mutant (Table 1) [58, 61]. Here, the mass difference corresponds directly to the incorporated ligand, demonstrating that in this case tryptic digestion also leads to removal of the first 27 amino acids. Thus, cleavage in this mutant does not remove the modified region, as expected.

Various organocatalyst-based hybrid catalysts were also prepared in this study [61]. For example, flavin **24** was used for the selective cysteine modification of the tHisF mutant Cys9Ala/Asp11Cys. This compound allows for direct quantification of chemical modification because it has chromophoric properties. In view of future en masse parallelized bioconjugation of mutant libraries in the process of directed evolution experiments (Fig. 3), the course of the chemical modification process was studied more

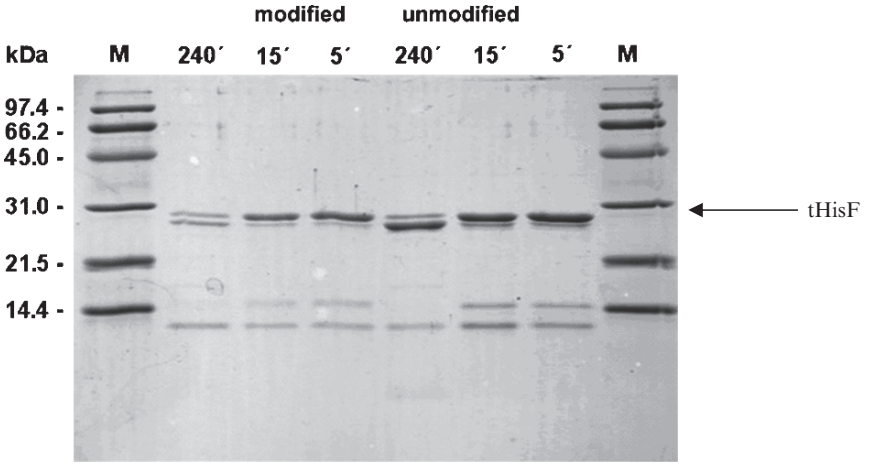

Fig. 14 SDS-PAGE (12.5% acrylamide) of samples from limited proteolysis (5, 15, and 240 min) of the unmodified tHisF mutant Cys9Ala/Asp11Cys and its bioconjugate with 5-iodacetamido-1,10-phenanthroline (**31**) [61]. The observed fragmentation pattern shows that modification does not significantly change the susceptibility of the tHisF mutant to selective trypsin digestion

Table 1 ESI-TOF MS analysis before and after tryptic digestion of chemical unmodified and modified tHisF mutants Cys9Ala/Asp11Cys and Cys9Ala/Leu50Cys [57, 61]

Protein	Modification	Undigested	Digested	Δ
Cys9Ala/Asp11Cys	None	27,683	24,678	3005
	With **22**	27,948	24,676	3272
Cys9Ala/Leu50Cys	None	27,682	24,669	3013
	With **22**	27,951	24,933	3018

Numbers refer to mass units

closely. In the bioconjugation experiments, 0.5, 1.0, and 2.0 equivalents of the flavin catalyst **24** were used. In order to check for possible unspecific modification of the host protein, the cysteine-free tHisF mutant Cys9Ala was studied under the same set of conditions. Two crucial results were noted. Firstly, bioconjugation occurs very selectively as evidenced by the extremely low degree of modification of the cysteine–free protein. MALDI-TOF MS corroborated this conclusion [61]. Secondly, it appears that the use of stoichiometric or slightly substoichiometric amounts of the flavin **24** in an en masse chemical modification of mutant libraries is feasible without subsequent purification. This finding is important with regard to achieving maximum throughput in future screening processes. In conclusion, the tHisF-based system appears to constitute a viable platform for performing directed evolution studies [61]. Of course, other thermophiles are probably just as well (or even better) suited, perhaps those with a larger/deeper anchoring pocket. Once a platform has been established, as in the case of the tHisF-system, the next step is to test catalysis.

3 Non-Covalent Anchoring of Ligands/Transition Metals in the Cavities of Proteins

Non-covalent bioconjugation has potential advantages over covalent versions described in Sect. 2, provided binding is strong and site-specific. Two of a number of possibilities are described here, one of them leading to the first case of proof-of-principle of the concept of directed evolution of hybrid catalysts (Fig. 3).

3.1 Serum Albumins as Host Proteins

Serum albumins are robust and easy to handle proteins that are present at high concentrations in blood plasma, functioning as transport carriers for a variety of compounds such as fatty acids, bile acids, bilirubin, and hemin [113]. It was known from X-ray work that iron-protoporphyrin dimethyl ester binds in the subdomain IB of human serum albumin (HSA) and that weak axial coordination by Tyr161 contributes to the binding [114–116]. Moreover, Gross had previously anchored water-soluble sulfonylated Fe^{III}- and Mn^{III}-corroles to various serum albumins and used these conjugates as catalysts in the H_2O_2-based asymmetric sulfoxidation of prochiral thioethers (up to 74% *ee* using WT) [117]. In addition, it had been reported that the sodium salts of di-, tri-, and tetrasulfonic acid derivatives of porphyrins, phthalocyanines, and corroles bind strongly to serum albumins [117–121], analogously to iron-protoporphyrin dimethyl ester [113].

Therefore, the use of the commercially available Cu^{II}-phthalocyanine complex **32** was considered [122], expecting it to bind strongly to the IB subdomain of HSA or to analogous regions of other serum albumins such as bovine serum albumin (BSA), which is also a cheap and robust protein.

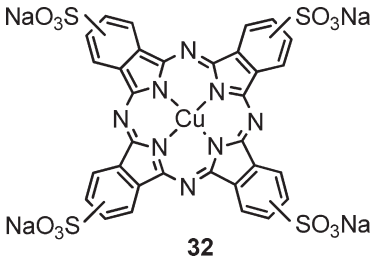

32

In order to get a better picture of the probable binding-mode, the X-ray data of HAS [114] was used to model the desired **32**/HSA complex (Fig. 15) [122]. Absolute proof that binding occurs in this manner was not obtained, but it is a good model.

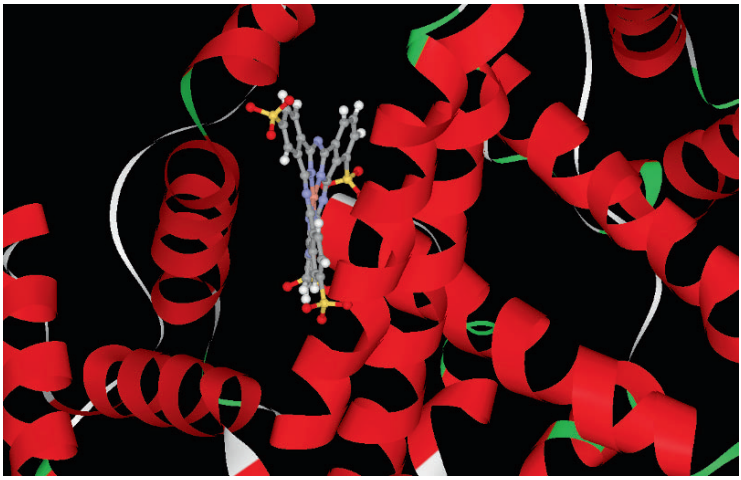

Fig. 15 Model of **32**/HSA [122] based on the X-ray structure of hemin/HSA [114–116]

The model reaction to be mediated by hybrid catalysts comprised of **32**/serum albumins, was the Diels–Alder reaction of the H_2O-soluble aza-chalcone **33** with cyclopentadiene **34** with formation of chiral adducts **35**. This reaction had been originally devised by Engberts [123, 124], who used Cu^{II}-complexes of amino acids in aqueous medium (*ee* up to 74%). Later it was employed by Feringa in the study of Cu^{II}-conjugates of DNA as catalysts [125].

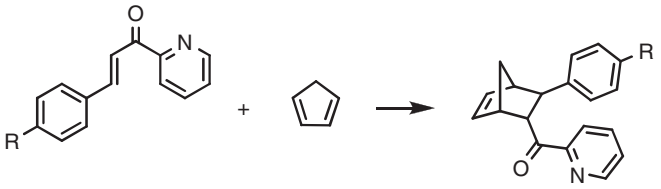

33 **a** R = H
b R = CH_3
c R = OCH_3
d R = NO_2
e R = Cl

34

35

Surprisingly, high enantioselectivities were observed when using BSA as the host harboring **32** (85–98% *ee* in favor of the *endo*-products **35**) [122]. In the case of **32**/HSA (Fig. 15), the reaction of **33a** with **34** led to an *ee*-value of only 85%. BSA or HSA alone did not catalyze the reaction. Since a good expression system for HSA has been reported [126, 127], this system could be employed in a future study regarding the directed evolution of enantioselective hybrid catalysts. Iterative CASTing (Fig. 2) based on the model in Fig. 15 could then be used to increase the enantioselectivity of the present Diels–Alder cycloaddition or of other Cu^{II}-catalyzed processes. However, a procedure for en masse purification of HSA mutants needs to be developed first.

3.2 Avidin or Streptavidin as the Host Protein

The first platform that provided proof-of-principle regarding the idea of directed evolution of hybrid catalysts (Fig. 3) was based on the so-called Whitesides system [128, 129] utilizing a biotinylated Rh-diphosphine of the type **36** (Fig. 16) [130]. Whitesides actually used avidin in combination with the analogous complex in which norbornadiene takes the place of cod. The respective complex was used as a single catalyst in the Rh-catalyzed hydrogenation of α-acetamido-acrylic acid, the observed *ee* ranging between 33 and 44% depending upon the conditions used [128, 129]. Ward has elegantly used chemical tuning (variation of spacer length in **36** and rational protein design (site-specific mutagenesis) to improve the enantioselectivity significantly in the same reaction using streptavidin, achieving *ee*s of >95% [131–135]. This is fundamentally different from the Darwinistic approach shown in Fig. 3. In the directed evolution study [130], the Rh-complex **36** was also employed, but the ester **37** instead of the acid was chosen as the substrate, because this facilitates easy extraction and medium-throughput analysis by gas chromatography [59, 130]. The reaction product **38** can be extracted with ethyl acetate in a parallel manner.

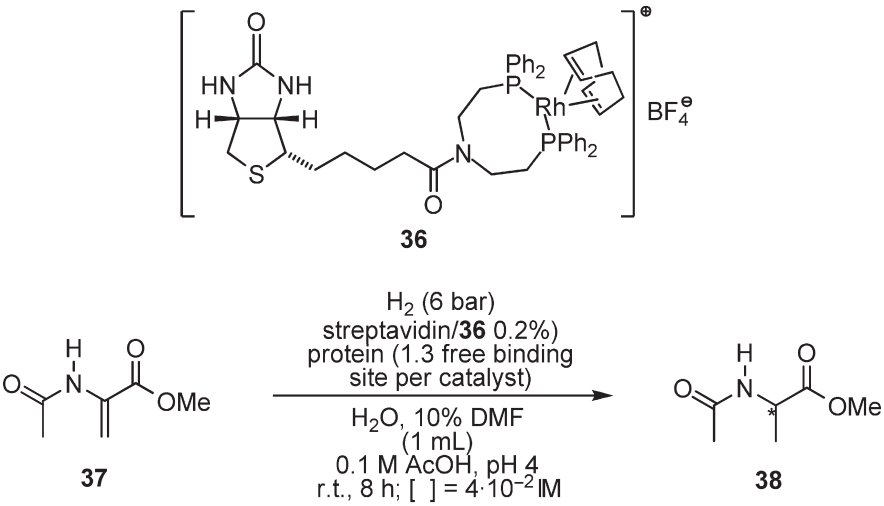

Fig. 16 Rh-catalyzed asymmetric hydrogenation of α-acetamido-acrylic acid ester **37** using streptavidin mutants as hosts for complexing **36** [130]

Avidin is not the ideal host protein, because production of eukaryotic proteins is both time consuming and low yielding. Therefore, streptavidin was chosen, a genetically unrelated bacterial protein that also binds biotin with high affinity. Several expression systems for streptavidin have been described [136–140], and some of them were compared. Unfortunately, problems with the insufficient expression level and purification in parallel form had to be dealt with. The best solution turned out to be based on pET11b-sav [141], which encodes 12 residues of T7-tag followed by Asp and Gln and residues 15 to 159 of the mature streptavidin. *E. coli* strain BL21(DE3) transformed with this plasmid and grown in Studier's autoinduction media [99], ZYP5052, requires less monitoring than conventional induction with IPTG at mid-log phase. Therefore, this allows multiple unattended overnight cultures [59]. Before reaction with **36**, streptavidin mutants were purified using standard agarose/iminobiotin affinity column chromatography. Streptavidin or streptavidin/biotin themselves do not catalyze the hydrogenation reaction. Unbound complex **36** does not occur because an excess of free binding site of streptavidin was present. Per tetramer of streptavidin, 3.8–3.9 free binding sites were determined by standard titration using fluorescence quenching of biotin/4-fluorescein [130].

This optimized adaptation was crucial in simplifying the screening task. However, the system is still not fully suited for screening thousands of mutants since it requires a 150-mL culture scale in order to provide a sufficient amount of streptavidin. Typically 1.04×10^{-7} mol of binding site was used, which is equivalent to ~1.7 mg protein (based on a MW of 16.5 kDa per monomer, and expecting 3.8–3.9 free binding sites per tetramer as obtained for the WT) [130]. Sometimes lower amounts of streptavidin were obtained for a given mutant. Then the culture scale had to be increased by up to fivefold and/or the amount of hybrid catalyst used

in the reaction decreased from 0.2 to 0.1%. Following titration of the mutant streptavidins for the purpose of determining the amount present, they were transferred into glass vessels of an in-house adapted reactor block [59, 130], which was used in the Chemspeed Accelerator SLT 100 Synthesizer. It is important to point out that traces of O_2 need to be removed from the reactors or it would otherwise destroy the Rh-catalyst. Enantioselectivity was determined by conventional gas chromatographic analysis of the reaction mixtures.

It became clear that this system fails to fulfill the technological requirements for implementing the concept of directed evolution of hybrid catalyst efficiently. Thus, two options were possible: (i) Invest more time in improving the (over) expression system for streptavidin, which would subsequently allow the practical formation of large libraries of mutant protein hosts (each mutant in sufficiently large quantities); or (ii) Use the partially optimized expression system described above, and then produce fairly small libraries. The latter strategy was chosen. Only a few hundred mutants in each mutagenesis experiment were generated and screened in what can be termed as "mini" directed evolution. Although still labor-intensive, this procedure led to proof-of-principle [130].

In an initial experiment, it was observed that WT streptavidin/**36** is a poor catalyst in the hydrogenation of **37**, leading to an *ee* of only 23% in favor of (*R*)-**38**. Rather than targeting the whole protein for amino acid substitution by error-prone PCR [38–44], CASTing [48–50] was applied. Unfortunately, an X-ray structure of the conjugate was not available. Therefore, the CAST sites for amino acid randomization were chosen on the basis of a model. The biotinylated Rh-complex **36** was modeled into the X-ray structure [142] of streptavidin/biotin using Moloc and Accelerys DS visualizer. Two major conformers were identified, meaning two slightly different positions of Rh. Figure 17 shows an excerpt of the modeled structure and the amino acid sites that appeared to be appropriate for CAST experiments [130].

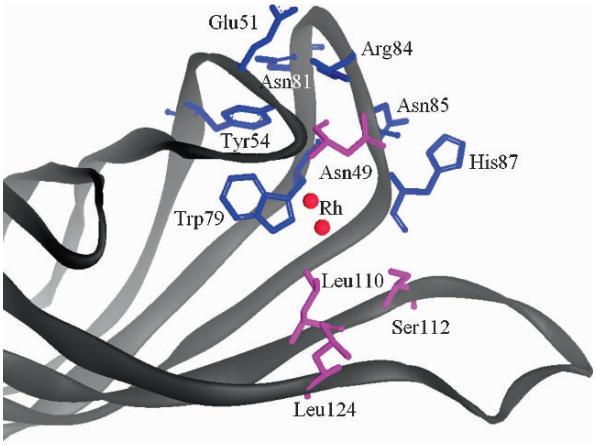

Fig. 17 Selected close (*purple*) and distal (*blue*) sites from Rh(I) centers (*red*) of two important calculated conformers of the complex streptavidin/**36** [130] based on the X-ray structure of streptavidin/biotin

Two types of sites for saturation mutagenesis were considered: The first are "close" positions, specifically Asn49, Leu110, Ser112, and Leu124. These are located about 4–6 Å away from the Rh(I) of the two calculated major conformers, which could influence directly the conformation of the catalyst or catalyst/substrate complex [130]. The second type of sites are more "distal": Glu51, Tyr54, Trp79, Asn81, Arg84, Asn85, His87, which are located further away from Rh(I). These second sphere CAST-positions could influence the structure of the enzyme as a whole because they are involved in hydrogen bonding between secondary elements. Saturation mutagenesis was initiated at positions 110, 112, and 124 using the QuikChange method (Stratagene) and pET11b-sav. In each saturation experiment about 200–300 clones were harvested and screened, which corresponds to an oversampling of about 95% coverage of the respective protein sequence space [49]. The best mutant **I** (Ser112Gly) led to 35% *ee* (*R*).

It is clear that a single round of saturation mutagenesis does not yet constitute an evolutionary process. Therefore, iterative CASTing [48], which is an embodiment of ISM, was performed using the gene that encodes mutant **I** and saturating at position 49. This led to a double mutant **II** having mutations Asn49His/Ser112Gly and showing an *ee* value of 54% (*R*) in the model reaction (Fig. 18) [130]. Finally, a third-generation saturation experiment was performed using the gene which encodes mutant **II** and focusing once more on position 112. This experiment was

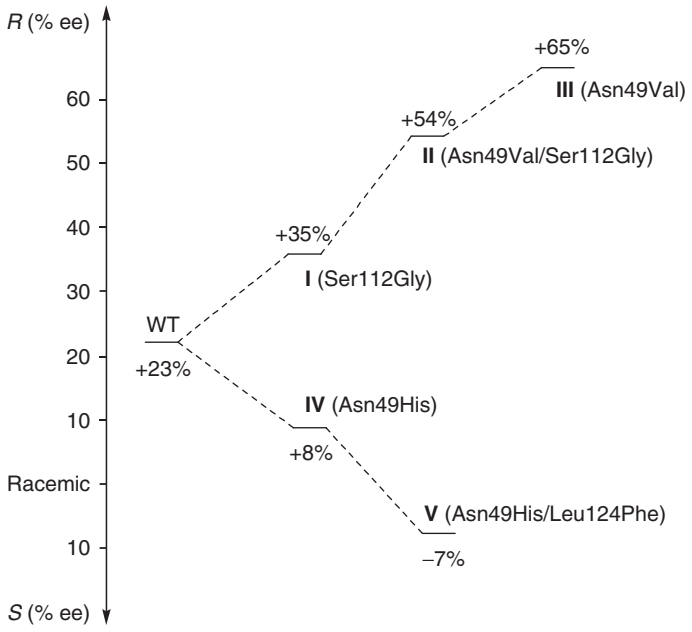

Fig. 18 Directed evolution of hybrid catalysts comprising mutants of streptavidin/**36**, the Rh-catalyzed hydrogenation **37**→**38** serving as the model reaction (40–90% yield) [130]

designed to test whether glycine at position 112 is really the best choice when combining with histidine at position 49. This provided the improved mutant **III** leading to an *ee* of 65% (*R*). Thus, the original mutation Ser112Gly was reverted back to serine (Fig. 18). This means that the best variant is characterized by a single mutation (Asn49Val). Thus, positions 51, 54, 79, 81, 84, 85, and 87 were considered. Unfortunately, saturation mutagenesis experiments were not successful because no soluble protein was obtained. In contrast, saturation mutagenesis at position 49 on WT template led directly to mutants **III** and **IV**. The latter is characterized by Asn49His. This variant has lower enantioselectivity than the WT, *ee* = 8% (*R*), suggesting the possibility of inverting stereoselectivity. Therefore, the plasmid encoding variant **IV** was utilized as a template for saturation mutagenesis at another site. Indeed, upon focusing on position 124, mutant **V** (Asn49His/Leu124Phe) was identified, which is (*S*)-selective, although not by a great degree (*ee* = 7%) [130]. It would be interesting to extend the present study by applying iterative saturation mutagenesis to residues in the second shell around the close amino acid positions already considered (49, 110, 112, and 124).

This work demonstrates for the first time that it is possible to apply the methods of directed evolution to increase and/or to invert enantioselectivity of a hybrid catalyst composed of a synthetic achiral transition metal catalyst anchored to a host protein [130]. Due to the technical problems associated with the inefficient expression system, only very small mutant libraries could be generated, which in itself was labor-intensive. Nevertheless, proof-of-principle has been provided [130].

4 Direct Binding of Transition Metal Salts to Designed Sites in Proteins

It can be argued that efforts of the type described in Sects. 1–3 can be replaced, at least in some cases, by metalloenzymes that nature already provides. Indeed, proteins such as P450 enzymes have been used as catalysts in organic chemistry, and directed evolution has been demonstrated to be useful in controlling regioselectivity of CH-activating hydroxylation [143–146]. It is also conceivable that directed evolution of other metalloenzymes can induce promiscuous behavior. A hypothetical example is to turn a natural Cu(II)-metalloenzyme into a stereoselective Diels–Alderase by the techniques of directed evolution. Such strategies are certainly logical and worthy of testing. However, an alternative concept can also be considered (Fig. 4, bottom): The construction by site-specific mutagenesis of a complexation site, which is specific for transition metal salts. In doing so, the potentially complexing amino acids should be placed in the protein appropriately so that the transition metal, but subsequently also a substrate, can bind, leading to a reaction. Moreover, it is advisable to be guided by nature, e.g., to see how the side-chains of amino acids in natural metalloenzymes bind transition metals. For example, in preliminary work two histidines and one aspartate were introduced in a geometrically correct manner into a thermostable protein in order to bind Cu(II) (Reetz et al., unpublished results). Such binding motifs are well known in certain metalloenzymes.

This "semi-synthetic" metalloenzyme was found to catalyze enantioselective Diels–Alder reactions (*ee* up to 30%) (Reetz et al., unpublished results). Following this initial step with the WT, directed evolution for optimizing the *ee* may prove to be a viable alternative strategy for putting the concept of directed evolution of hybrid catalysts into practice.

5 Conclusions and Perspectives

Directed evolution of hybrid catalysts in which transition metals are anchored to appropriate protein hosts is a novel concept, which in principle allows the optimization of a synthetic catalyst by genetic methods, specifically by relying on the Darwinistic principle [53–61]. It is thus fundamentally different from traditional (chemical) ways to optimize homogeneous transition metal catalysts in terms of activity and selectivity [1–5, 15–23]. Proof-of-principle was recently provided by utilizing the Whitesides system [128, 129] based on the supramolecular interaction of a biotinylated Rh/diphosphine complex and streptavidin [130]. Three rounds of iterative CASTing increased the enantioselectivity of the Rh-catalyzed hydrogenation of a prochiral olefin from *ee* = 23% to *ee* = 65% [130]. However, due to the insufficient expression system of streptavidin, other host proteins have to be considered. Serum albumins [122] or the thermostable tHisF [61] may prove to be acceptable. More work is needed to fulfill all requirements for constructing viable platforms upon which directed evolution can be performed in a practical manner. The idea of utilizing a thermostable protein as a host allows in principle the difficult problem of en masse purification of thousands of mutants to be solved by a simple heat treatment [61]. Ligand types should be chosen that bind transition metals so tightly that they do not move indiscriminately in the host protein. Once such practical platforms are available, chemists will have a fascinating tool in hand with which they can create active as well as regio-, enantio-, and diastereoselective hybrid catalysts for use in synthetic organic chemistry.

References

1. Noyori R (2002) Angew Chem Int Ed 41:2008
2. Sharpless KB (2002) Angew Chem Int Ed 41:2024
3. Jacobsen EN, Pfaltz A, Yamamoto H (1999) Comprehensive asymmetric catalysis, vol I–III. Springer, Berlin Heidelberg New York
4. Ager DJ (2005) Handbook of chiral fine chemicals. Marcel Dekker, New York
5. Blaser H-U, Schmidt E (2004) Asymmetric catalysis on industrial scales. Wiley-VCH, Weinheim
6. Lelais G, MacMillan DWC (2006) Adrichim Acta 39:79
7. Seayad J, List B (2005) Org Biomol Chem 3:719
8. List B (2002) Tetrahedron 58:5573
9. Berkessel A, Gröger H (2004) Asymmetric organocatalysis. VCH, Weinheim

10. Dalko PI, Moisan L (2001) Angew Chem Int Ed 40:3726
11. Drauz K, Waldmann H (2002) Enzyme catalysis in organic synthesis: a comprehensive handbook, vol I–III. Wiley-VCH, Weinheim
12. Faber K (2000) Biotransformations in organic chemistry. Springer, Berlin Heidelberg New York
13. Schmid A, Dordick JS, Hauer B, Kiener A, Wubbolts M, Witholt B (2001) Nature (London UK) 409:258
14. Koeller KM, Wong C-H (2001) Nature (London UK) 409:232
15. Gennari C, Piarulli U (2003) Chem Rev 103:3071
16. Dahmen S, Bräse S (2001) Synthesis 1431
17. Hoveyda AH (2002) In: Nicolaou KC, Hanko R, Hartwig W (eds) Handbook of combinatorial chemistry. Wiley-VCH, Weinheim, p 991
18. de Vries JG, de Vries AHM (2003) Eur J Org Chem 799
19. Reetz MT (2001) Angew Chem Int Ed 40:284
20. Francis MB, Jacobsen EN (1999) Angew Chem Int Ed 38:937
21. Berkessel A, Riedl R (2000) J Comb Chem 2:215
22. Ding K, Du H, Yuan Y, Long J (2004) Chem Eur J 10:2872
23. Reetz MT (2004) In: Ward MD (ed) Comprehensive coordination chemistry II. Elsevier, Amsterdam, p 509
24. Reetz MT, Sell T, Meiswinkel A, Mehler G (2003) Angew Chem Int Ed 42:790
25. Reetz MT (2008) Angew Chem Int Ed 47:2556
26. Hoen R, Boogers JAF, Bernsmann H, Minnaard AJ, Meetsma A, Tiemersma-Wegman TD, de Vries AHM, de Vries JG, Feringa BL (2005) Angew Chem Int Ed 44:4209
27. Klibanov AM (2001) Nature (London UK) 409:241
28. Liese A, Seelbach K, Wandrey C (2006) Industrial biotransformations. Wiley-VCH, Weinheim
29. Imanaka T, Atomi H (2002) In: Drauz K, Waldmann H (eds) Enzyme catalysis in organic synthesis: a comprehensive handbook, vol 1. Wiley-VCH, Weinheim, p 67
30. Cedrone F, Ménez A, Quéméneur E (2000) Curr Opin Struct Biol 10:405
31. Harris JL, Craik CS (1998) Curr Opin Chem Biol 2:127
32. Kazlauskas RJ (2000) Curr Opin Chem Biol 4:81
33. Li Q-S, Schwaneberg U, Fischer M, Schmitt J, Pleiss J, Lutz-Wahl S, Schmid RD (2001) Biochim Biophys Acta 1545:114
34. Reetz MT, Zonta A, Schimossek K, Liebeton K, Jaeger K-E (1997) Angew Chem Int Ed Engl 36:2830
35. Reetz MT, Wilensek S, Zha D, Jaeger K-E (2001) Angew Chem Int Ed 40:3589
36. Reetz MT (2004) Proc Natl Acad Sci U S A 101:5716
37. Reetz MT (2006) In: Gates BC, Knözinger H (eds) Advances in catalysis. Elsevier, San Diego, p 1
38. Arnold FH, Georgiou G (2003) Directed enzyme evolution: screening and selection methods. Humana, Totowa, NJ
39. Brakmann S, Johnsson K (2002) Directed molecular evolution of proteins (or how to improve enzymes for biocatalysis). Wiley-VCH, Weinheim
40. Brakmann S, Schwienhorst A (2004) Evolutionary methods in biotechnology (clever tricks for directed evolution). Wiley-VCH, Weinheim
41. Taylor SV, Kast P, Hilvert D (2001) Angew Chem Int Ed 40:3310
42. Powell KA, Ramer SW, del Cardayré SB, Stemmer WPC, Tobin MB, Longchamp PF, Huisman GW (2001) Angew Chem Int Ed 40:3948
43. Rubin-Pitel SB, Zhao H (2006) Comb Chem High Throughput Screening 9:247
44. Kaur J, Sharma R (2006) Crit Rev Biotechnol 26:165
45. Reetz MT (2004) In: Brakmann S, Schwienhorst A (eds) Evolutionary methods in biotechnology. Wiley-VCH, Weinheim, p 113
46. Reetz MT (2004) In: Robertson DE, Noel JP (eds) Methods in enzymology. Elsevier, San Diego, CA, p 238

47. Reetz MT (2006) In: Reymond J-L (ed) Enzyme assays – high-throughput screening, genetic selection and fingerprinting. Wiley-VCH, Weinheim, p 41
48. Reetz MT, Wang L-W, in part M. Bocola (2006) Angew Chem Int Ed 45:1236
49. Reetz MT, Carballeira JD (2007) Nat Protoc 2:891
50. Clouthier CM, Kayser MM, Reetz MT (2006) J Org Chem 71:8431
51. Parshall GW, Ittel SD (1992) Homogeneous catalysis: the applications and chemistry of catalysis by soluble transition metal complexes, 2nd ed. Wiley, New York
52. Cornils B, Herrmann WA (2004) Aqueous-phase organometallic catalysis. concepts and application, 2nd edn. Wiley-VCH, Weinheim
53. Reetz MT, Rentzsch M, Pletsch A, Maywald M (2002) Chimia 56:721
54. Reetz MT (2002) Tetrahedron 58:6595
55. Reetz MT (2001) Patent WO92,18645
56. Maiwald P (2001) Neue Liganden für die asymmetrische Katalyse. PhD thesis, Universität Bochum
57. Rentzsch M (2004) Integration von Übergangsmetallkatalysatoren in Proteine für die Anwendung evolutionsbasierter Optimierungsstrategien. PhD thesis, Universität Bochum
58. Pletsch A (2004) Untersuchungen zur gerichteten Evolution von Übergangsmetallkatalysatoren. PhD thesis, Universität Bochum
59. Maywald M (2005) Methodenentwicklung zur Anwendung genetischer Optimierungsstrategien auf semisynthetische Enzyme. PhD thesis, Universität Bochum
60. Reetz MT, Rentzsch M, Pletsch A, Maywald M, Maiwald P, Peyralans JJ-P, Maichele A, Fu Y, Jiao N, Hollmann F, Mondière R, Taglieber A (2007) Tetrahedron 63:6404
61. Taglieber A, Schulz F, Hollmann F, Rusek M, Reetz MT (2007) ChemBioChem 8:106
62. Qi D, Tann C-M, Haring D, Distefano MD (2001) Chem Rev 101:3081
63. Polgar L, Bender ML (1966) J Am Chem Soc 88:3153
64. Schultz PG (1988) Science 240:426
65. Khumtaveeporn K, DeSantis G, Jones JB (1999) Tetrahedron: Asymmetry 10:2563
66. Smith HB, Hartman FC (1988) J Biol Chem 263:4921
67. Nicholas KM, Wentworth Jr. P, Harwig CW, Wentworth AD, Shafton A, Janda KD (2002) Proc Natl Acad Sci USA 99:2648
68. Hamachi I, Shinkai S (1999) Eur J Org Chem 539
69. Barker PD (2003) Curr Opin Struct Biol 13:490
70. Kaiser ET (1988) Angew Chem Int Ed Engl 27:913
71. Hilvert D, Kaiser ET (1987) Biotechnol Genet Eng Rev 5:297
72. Davis BG (2003) Curr Opin Biotechnol 14:379
73. Eckermann AL, Barker KD, Hartings MR, Ratner MA, Meade TJ (2005) J Am Chem Soc 127:11880
74. Ohashi M, Koshiyama T, Ueno T, Yanase M, Fujii H, Watanabe Y (2003) Angew Chem Int Ed 42:1005
75. Ueno T, Koshiyama T, Ohashi M, Kondo K, Kono M, Suzuki A, Yamane T, Watanabe Y (2005) J Am Chem Soc 127:6556
76. Suckling CJ, Zhu LM (1993) Bioorg Med Chem Lett 3:531
77. van de Velde F, Könemann L, van Rantwijk F, Sheldon RA (2000) Biotechnol Bioeng 67:87
78. Hermanson GT (1996) Bioconjugate techniques. Academic, San Diego
79. Nakata E, Tsukiji S, Hamachi I (2007) Bull Chem Soc Jpn 80:1268
80. Wilson ME, Whitesides GM (1978) J Am Chem Soc 100:306
81. Lin C-C, Lin C-W, Chan ASC (1999) Tetrahedron: Asymmetry 10:1887
82. Reetz MT, Peyralans JJ-P, Maichele A, Fu Y, Maywald M (2006) Chem Commun 2006:4318
83. Lu Y (2005) Curr Opin Chem Biol 9:118
84. Lu Y, Valentine JS (1997) Curr Opin Struct Biol 7:495
85. Lu Y, Berry SM, Pfister TD (2001) Chem Rev 101:3047
86. Carey JR, Ma SK, Pfister TD, Garner DK, Kim HK, Abramite JA, Wang ZL, Guo ZJ, Lu Y (2004) J Am Chem Soc 126:10812

87. Kamphuis IG, Kalk KH, Swarte MBA, Drenth J (1984) J Mol Biol 179:233
88. Panella L, Broos J, Jin J, Fraaije MW, Janssen DB, Jeronimus-Stratingh M, Feringa BL, Minnaard AJ, de Vries JG (2005) Chem Commun 2005:5656
89. Reetz MT, Mehler G (2000) Angew Chem Int Ed 39:3889
90. Reetz MT, Ma JA, Goddard R (2005) Angew Chem Int Ed 44:412
91. Barrett AJ, Salvesen G (1986) In: Dingle JT, Gordon JL (eds) Research monographs in cell and tissue physiology, vol 12. Elsevier, Amsterdam
92. Kruithof CA, Casado MA, Guillena G, Egmond MR, van der Kerk-van Hoof A, Heck AJR, Klein Gebbink RJM, van Koten G (2005) Chem Eur J 11:6869
93. Douangamath A, Walker M, Beismann-Driemeyer S, Vega-Fernandez MC, Sterner R, Wilmanns M (2002) Structure 10:185
94. Beismann-Driemeyer S, Sterner R (2001) J Biol Chem 276:20387
95. Lang D, Thoma R, Henn-Sax M, Sterner R, Wilmanns M (2000) Science 289:1546
96. Sterner R, Höcker B (2005) Chem Rev 105:4038
97. Thoma R, Obmolova G, Lang DA, Schwander M, Jenö P, Sterner R, Wilmanns M (1999) FEBS Lett 454:1
98. Haeger M (2005) Dissertation, Universität Regensburg
99. Studier FW (2005) Protein Expression Purif 41:207
100. Walsh CT, Chen Y-CJ (1988) Angew Chem Int Ed Engl 27:333
101. Flitsch S, Grogan G (2002) In: Enzyme Drauz K, Waldmann H (eds) Catalysis in organic synthesis, vol 2. Wiley-VCH, Weinheim, p 1202
102. Kamerbeek NM, Janssen DB, van Berkel WJH, Fraaije MW (2003) Adv Synth Catal 345:667
103. Mihovilovic MD, Müller B, Schulze A, Stanetty P, Kayser MM (2003) Eur J Org Chem 2003:2243
104. Hilker I, Alphand V, Wohlgemuth R, Furstoss R (2004) Adv Synth Catal 346:203
105. Bolm C, Palazzi C, Beckmann O (2004) In: Beller M, Bolm C (eds) Transition metals for organic chemistry: building blocks and fine chemicals. Wiley-VCH, Weinheim, p 267
106. Murahashi S-I, Ono S, Imada Y (2002) Angew Chem Int Ed 41:2366
107. Strukul G (1998) Angew Chem Int Ed 37:1198
108. Servi S (1990) Synthesis 1990:1
109. Pohl M, Sprenger GA, Müller M (2004) Curr Opin Biotechnol 15:335
110. Stetter H (1976) Angew Chem Int Ed Engl 15:639
111. Breslow R (1958) J Am Chem Soc 80:3719
112. Enders D, Kallfass U (2002) Angew Chem Int Ed 41:1743
113. White RL, Spenser ID (1982) J Am Chem Soc 104:4934
114. Zunszain PA, Ghuman J, Komatsu T, Tsuchida E, Curry S (2003) BMC Struct Biol 3:6
115. Wardell M, Wang Z, Ho JX, Robert J, Ruker F, Ruble J, Carter DC (2002) Biochem Biophys Res Commun 291:813
116. Dockal M, Carter DC, Rüker F (1999) J Biol Chem 274:29303
117. Mahammed A, Gross Z (2005) J Am Chem Soc 127:2883
118. Gantchev TG, Ouellet R, van Lier JE (1999) Arch Biochem Biophys 366:21
119. Chatterjee S, Srivastava TS (2000) J Porphyrins Phthalocyanines 4:147
120. Ding Y, Lin B, Huie CW (2001) Electrophoresis 22:2210
121. Kragh-Hansen U, Chuang VTG, Otagiri M (2002) Biol Pharm Bull 25:695
122. Reetz MT, Jiao N (2006) Angew Chem Int Ed 45:2416
123. Otto S, Engberts JBFN (1999) J Am Chem Soc 121:6798
124. Otto S, Boccaletti G, Engberts JBFN (1998) J Am Chem Soc 120:4238
125. Roelfes G, Feringa BL (2005) Angew Chem 117:3294
126. Barr KA, Hopkins SA, Sreekrishna K (1992) Pharm Eng 12:48
127. Ohtani W, Nawa Y, Takeshima K, Kamuro H, Kobayashi K, Ohmura T (1998) Anal Biochem 256:56
128. Wilson ME, Whitesides GM (1978) J Am Chem Soc 100:306

129. Lin C-C, Lin C-W, Chan ASC (1999) Tetrahedron: Asymmetry 10:1887
130. Reetz MT, Peyralans J-P, Maichele A, Fu Y, Maywald M (2006) Chem Commun 2006:4318
131. Collot J, Gradinaru J, Humbert N, Skander M, Zocchi A, Ward TR (2003) J Am Chem Soc 125:9030
132. Thomas CM, Ward TR (2005) Chem Soc Rev 34:337
133. Ward TR (2005) Chem Eur J 11:3798
134. Klein G, Humbert N, Gradinaru J, Ivanova A, Gilardoni F, Rusbandi UE, Ward TR (2005) Angew Chem Int Ed 44:7764
135. Letondor C, Pordea A, Humbert N, Ivanova A, Mazurek S, Novic M, Ward TR (2006) J Am Chem Soc 128:8320
136. Bayer EA, Ben-Hur H, Wilchek M (1990) Methods Enzymol 184:80
137. Thompson LD, Weber PC (1993) Gene 136:243
138. Sano T, Cantor CR (1990) Proc Natl Acad Sci USA 87:142
139. Wu SC, Qureshi MH, Wong SL (2002) Protein Expression Purif 24:348
140. Wu S-C, Wong S-L (2002) Appl Environ Microbiol 68:1102
141. Gallizia A, de Lalla C, Nardone E, Santambrogio P, Brandazza A, Sidoli A, Arosio P (1998) Protein Expression Purif 14:192
142. Weber PC, Ohlendorf DH, Wendoloski JJ, Salemme FR (1989) Science 243:85
143. Meinhold P, Peters MW, Hartwick A, Hernandez AR, Arnold FH (2006) Adv Synth Catal 348:763
144. Lentz O, Feenstra A, Habicher T, Hauer B, Schmid RD, Urlacher VB (2005) Chem BioChem 7:345
145. Kumar S, Halpert JR (2005) Biochem Biophys Res Commun 336:1
146. Warman AJ, Roitel O, Neeli R, Girvan HM, Seward HE, Murray SA, McLean KJ, Joyce MG, Toogood H, Holt RA, Leys D, Scrutton NS, Munro AW (2005) Biochem Soc Trans 33:747

Top Organomet Chem (2009) 25: 93–112
DOI:10.1007/3418_2008_3

Artificial Metalloenzymes for Enantioselective Catalysis Based on the Biotin–Avidin Technology

Johannes Steinreiber and Thomas R. Ward

Abstract Artificial metalloenzymes can be created by incorporating an active metal catalyst precursor in a macromolecular host. When considering such artificial metalloenzymes, the first point to address is how to localize the active metal moiety within the protein scaffold. Although a covalent anchoring strategy may seem most attractive at first, supramolecular anchoring strategy has proven most successful thus far.

In this context and inspired by Whitesides' seminal paper, we have exploited the biotin–avidin technology to anchor a biotinylated active metal catalyst precursor within either avidin or streptavidin. A combined chemical and genetic strategy allows a rapid (chemogenetic) optimization of both the activity and the selectivity of the resulting artificial metalloenzymes. The chiral environment, provided by second coordination sphere interactions between the metal and the host protein, can be varied by introduction of a spacer between the biotin anchor and the metal moiety or by variation of the ligand scaffold. Alternatively, mutagenesis of the host protein allows a fine tuning of the activity and the selectivity.

With this protocol, we have been able to produce artificial metalloenzymes based on the biotin–avidin technology for the enantioselective hydrogenation of N-protected dehydroaminoacids, the transfer hydrogenation of prochiral ketones as well as the allylic alkylation of symmetric substrates. In all cases selectivities >90% were achieved. Most recently, guided by an X-ray structure of an artificial metalloenzyme, we have extended the chemogenetic optimization to a designed evolution scheme. Designed evolution combines rational design with combinatorial screening. In this chapter, we emphasize the similarities and the differences between artificial metalloenzymes and their homogeneous or enzymatic counterparts.

Key words Allylic alkylation, Artificial metalloenzyme, Biotin–avidin technology, Chemogenetic optimization, Designed evolution, Enantioselective catalysis, Hybrid catalyst, Hydrogenation, Streptavidin, Transfer hydrogenation,

J. Steinreiber and T.R. Ward (✉)
Department of Chemistry, University of Basel, Spitalstrasse 51, CH-4056 Basel, Switzerland
e-mail: thomas.ward@unibas.ch

Contents

Abbreviations

ee	Enantiomeric excess
WT	Wild-type
Sav	Streptavidin
Avi	Avidin
(strept)avidin	Either avidin or streptavidin
K_M	Michaelis–Menten constant
k_{cat}	Number of substrate molecules handled by one active site per second
v_{max}	Maximum velocity of the enzyme under the conditions of the experiment
DMSO	Dimethyl sulfoxide
EtOAc	Ethyl acetate
NBD	Norbornadiene
COD	Cyclooctadiene
MES	2-(*N*-morpholino)ethanesulfonic acid
MOPS	3-(*N*-morpholino)propanesulfonic acid
PYRPHOS	(3*R*,4*R*)-3,4-bis(diphenylphosphino)pyrrolidine

1 Introduction

In 1958 Frederick Sanger was awarded his first Nobel Prize in Chemistry for his studies on insulin [1]. He had determined its complete amino acid sequence, which proved that proteins have definite structures. Fifty years later, we have dramatically broadened our understanding of proteins and their role in vivo. Starting from amino acid building blocks, complex proteins have evolved to perform a variety of complex catalytic tasks. In addition to the amino acid's side chain reactivity, Nature often exploits cofactors and/or metal ions to complement its catalytic repertoire. It is estimated that one third of all enzymes are metalloproteins and that some of the most difficult biological transformations are mediated by these [2].

1.1 Background of Artificial Metalloenzymes

Artificial metalloenzymes, as reviewed here, are hybrid catalysts resulting from the introduction of a metal complex with catalytic activity into a macromolecular host, avidin or streptavidin (referred to as (strept)avidin hereafter). This provides a well-defined enantiopure second coordination sphere, thus potentially inducing selectivity in the catalyzed reaction [2–16]. The incorporation of an organometallic moiety within a protein may combine the advantages of both catalytic strategies, which are, in many regards, complementary (Table 1).

Enzymes can be improved by various protocols to overcome most of their inherent limitations, listed in Table 1. In particular, directed evolution, combined with an efficient screen or selection tool, has proven particularly versatile [17–20]. However, the ex nihilo creation of novel activities remains extremely challenging [21, 22].

We reasoned that one could mimic Nature by incorporating cofactors and metal ions to broaden the scope of accessible reactions catalyzed by protein scaffolds. Different approaches for the generation of artificial metalloenzymes have recently been reviewed [2–16]. Herein, we present the developments in the field of artificial metalloenzymes for enantioselective catalysis based on the biotin–avidin technology. The discussion includes a short introduction on the biotin–avidin technology followed by several examples of chemogenetic optimization of the performance of artificial metalloenzymes based on this technology.

1.2 Biotin–Avidin Technology

The biotin–avidin technology has found numerous applications both in fundamental and in applied research [23, 24]. This widespread technology relies on the affinity of biotin towards avidin ($K_a \sim 1 \times 10^{15}$ M^{-1}) and the homotetrameric nature of the protein, which allows binding of up to four (different) biotinylated probes. It has been

Table 1 Typical features of enzymatic and homogeneous catalysis

Features	Enzymes	Homogeneous catalysts
Enantiomers	Single	Both
Reaction conditions	Mild	Harsh
Substrate scope	Limited	Large
Functional group tolerance	Large	Small
Typical substrates	Flexible	Apolar
Reaction repertoire	Small	Large
Solvent compatibility	Aqueous > organic	Organic > aqueous
Optimization	Genetic	Chemical
Second coordination sphere	Well-defined	Ill-defined
Turnover numbers	Large	Modest

shown that derivatization of the valeric acid side chain of biotin does not decrease too significantly the affinity of avidin for the biotinylated probe. Both avidin (Avi, from egg-white) and its bacterial relative streptavidin (Sav, from *Streptomyces avidinii*, 32% sequence homology with avidin) display similar quaternary structures (homotetrameric eight-stranded β-barrel) as well as comparable affinities towards biotinylated probes. In the past 40 years, the biotin–avidin technology has been applied to affinity chromatography, diagnostics, immunoassays, drug targeting, etc. [25].

Most applications of the biotin–avidin technology do not rely on the incorporation of the biotinylated probe *within* the protein environment provided by (strept) avidin. Typically, the introduction of a long spacer (at least five atoms) between the biotin anchor and the probe is recommended (Fig. 1). The biotin–avidin technology can thus be regarded as a molecular velcro that allows the bringing together of up to four biotinylated probes.

With the aim of creating enantioselective catalysts, we wished to exploit the chiral environment provided by (strept)avidin upon incorporation of an achiral biotinylated metal catalyst. For this purpose, short spacers between the biotin anchor and the metal center should ensure that the latter is embedded within the protein (cf. Fig. 2).

1.3 Whitesides' Seminal Idea

Asymmetric hydrogenation is the archetype of homogeneous catalysis [26]. Wilkinson and Osborn reported that $[RhCl(PPh_3)_3]$ catalyzes the homogeneous hydrogenation of olefins [27]. This hydrogenation catalyst was rapidly adapted to an enantioselective

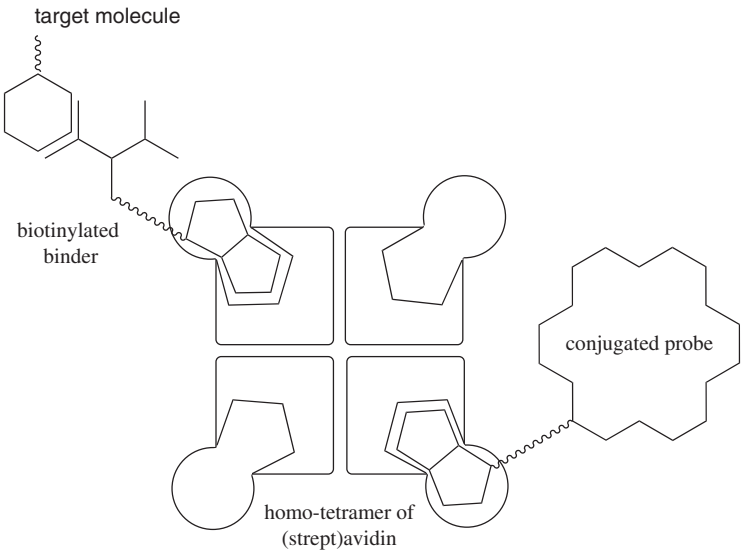

Fig. 1 Basic principle of the biotin–avidin technology. The homotetrameric nature of the protein allows binding of up to four (different) biotinylated probes

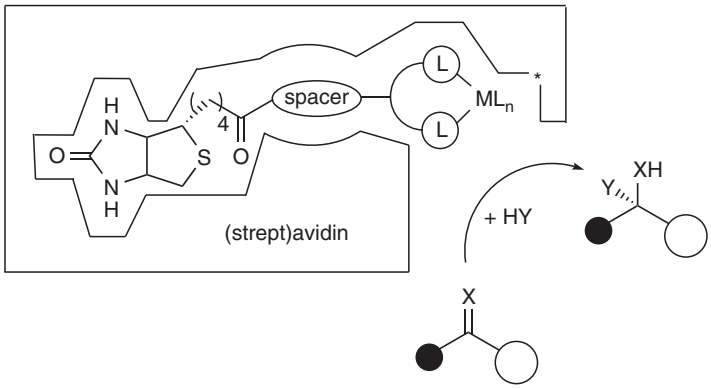

Fig. 2 Biotin–avidin technology: Artificial metalloenzymes [M(L_n)(biotin-ligand)]⊂(strept)avidin for enantioselective catalysis are based on the anchoring of a catalytically active metal fragment within a host protein via a ligand, a spacer, and biotin. Chemical optimization can be achieved either by varying the spacer or the metal chelate moiety (ML_n). Saturation mutagenesis at a position close to the metal moiety (*) can be used for genetic optimization

version by replacement of the achiral phosphine ligands [28] with enantiopure analogs (e.g. CAMP [29]) as well as chelating diphosphines (DIPAMP [30], DIOP [31], BINAP [32] and DuPhos [33]).

Rather than exploiting the first coordination sphere to induce selectivity, Whitesides suggested the introduction of an achiral homogeneous biotinylated catalyst within avidin, to form a hybrid catalyst where chirality is present in the second coordination sphere (Fig. 2 and Scheme 1a) [34].

Anchoring of a biotinylated rhodium-diphosphine in avidin resulted in an artificial metalloenzyme for the reduction of *N*-acetamidoacrylate. Using 0.2 mol% catalyst at 0 °C and 1 bar H_2, *N*-acetamidoalanine was produced quantitatively in 41% ee (*S*) (Scheme 1a) [34]. In 1999, Chan et al. relied on an enantiopure biotinylated PYRPHOS-ligand to hydrogenate itaconic acid (Scheme 1b) [35]. Depending on the configuration of the ligand (*S*,*S* or *R*,*R*) and the operating conditions, the ee of the product varied between 48% (*R*) and 26% (*S*).

Inspired by the visionary paper of Whitesides, we adapted and extended the concept of artificial metalloenzymes (or hybrid catalysts) based on the biotin–avidin technology to enantioselective hydrogenation, transfer hydrogenation, and allylic alkylation reactions, which are summarized herein.

2 Results of the Chemogenetic Optimization of Artificial Metalloenzymes Based on the Biotin–Avidin Technology

Inspired by the pioneering work of Whitesides [34], we endeavored to use the modern tools of genetic and chemical engineering to control the second coordination sphere of the homogeneous catalyst for hydrogenation [36–42]. The main

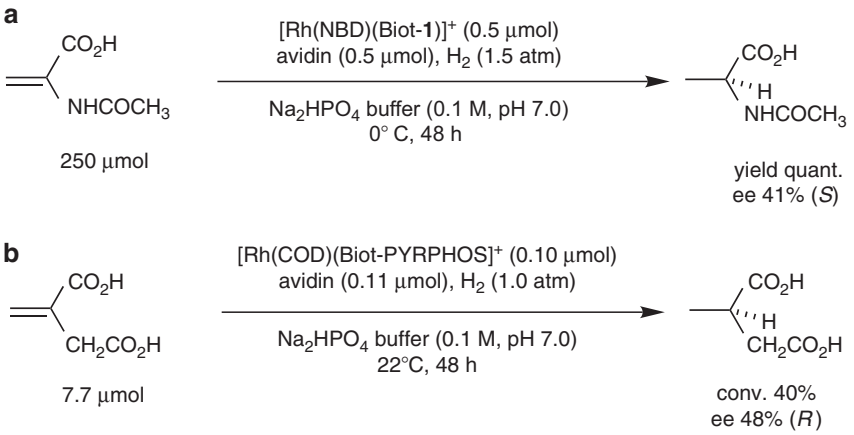

Scheme 1 Artificial metalloenzymes based on the biotin–avidin technology for the hydrogenation of alkenes. Operating conditions used by **a** Whitesides [34] and **b** Chan [35]

stages are (i) mutation and overexpression of the (strept)avidin isoform in a suitable host, (ii) isolation and quantification of the activity of the mutated (strept)avidin, (iii) synthesis of the biotinylated catalyst precursor and incorporation within (strept)avidin, (iv) catalysis, and (v) product isolation and analysis.

For optimization purposes, we rely on both chemical and genetic diversity (Fig. 2). The chemogenetic diversity matrix consists of a ligand scaffold, a spacer, and genetic mutations performed on the (strept)avidin host protein [4]. Whereas genetic engineering has been very successful in elucidating and modifying an enzyme's activity and selectivity, we showed that an artificial metalloenzyme could be modified either genetically or chemically (Fig. 3) [36] to improve its enantioselectivity, thus paving the way for further directed evolution of artificial metalloenzymes [43].

The general strategy that we employed initially was a chemogenetic approach – a term initially coined by Distefano [12] – whereby both the various components of the metal complex (e.g., the metal, the first coordination sphere, and the "spacer" linking it to the biotin anchor) as well as the protein "scaffold" were subjected to optimization. The chemogenetic approach to artificial enzymes has the potential for providing hybrid protein catalysts "made to order" [4]. Our preferred methodology is a combination of rational design and combinatorial screening leading to the "evolution" of the enzyme, for which we borrow the term "designed evolution" (Fig. 4) [44].

Designed evolution incorporates the need for rational decisions on choices of scaffolds and elements to combine, followed by several rounds of screening to perfect those elements that cannot be predicted a priori. It is noteworthy that the reaction conditions, such as a requirement for high temperatures or extreme pH, may impose evolutionary restrictions on the protein scaffold and that for extensive screening it is preferable to start with an appropriately robust scaffold [45, 46]. Due to the number of possible combinations of protein hosts, it

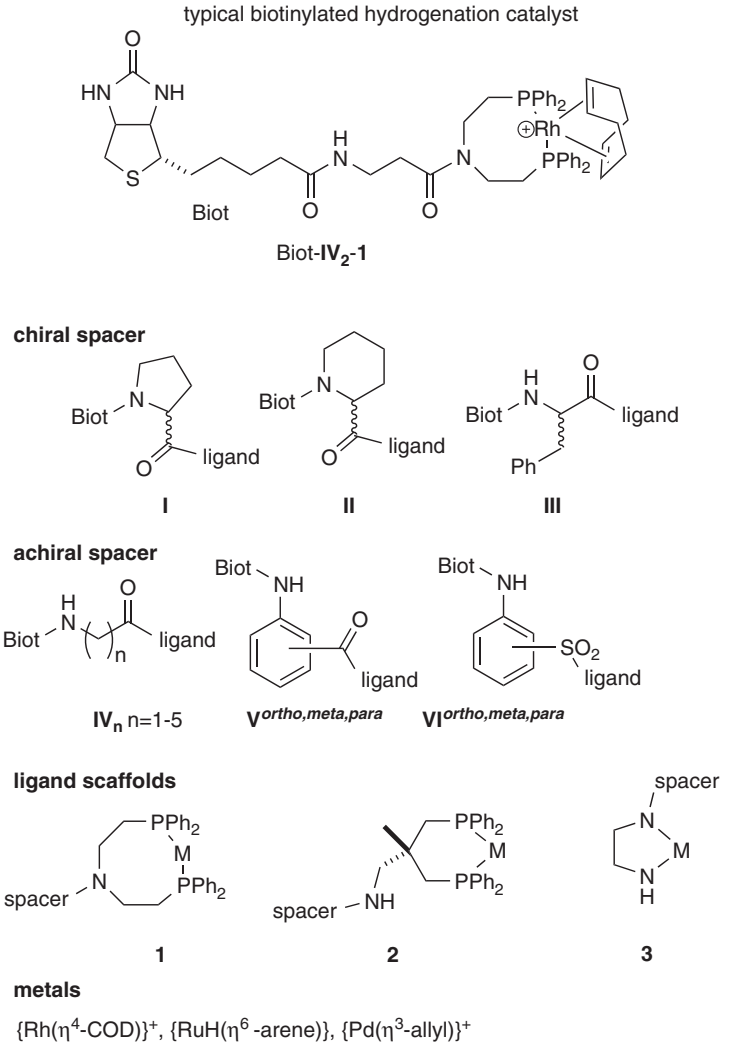

Fig. 3 Chemical diversity generated by different spacers, ligands, and metals as applied in the chemogenetic designed evolution described herein

is also convenient to limit the variations to a few designed choices, e.g., avidin and streptavidin. The latter provides a deeper binding pocket for the biotinylated metal complex. It is envisaged that as we learn more about the reaction mechanisms of these particular hybrid catalysts, particularly as concerns the second coordination sphere, we will be able to make wiser choices for designed evolution, optimally leaving the really fine-tuning to genetic, evolutionary approaches.

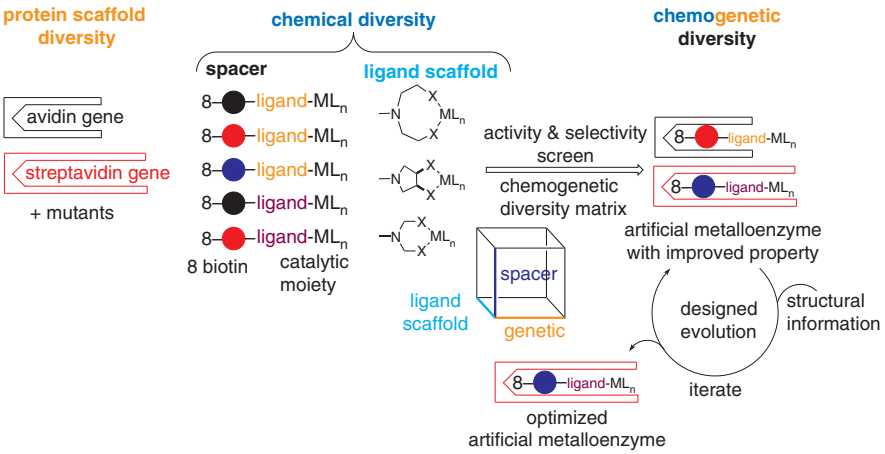

Fig. 4 Starting with a subset of appropriate protein scaffolds and chemically diverse homogeneous catalysts, a chemogenetic diversity matrix can be used to screen for improved characteristics. Designed evolution consists of iterative rounds of screening and selection of the chemogenetic diversity that is introduced, at least partially, according to the structural information available

2.1 Hydrogenation

Applying this designed evolution strategy we were able to improve the artificial hydrogenases of Whitesides and Chan significantly [36–42]. Using wild-type streptavidin (WT Sav) combined with Biot-**1** (Fig. 3) as a starting point, two steps of evolution of the artificial enzyme (first step is chemical optimization; second step is genetic optimization) lead to reversal and improvement of enantioselectivity for the hydrogenation of α-acetamidocinnamic acid from 96% ee in favor of (*R*) to 88% ee in favor of (*S*) (Fig. 5) [38, 40].

Further studies showed that introduction of chiral amino acid spacers – proline **I** or phenylalanine **III** – between the biotin anchor and the flexible aminodiphosphine moiety **1**, combined with saturation mutagenesis at position S112 of streptavidin, affords second generation artificial hydrogenases displaying improved organic solvent tolerance, reaction rates, and selectivities (≥95% ee for both enantiomers) (Scheme 2) [36, 39].

Many organic substrates are only poorly soluble in water, thus limiting the scope of aqueous phase catalysis. The addition of either an organic co-solvent or a surfactant often allows this serious limitation to be overcome. In order to investigate the robustness and performance of artificial metalloenzymes in organic solvents, we tested them in the presence of increasing amounts of dimethyl sulfoxide (DMSO) or ethyl acetate under biphasic conditions [39, 41]. The first generation catalyst [Rh(COD)(Biot-**1**)]$^+$ performs poorly in the presence of organic solvents (Table 2, entry 1 vs. entries 2 and 3). In strong contrast, for the catalyst [Rh(COD)(Biot-**I-1**)]$^+$ including a constrained proline spacer, the conversion and ee remained high (entries 4–6) in the presence of organic solvents. Although the catalyst affords

nearly racemic product in the absence of host protein, the chirality of the product is dictated by the absolute configuration of the spacer upon incorporation within (strept)avidin (entry 4 vs. 6, *R* or *S*). In addition, the immobilization of the artificial metalloenzyme using commercially available biotin-sepharose gave comparable results to the homogeneous counterparts [Rh(COD)(Biot-**1**)]$^+$ (entry 7 vs. 1).

The kinetic parameters for selected artificial hydrogenases were determined and the Michaelis–Menten parameters are listed in Table 3. The reactions were carried out at 2 bars hydrogen pressure and room temperature, with the more soluble substrate *N*-acetamidoacrylic acid.

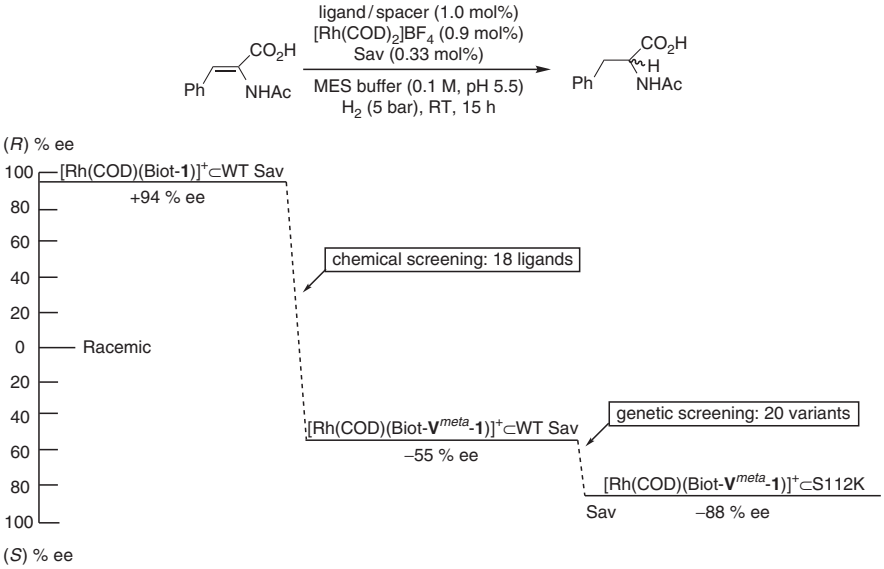

Fig. 5 Two steps of evolution of [Rh(COD)(Biot-**1**)]$^+$⊂WT Sav (first step is chemical optimization; second step is genetic optimization) [38, 40]

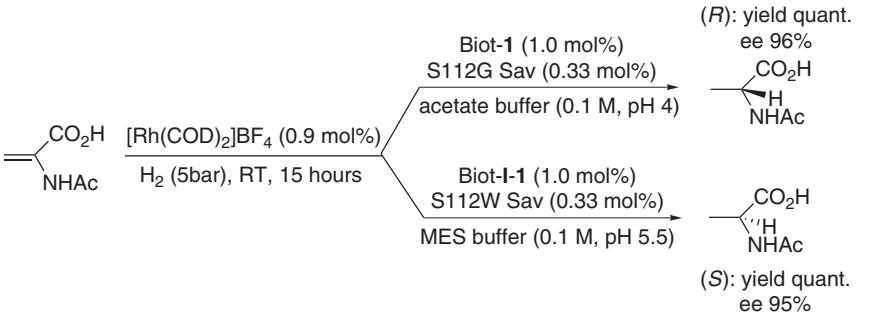

Scheme 2 Summary of selected results of the asymmetric hydrogenation improved by designed evolution [36, 39]

All catalytic systems studied display Michaelis–Menten behavior. Compared to the protein-free catalyst (Table 3, entry 1) all artificial hydrogenases display higher affinity for the substrate (i.e., smaller K_M, entries 2–4) and increased turnover frequencies (i.e., larger k_{cat}). It thus appears that incorporation of a biotinylated catalyst within streptavidin contributes to improve both its selectivity and its activity. We hypothesize that this latter feature may be caused by the accumulation of the hydrophobic substrate and H_2 in the vicinity of the active site, which bears hydrophobic amino acid residues.

In summary, relying on a chemogenetic optimization procedure, we have produced artificial hydrogenases based on the biotin–avidin technology for the enantioselective reduction of N-protected dehydroaminoacids [up to 96% ee (*R*) and 95% ee (*S*)] [36, 39]. Next, we outline our recent findings in artificial allylic alkylases based on a similar strategy.

2.2 Allylic Alkylation

C–C bond-forming reactions play an important role in asymmetric synthesis. In homogenous catalysis, palladium-catalyzed reactions are used for the construction

Table 2 Selected results for the synthesis of *N*-acetyl alanine in the presence of organic solvents or with immobilized artificial metalloenzyme (on sepharose) [39][a]

Entry	Ligand	Protein	Organic solvent	ee[b] (conv.)
1	Biot-**1**	WT Sav	DMSO 9%	94 (quant.)
2	Biot-**1**	WT Sav	DMSO 45%	16 (71)
3	Biot-**1**	WT Sav	EtOAc	30 (56)
4	Biot-(*S*)-**I**-**1**	S112M Sav	DMSO 45%	69 (quant.)
5	Biot-(*S*)-**I**-**1**	S112M Sav	EtOAc	64 (quant.)
6	Biot-(*R*)-**I**-**1**	WT Sav	DMSO 45%	−87 (quant.)
7	Biot-**1** + Biot-sepharose	WT Sav	DMSO 9%	83 (quant.)

[a]Conditions: $[Rh(COD)_2]BF_4$ (0.9 mol%), Biot-**1** (1.0 mol%), WT Sav (0.33 mol%), MES buffer (0.1 M, pH 5.5), H_2 (5 bar), RT, 15 h

[b]Positive- and negative ee values correspond to the (*R*)- and (*S*)-enantiomers, respectively

Table 3 Michaelis–Menten parameters for the reduction of *N*-acetamidoacrylic acid with selected artificial hydrogenases at 2 bars H_2 and room temperature[a]

Entry	Ligand	Protein	DMSO (%)	v_{max} (mM min^{-1})	k_{cat} (min^{-1})	K_M (mM)
1	Biot-**1**	–	9	0.173	3.06	7.38
2	Biot-**1**	WT Sav	9	0.254	4.49	3.18
3	Biot-(*R*)-**I**-**1**	WT Sav	30	0.695	12.30	4.36
4	Biot-(*R*)-**I**-**1**	WT Avi	30	0.634	11.23	4.80

[a]Conditions: $[Rh(COD)_2]BF_4$ (0.62 μmol), ligand (0.62 μmol), protein (0.207 μmol), MES buffer (0.1 M, pH 5.5, 10 mL), H_2 (2 bar), RT

of complex organic molecules via C–C bond-forming reactions [47]. As this versatile precious metal is absent in natural enzymes, Nature has implemented different strategies to create C–C bonds using enzymes (C–C lyases) [48].

Among asymmetric bond-forming reactions, the metal-catalyzed asymmetric allylic alkylation (AAA) is versatile and has found numerous applications [49]. While palladium involves a net retention via a double inversion mechanism with "soft" nucleophiles and a net inversion path with "hard" nucleophiles, many other metals also catalyze allylic alkylation (e.g., Rh, Ru, Ir, Mo, W, and Cu), which may involve different stereochemical courses [49].

Since the AAA in aqueous solution has been most studied with Pd(diphosphine)-bearing catalysts, we screened the library of biotinylated diphosphine ligands that were initially used in the hydrogenation study (Sect. 2.1). Our initial experiments focused on symmetric 1,3-diphenylallyl acetate and dimethylmalonate as soft nucleophiles (Scheme 3) [50]. It is widely accepted that the enantiodiscrimination event occurs through the external attack of a soft nucleophile on a palladium η^3-allyl intermediate. The AAA thus bears resemblance to enzymatic reactions, in which a reactant need not necessarily bind to the active site of the enzyme for the reaction to proceed with high stereoselectivity [51]. The second coordination sphere may thus play an important role in ensuring selectivity.

In order to favor the alkylation over the hydrolysis of the acetate-bearing substrate in aqueous media, the addition of a cationic surfactant proved beneficial (Table 4, entries 1–3). Having identified suitable reaction conditions for the AAA catalyzed by artificial metalloenzymes, we proceeded to screen the diversity matrix provided by combining 22 (strept)avidin isoforms with 13 [Pd(η^3-allyl)(Biot-spacer-**1**)]$^+$ type complexes. The results are summarized as a fingerprint in Fig. 6 and selected results are listed in Table 4 (entries 4–8).

In contrast to artificial hydrogenases, only selected biotinylated catalyst⊂(strept)avidin combinations yielded active catalysts. In this context, rigid spacers bearing

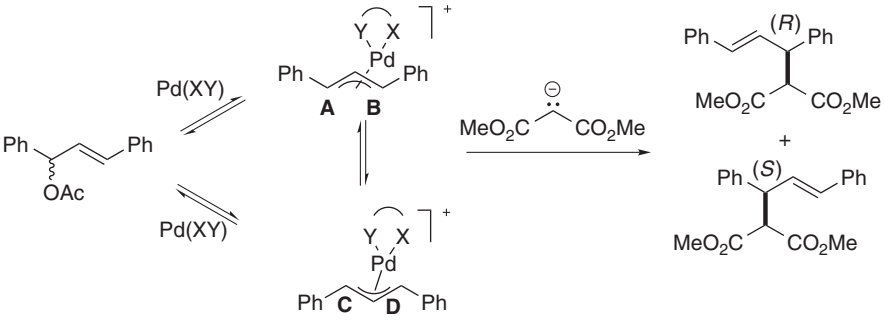

A and **D**: nucleophilic attack to form the (*R*)-enantiomer
B and **C**: nucleophilic attack to form the (*S*)-enantiomer

Scheme 3 Asymmetric allylic alkylation of symmetric 1,3-diphenylallyl acetate by malonic dimethylester

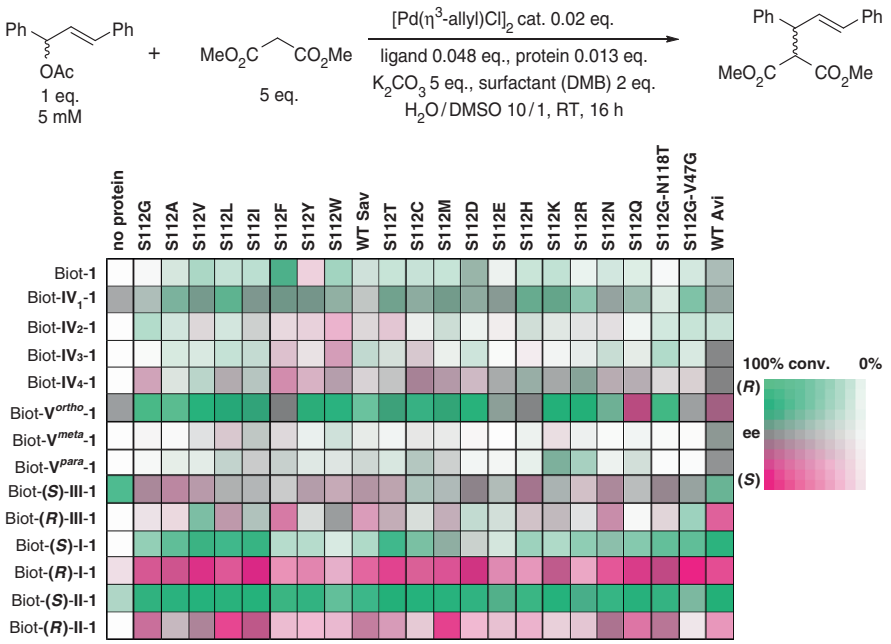

Fig. 6 Fingerprint of the chemoenzymatic screening for improved activity (*color depth*) and selectivity (*color change*). *DMB* didocyldimethylammonium bromide [50]

Table 4 Selected results for the AAA using different spacers and Sav isoforms [50][a]

Entry	Spacer	Sav isoform	ee (conv.)[b]
1	**I**	–	– (<5)
2	No spacer	WT Sav	14 (<5)[c]
3	No spacer	WT Sav	29 (21)
4	**V**^{ortho}	S112A	90 (95)
5	**V**^{ortho}	S112A	93 (20)[c]
6	**V**^{ortho}	S112Q	−31 (96)
7	(*R*)-**II**	S112M	−73 (88)
8	(*R*)-**I**	S112G-V47G	−82 (82)
9	**V**^{ortho}	S112A	95 (94)[d]

[a]Reaction conditions: The catalyst precursor was prepared in situ from [PdCl(η^3-Ph$_2$ allyl)]$_2$ (0.02 equiv) and the biotinylated ligand (0.048 equiv) in DMSO, and an aqueous solution of (strept)avidin (binding sites: 0.054 equiv), K_2CO_3 (5 equiv), DMB (2 equiv), $H_2C(CO_2Me)_2$ (5 equiv), and allylic acetate (1 equiv, final concentration 4 mM) was added. Final volume 435 μL, DMSO/H_2O = 1:10. The reaction mixture was stirred for 16 h at RT

[b]Positive- and negative ee values correspond to the (*R*)- and (*S*)-enantiomers, respectively

[c]No DMB was added

[d]At 40 °C for 1 h, 50% DMSO, no DMB added (Lo and Ward, unpublished results)

one or two carbon atoms between the amino-acid functionalities proved most active: the *ortho*-substituted aromatic amino acid spacer $\mathbf{V}^{ortho}$ yielded mostly (*R*)-alkylation products, except when combined with S112Q Sav (entries 4–6). The most (*S*)-selective catalysts included an (*R*)-piperidine and proline spacer (Biot-(*R*)-**II**-**1** and Biot-(*R*)-**I**-**1**) (entries 7, 8). Initially, the use of surfactant with these artificial lyases was essential as the yield dropped to 20% in its absence (entry 5). However, since the selectivities of the catalytic runs performed in their presence were comparable to those performed without DMB, we hypothesize that the structure of the protein is not significantly affected by the presence of surfactant. Most recently, we have shown that the artificial alkylases can operate in 50% DMSO without addition of DMB, affording alkylation products in up to 95% ee (entry 9) (Lo and Ward unpublished results).

In contrast to other reactions implemented so far with artificial metalloenzymes there is, to the best of our knowledge, no enzyme known that catalyzes such C–C bond-forming allylic alkylations. The final section of this chapter focuses on carbonyl reduction via a transfer hydrogenation mechanism.

2.3 Transfer Hydrogenation

The reduction of C=O and C=N bonds is a fundamental reaction that has been investigated with both enzymatic [48] and homogeneous [52] catalysis. Both systems achieve high levels of enantioselectivity. However, enzymes such as alcohol dehydrogenase need precious cofactors like NAD(P)H, which have to be regenerated (mostly done using whole cell fermentations). Homogeneous transfer hydrogenation (Meerwein–Ponndorf–Verley reduction) based on d^6-piano-stool complexes has proven to be efficient and selective by regenerating the organometallic hydride by a β-H abstraction between the catalyst precursor and a sacrificial hydrogen donor (e.g., isopropanol or formate, Scheme 4) [53, 54]. The transfer hydrogenation mechanism by d^6-piano-stool complexes is well-studied and it is generally accepted that the prochiral substrate does not bind to the metal. Instead, it proceeds via a second coordination sphere mechanism where a hydride and a proton are delivered to the C=O (or C=N) moiety (Scheme 4). In this context, acetophenone derivatives are preferred substrates as C–H···π interactions occur between the substrate's aryl group and the η^6-capping arene [55]. The asymmetric transfer hydrogenation of dialkyl ketones thus remains challenging for such catalysts [56]. Alcohol dehydrogenases solve this problem with an exquisitely tailored second coordination sphere of the active site [48].

Assuming that the enantioselection mechanism for artificial transfer hydrogenases using biotinylated d^6-piano-stool complexes should be similar to the homogeneous systems, we initially focused on the reduction of prochiral acetophenone derivatives [57–59]. Systematic variation of the pH revealed that these systems perform best at pH 6.25. As the pH rises during catalysis, we used a mixed buffer consisting of a sodium formate and boric acid mixture. Addition of MOPS further contributed to stabilization of the pH and improved the selectivity of the system.

Having identified suitable conditions, we proceeded to screen 21 biotinylated d^6-piano-stool complexes with the 20 Sav isoforms (S112X) resulting from saturation mutagenesis at position S112. The reduction of several acetophenone derivatives was achieved with [RuH(η^6-arene)(Biot-spacer-**3**)]⊂Sav with good activities and selectivities (Table 5). Most remarkably, the choice of capping arene (benzene or *p*-cymene) was shown to exert a strong influence on the enantiomer produced preferentially (entries 1 vs. 2, 3 vs. 4). This propensity can partially be overruled by introduction of cationic residues at position S112 (e.g., S112K), favoring (*S*)-products with modest conversions and selectivity (entry 5 vs. 6). With this first

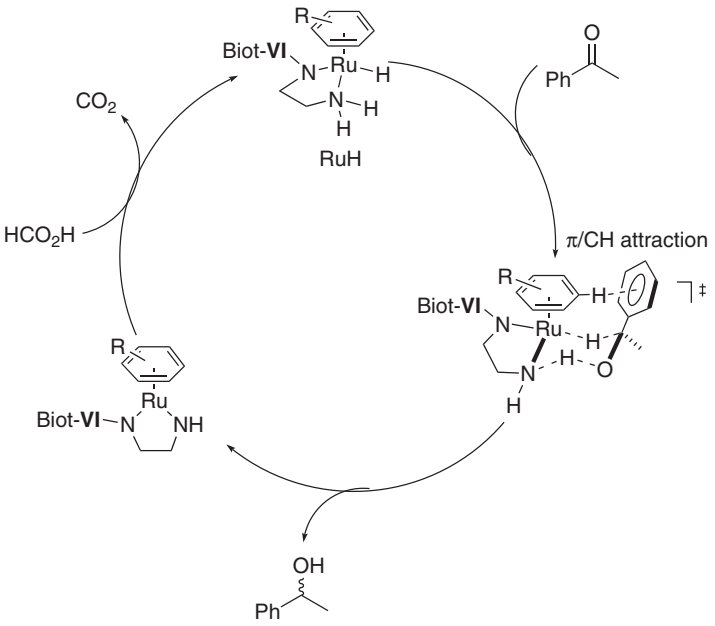

Scheme 4 Catalytic cycle for the Ru-catalyzed transfer hydrogenation of acetophenone and reduction of the Ru-catalyst by formate to form the Ru-hydride RuH

generation artificial transfer hydrogenases, dialkyl alcohols were produced with only modest enantioselectivity (entries 7, 8).

After many unsuccessful attempts, we were fortunate to crystallize the most promising (*S*)-selective artificial transfer hydrogenase: [RuCl(η^6-benzene)(Biot-VI^{para}-**3**)]⊂S112K Sav (Fig. 7) [57]. Several noteworthy features are apparent from this X-ray structure:

i. The Ru-occupancy in the refined structure is only 20%.
ii. The absolute configuration of the metal is (*S*)-Ru. This configuration is predicted to afford (*S*)-reduction products in the homogeneous system. Interestingly, (*S*)-reduction products are produced preferentially with [RuCl(η^6-benzene)(Biot-**VI**^{para}-**3**)]⊂S112K Sav.

Table 5 Selected results for the transfer hydrogenation of prochiral ketones by artificial metalloenzymes [59]

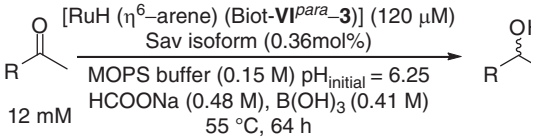

Entry	R	η⁶-arene	Sav isoform	ee (conv.)[a] (%)
1	4-Bromophenyl	*p*-Cymene	S112N	82 (94)
2	4-Bromophenyl	Benzene	S112T	−55 (90)
3	2-Pyridyl	*p*-Cymene	S112F	76 (95)
4	2-Pyridyl	Benzene	S112R	−70 (95)
5	Phenyl	*p*-Cymene	S112Y	90 (95)
6	Phenyl	*p*-Cymene	S112K	−20 (64)
7	CH_2CH_2Ph	*p*-Cymene	S112A	48 (98)
8	CH_2CH_2Ph	Benzene	S112A	52 (58)

[a]Positive- and negative ee values correspond to the (*R*)- and (*S*)-enantiomers, respectively

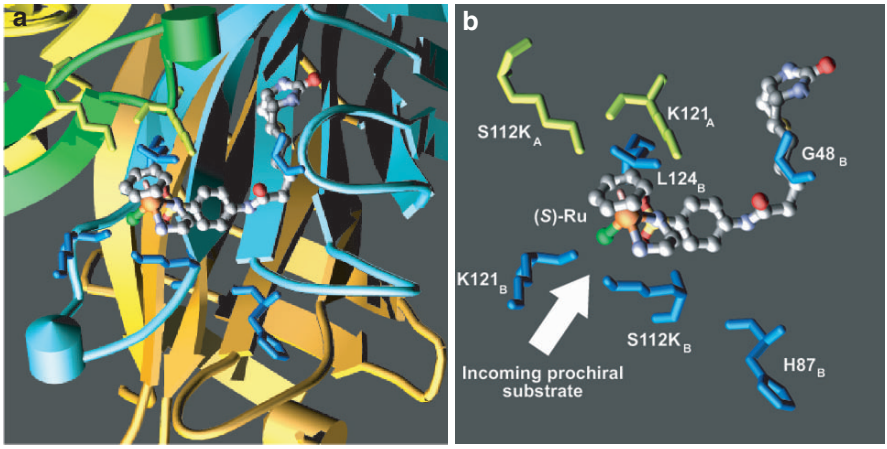

Fig. 7 X-ray crystal structure of [RuCl(η⁶-benzene)(Biot-**VI**^{para}-**3**)]⊂S112K Sav [57]. **a** Only monomer B (*blue*) is occupied by the biotinylated catalyst (*ball and stick representation*). Monomer A is shown in *green*, C *orange*, and D *yellow*. **b** Highlight of close contacts between the structure of [RuCl(benzene)(Biot-**VI**^{para}-**3**)] and amino acid residues of both monomers A and B of S112K Sav

iii. Residues K112 and K121 are in the close proximity of the Ru-center. Importantly, both residues from monomers A and B contribute to encapsulate the piano-stool moiety in a well-defined chiral environment.
iv. Residue L124 of monomer B (where the biotinylated catalyst is located) displays a close contact to the SO_2 group of the ligand.

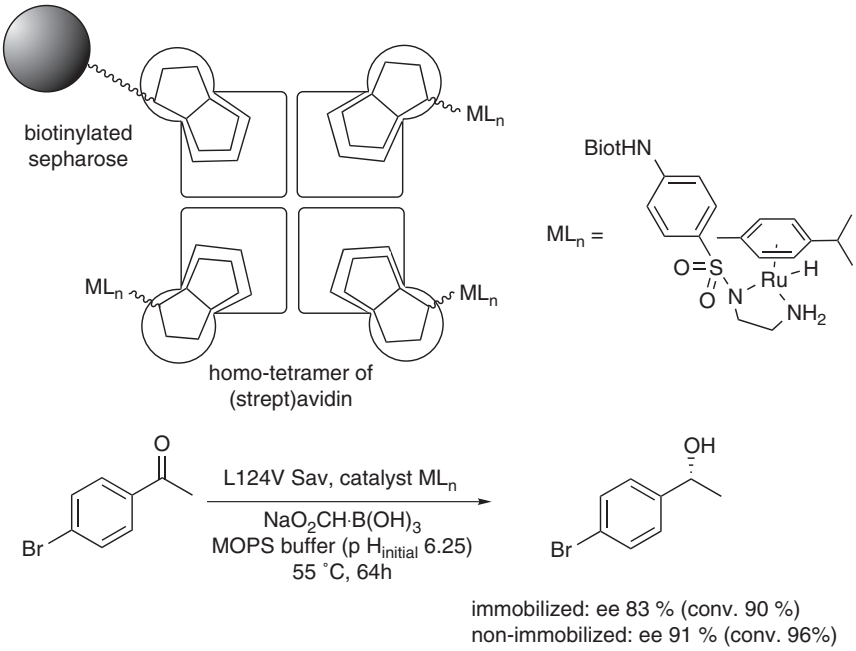

Fig. 8 Overcoming the purification bottleneck via immobilization of streptavidin isoforms using biotin-sepharose [57]

Based on these observations, we designed a second round of Sav isoforms bearing mutations at either position 121 or 124. These two positions were subjected to saturation mutagenesis using either S112A, which is (*R*)-selective; S112K Sav, which is (*S*)-selective; or WT Sav as the background. These 120 Sav isoforms were combined with either [RuH(η^6-benzene)(Biot-**VI**^{para}-**3**)] or with [RuH(η^6-*p*-cymene)(Biot-**VI**^{para}-**3**)] and tested for the reduction of *p*-bromoacetophenone and 4-phenyl-2-butanone, thus yielding a total of 480 catalytic runs.

In contrast to enzymatic catalyst optimization, artificial metalloenzymes require *purified* protein samples in *milligram* quantities. These requirements severely slow down the screening process, the bottleneck being the protein purification by affinity chromatography, followed by dialysis and lyophilization. To accelerate this process, a straightforward extraction–immobilization protocol with biotin-sepharose was implemented to capture functional Sav from crude cellular extracts (Fig. 8) [39, 57]. This procedure significantly hastened the optimization process, at the cost of a slight erosion in selectivity.

The result of the screening of the immobilized artificial transfer hydrogenases is displayed as a fingerprint in Fig. 9. The most promising results of artificial transfer hydrogenases were subsequently reproduced using the purified non-immobilized

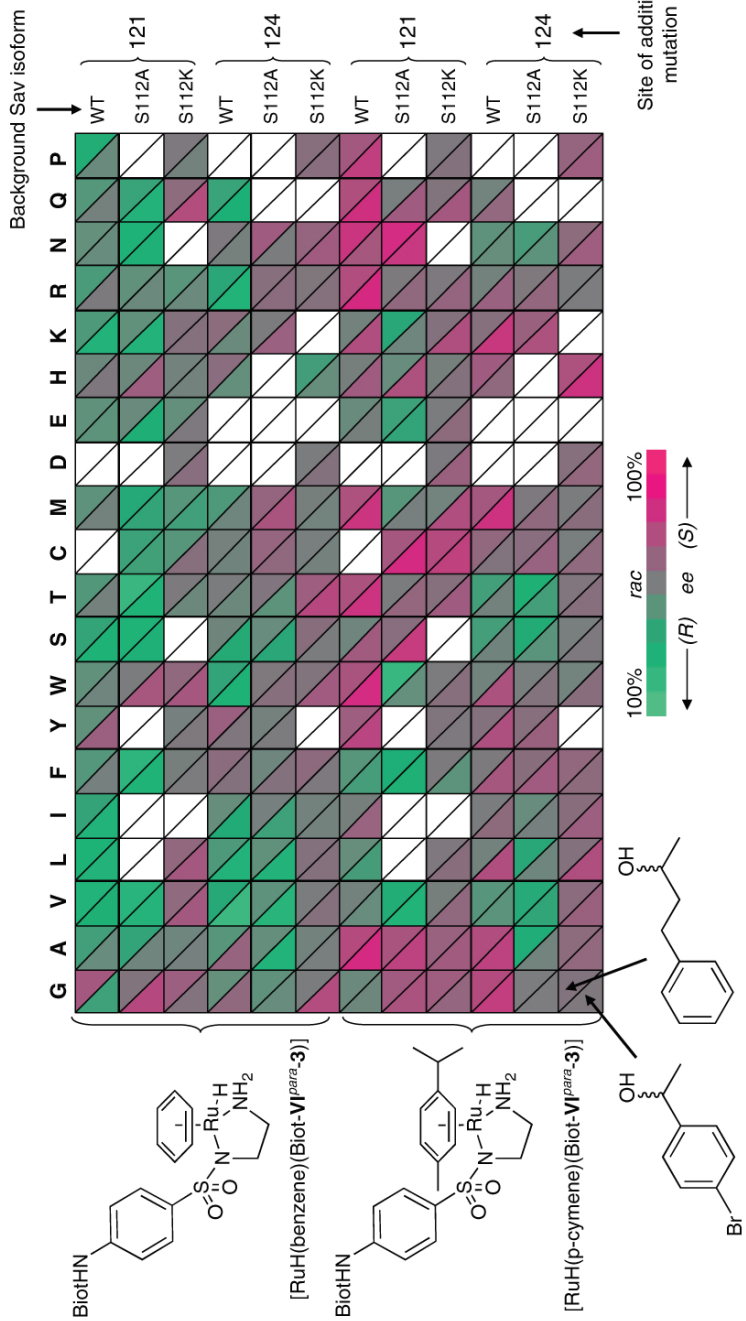

Fig. 9 Fingerprint display of the results for the chemogenetic optimization of the reduction of 4-bromo acetophenone and 4-phenyl-2-butanone in the presence of biotin-sepharose-immobilized artificial transfer hydrogenases [RuH(η^6-arene)(Biot-**VI**^{para}-**3**)]⊂streptavidin mutant [57]

Table 6 Summary of selected results for the catalytic experiments with purified homogeneous artificial metalloenzymes [η⁶-(arene)RuH(Biot-**VI**^{para}-**3**)]⊂Sav

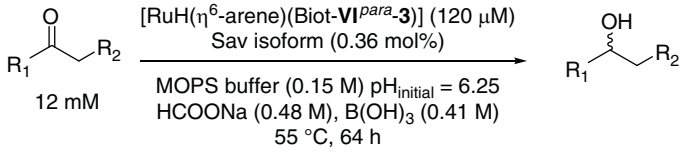

Entry	R_1/R_2	Arene	Sav isoform	ee (conv.)[a] (%)
1	4-Bromophenyl/H	*p*-Cymene	L124V	91 (96)
2	4-Bromophenyl/H	Benzene	S112A K121N	−75 (98)
3	4-Bromophenyl/H	*p*-Cymene	S112A K121N	70 (89)
4	4-Tolyl/H	*p*-Cymene	L124V	96 (97)
5	2-Pyridyl/H	Benzene	S112A K121N	−92 (quant.)
6	CH_2CH_2Ph/H	*p*-Cymene	S112A K121S	77 (98)
7	CH_2CH_2Ph/H	Benzene	S112A K121W	84 (99)
8	$CH_2CH_2OCH_2Ph/H$	*p*-Cymene	S112A K121T	90 (quant.)
9	CH_2Ph/CH_3	*p*-Cymene	S112A K121T	46 (50)

[a]Positive- and negative ee values correspond to the (*R*)- and (*S*)-enantiomers, respectively

catalysts in the presence of various substrates (Table 6). From this extensive screening several interesting trends emerge:

i. For acetophenone derivatives, selectivities of up to 96% (*R*) and 92% (*S*) were obtained (entries 1–5). Strikingly the substitution of benzene for *p*-cymene in the presence of the double mutant S112A K121N gives near mirror images for the reduction of acetophenone derivatives (entries 2 vs. 3).
ii. The best Sav isoforms originate from the S112A background. We speculate that a small side chain at position S112 may allow increased influence of beneficial K121X or L124X mutations.
iii. Saturation mutagenesis at position K121 is more effective for the optimization of enantioselectivity than at position L124. We hypothesize that the double interaction with the piano-stool complex itself and the substrate may be beneficial. Interaction with the substrate seems to play an important role for the enantioselective reduction of dialkyl ketones. Since no CH···π interaction is possible with the dialkyl substrate, the enantiodiscrimination must arise from interactions with the protein, as in the case of natural enzymes.
iv. While the enantioselectivity for acetophenone derivatives can be improved to >90% with Sav isoforms bearing single point mutations, a designed evolution protocol was required to identify double mutants for dialkyl ketones with similar selectivities (entries 1 vs. 8). As the CH···π interaction cannot operate for dialkylketones, the influence of the η⁶-arene on the enantioselectivity is much less pronounced than with acetophenone derivatives (entries 6, 7). Thus, the improved selectivity relies mostly on the evolved secondary coordination sphere and not on the η⁶-arene···substrate interactions, which is typical for homogeneous catalysts.
v. Interestingly, substitution of a methyl by an ethyl group in the substrate affords low reaction yields. Such substrate specificity is similar to that of yeast alcohol

dehydrogenases which, in general, only accept aldehydes and methyl ketones as substrates [48].

3 Conclusion and Perspectives

This chapter summarizes the development of artificial metalloenzymes for enantioselective catalysis based on the biotin–avidin technology. In the past 5 years and relying on a chemo-genetic optimization procedure, we have been able to produce hybrid catalysts for hydrogenation, transfer hydrogenation as well as for allylic alkylation reactions, with selectivities exceeding 90% ee. As outlined, these systems combine attractive features both of homogeneous catalysts as well as of enzymes.

The next challenges in the field of artificial metalloenzymes include:

i. Increasing the turnover number and turnover frequency of these systems to render these systems cost-competitive with the best enzymatic or homogeneous catalysts. Much along the lines of enzyme optimization, one should develop a rapid activity screen and apply it in combination with a directed evolution scheme.
ii. Investigating reactions that are challenging both for homogeneous and enzymatic catalysts. In this context, most of our current effort focuses on selective oxidation reactions. We speculate that, in the spirit of methane monooxygenase, the second coordination sphere interactions may prevent the thermodynamically favored over-oxidation of the product.
iii. Extending the concept of artificial metalloenzymes towards red biotechnology applications. For this purpose, we are currently testing artificial hydrolases for phosphodiester hydrolysis (restriction enzymes) as well as amide hydrolysis (proteases). We speculate that the large contacts between the streptavidin host and the macromolecule (DNA or protein) may allow the achievement of unrivalled levels of selectivity.

References

1. Sanger F (1959) Science 129:1340
2. Lu Y (2006) Inorg Chem 45:9930
3. Bornscheuer UT, Kazlauskas RJ (2004) Angew Chem Int Ed 43:6032
4. Creus M, Ward TR (2007) Org Biomol Chem 5:1835
5. Crow JM (2007) Chem World 4:50
6. Davis BG (2003) Curr Opin Biotechnol 14:379
7. Hayashi T, Hisaeda Y (2002) Acc Chem Res 35:35
8. Kraemer R (2006) Angew Chem Int Ed 45:858
9. Letondor C, Ward TR (2006) ChemBioChem 7:1845
10. Lu Y (2005) Curr Opin Chem Biol 9:118
11. Lu Y, Berry SM, Pfister TD (2001) Chem Rev 101:3047
12. Qi D, Tann C-M, Haring D, Distefano MD (2001) Chem Rev 101:3081
13. Steinreiber J, Ward TR (2008) Coord Chem Rev 252:751
14. Thomas CM, Ward TR (2005a) Chem Soc Rev 34:337
15. Thomas CM, Ward TR (2005b) Appl Organometal Chem 19:35
16. Ueno T, Satoshi A, Yokoi N, Watanabe Y (2007) Coord Chem Rev 251:2717

17. Arnold FH (1998) Acc Chem Res 31:125
18. Morley KL, Kazlauskas RJ (2005) Trends Biotechnol 23:231
19. Peisajovich SG, Tawfik DS (2007) Nat Methods 4:991
20. Reetz MT (2004) Meth Enzymol 388:238
21. Park H-S, Nam S-H, Lee JK, Yoon CN, Mannervik B, Benkovic SJ, Kim H-S (2006) Science 311:535
22. Seelig B, Szostak JW (2007) Nature 448:828
23. Wilchek M, Bayer EA (1990a) Methods Enzymol 184:5
24. Wilchek M, Bayer EA (1990b) Methods Enzymol 184:14
25. McMahon RJ (2008) Avidin–biotin interactions (methods in molecular biology) Springer, Berlin Heidelberg New York
26. Knowles WS, Noyori R (2007) Acc Chem Res 40:1238
27. JA, Osborn FH, Jardine JF, Young G Wilkinson (1966) J Chem Soc A: 1711
28. Blaser H-U, Malan C, Pugin B, Spindler F, Steiner H, Studer M (2003) Adv Synth Catal 345:103
29. Knowles WS, Sabacky MJ, Vineyard BD (1972) J Chem Soc Chem Commun 1972:10
30. Knowles WS (2002) Angew Chem Int Ed 41:1998
31. Kagan HB, Dang Tuan P (1972) J Am Chem Soc 94:6429
32. Noyori R (2002) Angew Chem Int Ed 41:2008
33. Burk MJ (2000) Acc Chem Res 33:363
34. Wilson ME, Whitesides GM (1978) J Am Chem Soc 100:306
35. Lin C-C, Lin C-W, Chan ASC (1999) Tetrahedron: Asymmetry 10:1887
36. Collot J, Gradinaru J, Humbert N, Skander M, Zocchi A, Ward TR (2003) J Am Chem Soc 125:9030
37. Collot J, Humbert N, Skander M, Klein G, Ward TR (2004) J Organometal Chem 689:4868
38. Klein G, Humbert N, Gradinaru J, Ivanova A, Gilardoni F, Rusbandi UE, Ward TR (2005) Angew Chem Int Ed 44:7764
39. Rusbandi Untung E, Lo C, Skander M, Ivanova A, Creus M, Humbert N, Ward Thomas R (2007) Adv Synth Catal 349:1923
40. Skander M, Humbert N, Collot J, Gradinaru J, Klein G, Loosli A, Sauser J, Zocchi A, Gilardoni F, Ward TR (2004) J Am Chem Soc 126:14411
41. Skander M, Malan C, Ivanova A, Ward TR (2005) Chem Commun 2005:4815
42. Ward TR (2005) Chem Eur J 11:3798
43. Reetz MT, Peyeralans JJ-P, Maichele A, Fu Y, Maywald M (2006) Chem Commun 2006:4318
44. Petrounia IP, Arnold FH (2000) Curr Opin Biotechnol 11:325
45. Le Trong I, Humbert N, Ward TR, Stenkamp RE (2006) J Mol Biol 356:738
46. Loosli A, Rusbandi UE, Gradinaru J, Bernauer K, Schlaepfer CW, Meyer M, Mazurek S, Novic M, Ward TR (2006) Inorg Chem 45:660
47. Tsuji J (2004) Palladium reagents and catalysts: new perspectives for the 21st century. Wiley, Chichester
48. Faber K (2004) Biotransformation in organic chemistry, 5th edn. Springer, Berlin Heidelberg New York
49. Trost BM (2004) J Org Chem 69:5813
50. Pierron J, Malan C, Creus M, Gradinaru J, Hafner I, Ivanova A, Sardo A, Ward TR (2008) Angew Chem Int Ed Engl 47:701
51. Wendt KU, Schulz GE, Corey EJ, Liu DR (2000) Angew Chem Int Ed 39:2812
52. Jacobsen EN, Pfaltz A, Yamamoto H (1999) Comprehensive asymmetric catalysis. Springer, Berlin Heidelberg New York
53. Noyori R, Hashiguchi S (1997) Acc Chem Res 30:97
54. Samec JSM, Bäckvall J-E, Andersson PG, Brandt P (2006) Chem Soc Rev 35:237
55. Yamakawa M, Yamada I, Noyori R (2001) Angew Chem Int Ed 40:2818
56. Schlatter A, Kundu MK, Woggon WD (2004) Angew Chem Int Ed 43:6731
57. Creus M, Pordea A, Rossel T, Sardo A, Letondor C, Ivanova A, Letrong I, Stenkamp RE, Ward TR (2008) Angew Chem Int Ed Engl 47:1400
58. Letondor C, Humbert N, Ward TR (2005) Proc Natl Acad Sci USA 102:4683
59. Letondor C, Pordea A, Humbert N, Ivanova A, Mazurek S, Novic M, Ward TR (2006) J Am Chem Soc 128:8320

Index